UNIVERSIDADE FEDERAL DE VIÇOSA

Climatic suitability and potential distribution of South American tropical moist forests from the Last Glacial Maximum to 2100

Mathias Viana Vicari
Doctor Scientiae

VIÇOSA - MINAS GERAIS
2025

MATHIAS VIANA VICARI

Climatic suitability and potential distribution of South American tropical moist forests from the Last Glacial Maximum to 2100

Thesis submitted to the Applied Meteorology Graduate Program of the Universidade Federal de Viçosa in partial fulfillment of the requirements for the degree of *Doctor Scientiae*.

Adviser: Jackson Martins Rodrigues

Co-adviser: Gustavo Reis de Brito

VIÇOSA - MINAS GERAIS
2025

Ficha catalográfica elaborada pela Biblioteca Central da Universidade Federal de Viçosa - Campus Viçosa

T

V628c
2025

Vicari, Mathias Viana, 1988-
Climatic suitability and potential distribution of South American tropical moist forests from the Last Glacial Maximum to 2100 / Mathias Viana Vicari. – Viçosa, MG, 2025.
1 tese eletrônica (129 f.): il. (algumas color.).

Texto em inglês.
Inclui apêndices.
Orientador: Jackson Martins Rodrigues.
Tese (doutorado) - Universidade Federal de Viçosa, Departamento de Engenharia Agrícola, 2025.
Inclui bibliografia.
DOI: https://doi.org/10.47328/ufvbbt.2025.837
Modo de acesso: World Wide Web.

1. Mudanças climáticas - América do Sul.
2. Paleoclimatologia. 3. Ecologia das florestas tropicais.
I. Rodrigues, Jackson Martins, 1984-. II. Universidade Federal de Viçosa. Departamento de Engenharia Agrícola. Programa de Pós-Graduação em Meteorologia Aplicada. III. Título.

CDD 22. ed. 551.698

Bibliotecário(a) responsável: Bruna Silva CRB-6/2552

MATHIAS VIANA VICARI

Climatic suitability and potential distribution of South American tropical moist forests from the Last Glacial Maximum to 2100

Thesis submitted to the Applied Meteorology Graduate Program of the Universidade Federal de Viçosa in partial fulfillment of the requirements for the degree of *Doctor Scientiae*.

APPROVED: July 16, 2025.

Assent:

Mathias Viana Vicari
Author

Jackson Martins Rodrigues
Adviser

To Maísa, Nayara, and Peter.

ACKNOWLEDGMENTS

First and foremost, I thank God for His guidance, strength, and grace throughout every step of this journey. Without His presence in my life, none of this would have been possible.

I would like to express my deepest gratitude to my advisor, Prof. Jackson Martins Rodrigues, for his guidance, patience, and support throughout this journey. I am especially grateful for his constant availability and willingness to respond to the countless messages I sent, always encouraging me and providing direction in my decisions and actions.

I am also sincerely thankful to Prof. Flávio Barbosa Justino, Prof. Paulo Hamakwa, and Prof. Marcos Heil for their valuable contributions and insights to my academic development. I would also like to thank Graça, the program secretary, for her attention and patience throughout this process. I extend special thanks to Prof. Gustavo Reis de Brito for his essential support, patience, and guidance throughout all the modeling and ecological analyses.

I sincerely thank Prof. João Augusto Alves Meira Neto, Prof. Gustavo Reis de Brito, Prof. Douglas da Silva Lindemann, and Prof. Carlos Diego de Sousa Gurjão for their participation in the examination committee, as well as for their valuable contributions, insightful suggestions, and generosity in sharing their knowledge and expertise, which greatly enriched this work.

I carry immense gratitude for my family, whose unconditional support has been a steady foundation along this journey. But above all, I dedicate my deepest admiration and love to my wife Nayara, my daughter Maísa, and Peter, for being a source of presence, comfort, and light in the most challenging moments. Their love, patience, and understanding were indispensable, and without them, this achievement would simply not have been possible.

I am also thankful to my parents, my sister, my parents-in-law, and my brother-in-law for their unwavering support. A special thanks goes to my friends Luiz Alberto Santana and Rodrigo Siqueira Batista for their friendship, trust, and encouragement, and to the band Iron Maiden, for the energy that fueled every late-night writing session.

Finally, I thank the Federal University of Viçosa for the opportunity to pursue and complete this postgraduate program.

This work has been sponsored by the following Brazilian research agencies: Coordination for the Improvement of Higher Education Personnel

(CAPES; Financing code 001), Minas Gerais State Foundation for Research Aid (FAPEMIG) and National Council of Scientific and Technological Development (CNPq).

“Our planet is a lonely speck in the great enveloping cosmic dark. In our obscurity, in all this vastness, there is no hint that help will come from elsewhere to save us from ourselves.”

Carl Sagan, Pale Blue Dot: A Vision of the Human Future in Space (1994)

ABSTRACT

VICARI, Mathias Viana, D.Sc., Universidade Federal de Viçosa, July, 2025. **Climatic suitability and potential distribution of South American tropical moist forests from the Last Glacial Maximum to 2100**. Adviser: Jackson Martins Rodrigues. Co-adviser: Gustavo Reis de Brito.

This thesis analyzes the climatic suitability and potential distribution of South American tropical moist forests from the Last Glacial Maximum to the year 2100. It investigates how past, present, and future climatic conditions have influenced and may continue to influence the spatial patterns of these ecosystems. Chapter 2 assesses the climatic suitability of tropical forests throughout the Late Quaternary, encompassing both glacial and post-glacial periods, with a focus on eight key intervals: the Last Glacial Maximum (LGM), Heinrich Stadial 1 (HS1), Bølling–Allerød (BA), Younger Dryas (YD), the Holocene (subdivided into early, middle, and late phases) and the present. The objective is to understand how colder and more variable climatic regimes shaped the spatial configuration of forest habitats and how the transition to more stable interglacial conditions, from the Holocene to the present, influenced the expansion, contraction, or persistence of climatically suitable areas. This approach highlights the responses of tropical forests to gradual warming and changes in moisture regimes that followed the end of the last glacial period. Chapter 3 focuses on future scenarios, projecting climatic suitability under contemporary conditions (1970–2000) and across four time intervals between 2021 and 2100. Using ecological niche modeling with the MaxEnt algorithm and CMIP6 climate data, the study simulates the impacts of different socioeconomic pathways (SSP1–2.6, SSP2–4.5, SSP3–7.0, and SSP5–8.5) on forest distribution. The models predict a general decline in suitable areas, particularly under high-emission scenarios, raising concerns about the resilience of tropical forests in the face of accelerating climate change. By integrating paleoecological, current, and future data, this research provides a comprehensive understanding of the biogeographical dynamics of South American tropical forests and offers valuable insights for conservation planning amid ongoing global climatic disruptions.

Keywords: Tropical moist forests; Climatic suitability; Ecological niche modeling; Paleoclimatology; Climate change; Last Glacial Maximum; Future scenarios; South America

RESUMO

VICARI, Mathias Viana, D.Sc., Universidade Federal de Viçosa, julho de 2025. **Mudanças climáticas na América do Sul nos últimos 21.000 anos e os impactos na distribuição de vegetações**. Orientador: Jackson Martins Rodrigues. Coorientador: Gustavo Reis de Brito.

Esta tese analisa a adequabilidade climática e a distribuição potencial das florestas tropicais úmidas da América do Sul desde o Último Máximo Glacial até o ano de 2100. Investiga como as condições climáticas passadas, presentes e futuras influenciaram e podem continuar a influenciar os padrões espaciais desses ecossistemas. O Capítulo 2 avalia a adequabilidade climática das florestas tropicais ao longo do Quaternário Tardio, abrangendo tanto a era glacial quanto o período pós-glacial, com foco em oito intervalos-chave: Último Máximo Glacial (LGM), Estádio de Heinrich 1 (HS1), Bølling–Allerød (BA), Dryas Recente (YD), Holoceno (subdividido em inicial, médio e tardio) e o presente. O objetivo é compreender como regimes climáticos mais frios e variáveis moldaram a configuração espacial dos habitats florestais e de que forma a transição para condições interglaciais mais estáveis, do Holoceno ao presente, influenciou a expansão, contração ou persistência das áreas climaticamente adequadas. Essa abordagem evidencia as respostas das florestas tropicais ao aquecimento gradual e às mudanças nos regimes de umidade que se seguiram ao fim da última era glacial. O Capítulo 3 foca nos cenários futuros, projetando a adequabilidade climática sob condições contemporâneas (1970–2000) e em quatro intervalos de tempo entre 2021 e 2100. Utilizando modelagem de nicho ecológico com o algoritmo MaxEnt e dados climáticos do CMIP6, são simulados os impactos de diferentes trajetórias socioeconômicas (SSP1–2.6, SSP2–4.5, SSP3–7.0 e SSP5–8.5) sobre a distribuição das florestas. Os modelos preveem um declínio geral das áreas adequadas, especialmente sob cenários de altas emissões, levantando preocupações sobre a resiliência das florestas tropicais diante do acelerado processo de mudança climática. Ao integrar dados paleoecológicos, atuais e futuros, o estudo contribui para uma compreensão mais profunda da dinâmica biogeográfica das florestas sul-americanas e oferece subsídios relevantes para o planejamento da conservação frente às perturbações climáticas globais.

Palavras-chave: Florestas tropicais úmidas; Adequabilidade climática; Modelagem de nicho ecológico; Paleoclimatologia; Mudanças climáticas; Último Máximo Glacial; Cenários futuros; América do Sul

SUMMARY

1. General Introduction

The tropical and subtropical forests of South America represent some of the most biodiverse and critical ecosystems on the planet (Almazroui et al., 2021; Anjos, 2021; Borma et al., 2022). Biomes such as the Amazon Rainforest and the Atlantic Forest play essential roles in global and regional climate regulation, the carbon cycle, and the maintenance of a vast array of species and ecosystem functions (Artaxo et al., 2022; Borma et al., 2022; da Rocha et al., 2009; Ribeiro et al., 2009; Vancine et al., 2024).

The Amazon, as the largest tropical rainforest in the world, has a profound impact on Earth's climate due to its role in global energy, moisture, and carbon balances (Artaxo et al., 2022; da Rocha et al., 2009). Although the Atlantic Forest has been reduced to fragments (Ribeiro et al., 2009; Tabarelli et al., 2010; Vancine et al., 2024), it remains a major biodiversity hotspot (Ribeiro et al., 2009; Tabarelli et al., 2010).

However, these ecosystems are under increasing pressure due to a range of human-induced threats, such as deforestation, habitat fragmentation, intensive land use, wildfires, and hunting, which have led to alarming biodiversity losses and degradation of essential ecosystem services (Ribeiro et al., 2009; Tabarelli et al., 2010; Malhi et al., 2008; Miranda, 2019; Rezende et al., 2018; Vancine et al., 2024; Welch et al., 2013). In parallel, global climate change is emerging as a significant and escalating threat (Almazroui et al., 2021; Hacon et al., 2019; IPCC, 2023; Vale et al., 2021). Rising temperatures, altered precipitation patterns, and increased frequency and intensity of extreme events such as droughts and floods pose additional challenges to the persistence and functioning of these forests (Almazroui et al., 2021; Vale et al., 2021).

The combination of these anthropogenic pressures may lead to ecological tipping points (Bottino et al., 2024) and abrupt shifts in ecosystem states, such as the savannization of forested areas (Bottino et al., 2024; Lyra et al., 2016; Sales et al., 2021).

To understand the vulnerability and resilience of South America's tropical and subtropical forests in the face of climate change, it is crucial to examine their responses across different temporal scales. Paleoecological and paleoclimatic studies provide a long-term perspective, revealing how these ecosystems responded to major

climatic shifts in the past (Behling et al., 1995; Flantua et al., 2015; Hermanowski et al., 2012; Li et al., 2024).

The Last Glacial Maximum (LGM), which occurred approximately between 19.000 and 23.000 cal years ago (Pinaya et al., 2024), was characterized by environmental conditions drastically different from those of the present. Temperatures across tropical and subtropical South America were significantly lower (Pinaya et al., 2019; 2024), and atmospheric CO_2 concentrations were considerably reduced (Borma et al., 2022; Hermanowski et al., 2012; Pinaya et al., 2024). Precipitation patterns also changed: the South American monsoon system was weaker, leading to overall lower precipitation rates in the Amazon (Borma et al., 2022), with paleorecords indicating drier conditions in parts of eastern and central Amazonia (Hermanowski et al., 2012), while other regions of the continent experienced corridors of cold and humid forest (Pinaya et al., 2024).

The LGM shaped both Amazonian and Atlantic Forest ecosystems, driving plant population displacements, community rearrangements, and the formation of no-analogue vegetation types (Flantua et al., 2015). Cold-adapted species expanded into lowland areas (Behling et al., 1995; Hermanowski et al., 2012), and grasslands expanded into regions now occupied by forests, such as southern Brazil (Behling et al., 1995; Colinvaux et al., 2000).

Tropical rainforest persisted in large parts of the Amazon Basin, although possibly with less dense structure in some areas (Colinvaux et al., 2000; Hermanowski et al., 2012). The climatic transition from the LGM to the pre-industrial period represents a valuable "natural experiment" for testing vegetation responses to major temperature shifts and can help validate models used to project future scenarios (Colinvaux et al., 2000).

Future climate projections, based on global and regional climate models and Shared Socioeconomic Pathways (SSPs) (Almazroui et al., 2021; Anjos, 2021; IPCC, 2023), indicate that temperatures across South America will continue to rise significantly (Almazroui et al., 2021; Vale et al., 2021), particularly within the tropical belt (Almazroui et al., 2021).

Mean annual precipitation is expected to decrease in some regions while increasing in others (Almazroui et al., 2021), with particularly notable trends of moisture reduction in forest biomes (Almazroui et al., 2021; Vale et al., 2021). More pessimistic scenarios project more severe changes than optimistic ones (Almazroui et

al., 2021). These projected changes suggest profound modifications in vegetation distribution and composition, including potential expansion of savannas and Cerrado and a reduction of tropical and seasonal forests (Oliveira-Filho & Ratter, 2002; Pennington et al., 2018; Thomas et al., 2004; Vale et al., 2021), with major impacts on biodiversity (Ribeiro et al., 2009; Tabarelli et al., 2010; Thomas et al., 2004; Vale et al., 2021) and regional climate regulation (Almazroui et al., 2021).

This doctoral thesis aims to fill a knowledge gap regarding how South American tropical and subtropical forests respond to major climatic disturbances by examining both past dynamics and future projections. By integrating these two perspectives, it is possible to obtain a more comprehensive understanding of the sensitivity, adaptability, and resilience of these ecosystems under different climate regimes, and to better anticipate potential future impacts in a context of rapid and unprecedented change.

This work is organized as follows:

- ✓ Chapter 2 investigates the climatic suitability of South American tropical forests throughout the Late Quaternary, encompassing both glacial and post-glacial periods, with a focus on eight key intervals: the Last Glacial Maximum (LGM), Heinrich Stadial 1 (HS1), Bølling–Allerød (BA), Younger Dryas (YD), and the Holocene subdivided into three phases: Early Holocene, Middle Holocene, and Late Holocene, in addition to the present. The analysis aims to understand how colder and more variable glacial conditions shaped the potential spatial patterns of these forest formations, and how the transition to more stable interglacial regimes, from the Holocene to the present, influenced trends of expansion, contraction, or stability in climatically suitable areas in response to post-glacial environmental changes.
- ✓ Chapter 3 is dedicated to future projections of climatic suitability, based on contemporary climate conditions (1970–2000) and on projected scenarios for the periods 2021–2040, 2041–2060, 2061–2080, and 2081–2100. The modeling is conducted using CMIP6 climate scenarios (SSP1–2.6, SSP2–4.5, SSP3–7.0, and SSP5–8.5), with the aim of assessing the potential impacts of climate change on the future distribution of tropical forests.
- ✓ Chapter 4 presents the general conclusions, integrating the results obtained across the three temporal scales (glacial, interglacial, and future), and discussing their

implications for the resilience of South American tropical forests and for conservation strategies in the face of climate change.

This study aims to contribute to the advancement of knowledge on the historical ecology and future of South American forests, providing essential insights to inform conservation and management decisions in a rapidly changing climatic world.

REFERENCES

Almazroui, M., Ashfaq, M., Islam, M.N. et al. Assessment of CMIP6 Performance and Projected Temperature and Precipitation Changes Over South America. Earth Syst Environ 5, 155–183 (2021). https://doi.org/10.1007/s41748-021-00233-6

Anjos, L. J. S., de Souza, E. B., Amaral, C. T., Igawa, T. K., & de Toledo, P. M. (2021). Future projections for terrestrial biomes indicate widespread warming and moisture reduction in forests up to 2100 in South America. Global Ecology and Conservation, 25, e01441. https://doi.org/10.1016/j.gecco.2020.e01441

Artaxo, P., et al. (2022). Tropical and boreal forest–atmosphere interactions: A review. Tellus B: Chemical and Physical Meteorology, 74(1), 24–163. https://doi.org/10.16993/tellusb.34

Behling, H. (1995). Investigations into the Late Pleistocene and Holocene history of vegetation and climate in Santa Catarina (S Brazil). Vegetation History and Archaeobotany, 4, 127–152.

Borma, L. S., Costa, M. H., da Rocha, H. R., Arieira, J., Nascimento, N. C. C., Jaramillo-Giraldo, C., et al. (2022). Beyond carbon: The contributions of South American tropical humid and subhumid forests to ecosystem services. Reviews of Geophysics, 60, e2021RG000766. https://doi. org/10.1029/2021RG000766

Bottino, M. J., Nobre, P., Giarolla, E., Lyra, A. A., Marengo, J. A., & Sampaio, G. (2024). Amazon savannization and climate change are projected to increase dry season length and temperature extremes over Brazil. Scientific Reports, 14, 5131. https://doi.org/10.1038/s41598-024-55176-5

Colinvaux, P. A., De Oliveira, P. E., & Bush, M. B. (2000). Amazonian and neotropical plant communities on glacial time-scales: The failure of the aridity and refuge hypotheses. Quaternary Science Reviews, 19(1–5), 141–169

da Rocha, H. R., Manzi, A. O., Cabral, O. M., Miller, S. D., Goulden, M. L., et al. (2009). Patterns of water and heat flux across a biome gradient from tropical forest to savanna in Brazil. Journal of Geophysical Research: Biogeosciences, 114, G00B12. https://doi.org/10.1029/2007JG000640

Flantua, S. G. A., Hooghiemstra, H., Grimm, E. C., Behling, H., Bush, M. B., González-Arango, C., Gosling, W. D., Ledru, M.-P., Lozano-García, S., Maldonado,

A., Prieto, A. R., Rull, V., & Van Boxel, J. H. (2015). Updated site compilation of the Latin American Pollen Database. Review of Palaeobotany and Palynology, 223, 104–115. http://dx.doi.org/10.1016/j.revpalbo.2015.09.008

Hacon, S. D. S., de Oliveira, B. F. A., & Silveira, I. (2019). A review of the health sector impacts of 4 °C or more temperature rise. In C. Nobre, J. Marengo, & W. Oyama (Eds.), Climate change risks in Brazil (pp. 67–129). Springer International Publishing. https://doi.org/10.1007/978-3-319-92881-4_4

Hermanowski, B., Behling, H., Pillar, V. D., Berrio, J. C., Van der Hammen, T., & Bush, M. B. (2012). Environmental changes in southeastern Amazonia during the last 25,000 years revealed from a paleoecological record. Quaternary Research, 77(1), 138–148.

IPCC. (2023). Summary for Policymakers. In H. Lee & J. Romero (Eds.), Climate Change 2023: Synthesis Report. Contribution of Working Groups I, II and III to the Sixth Assessment Report of the Intergovernmental Panel on Climate Change (pp. 1–34). IPCC. https://doi.org/10.59327/IPCC/AR6-9789291691647.001

Li, C., Dallmeyer, A., Ni, J., Chevalier, M., Willeit, M., Andreev, A. A., Cao, X., Schild, L., Heim, B., & Herzschuh, U. (2024). Global biome changes over the last 21,000 years inferred from model–data comparisons. EGUsphere. Advance online publication. https://doi.org/10.5194/egusphere-2024-1862

Lyra, A. de A., Chou, S. C., & Sampaio, G. de O. (2016). Sensitivity of the Amazon biome to high resolution climate change projections. Acta Amazonica, 46(2), 175–188. https://doi.org/10.1590/1809-4392201502225

Malhi, Y., Roberts, J. T., Betts, R. A., Killeen, T. J., Li, W., & Nobre, C. A. (2008). Climate change, deforestation, and the fate of the Amazon. Science, 319(5860), 169–172. https://doi.org/10.1126/science.1146961

Miranda, E. B. P., Menezes, J. F. S., Farias, C. C. L., Munn, C., & Peres, C. A. (2019). Species distribution modeling reveals strongholds and potential reintroduction areas for the world's largest eagle. PLoS ONE, 14(5), e0216323. https://doi.org/10.1371/journal.pone.0216323

Oliveira-Filho, A. T., & Ratter, J. A. (2002). Vegetation physiognomies and woody flora of the Cerrado biome. In P. S. Oliveira & R. J. Marquis (Eds.), The Cerrados of Brazil (pp. 91–120). Columbia University Press. https://doi.org/10.7312/oliv12042-007

Pennington, R. T., Lehmann, C. E. R., & Rowland, L. M. (2018). Tropical savannas and dry forests. Current Biology, 28(9), R541–R545. https://doi.org/10.1016/j.cub.2018.03.014

Pinaya, J. L. D., Cruz, F. W., Ceccantini, G. C. T., Corrêa, P. L. P., Pitman, N., Vemado, F., Lopez, M. S., Pereira Filho, A. J., Grohmann, C. H., Chiessi, C. M., Stríkis, N. M., & De Oliveira, P. E. (2019). Brazilian montane rainforest expansion

induced by Heinrich Stadial 1 event. Scientific Reports, 9(17912). (2019) 9:17912 https://doi.org/10.1038/s41598-019-53036-1

Rezende, C. L., Scarano, F. R., Assad, E. D., Joly, C. A., Metzger, J. P., Strassburg, B. B. N., et al. (2018). From hotspot to hopespot: An opportunity for the Brazilian Atlantic Forest. Perspectives in Ecology and Conservation, 16(4), 208–214. https://doi.org/10.1016/j.pecon.2018.10.002

Ribeiro, M. C., Metzger, J. P., Martensen, A. C., Ponzoni, F. J., & Hirota, M. M. (2009). The Brazilian Atlantic Forest: How much is left, and how is the remaining forest distributed? Implications for conservation. Biological Conservation, 142(6), 1141–1153. https://doi.org/10.1016/j.biocon.2009.02.021

Sales, L. P., Kissling, W. D., Galetti, M., Naimi, B., & Pires, M. M. (2021). Climate change reshapes the eco-evolutionary dynamics of a Neotropical seed dispersal system. Global Ecology and Biogeography, 30(1), 117–127. https://doi.org/10.1111/geb.13271

Tabarelli, M., Aguiar, A. V., Ribeiro, M. C., Metzger, J. P., & Peres, C. A. (2010). Prospects for biodiversity conservation in the Atlantic Forest: Lessons from aging human-modified landscapes. Biological Conservation, 143(10), 2328–2340. https://doi.org/10.1016/j.biocon.2010.02.005

Thomas, C. D., Cameron, A., Green, R. E., Bakkenes, M., Beaumont, L. J., Collingham, Y. C., Erasmus, B. F., de Siqueira, M. F., Grainger, A., Hannah, L., Hughes, L., Huntley, B., van Jaarsveld, A. S., Midgley, G. F., Miles, L., Ortega-Huerta, M. A., Peterson, A. T., Phillips, O. L., & Williams, S. E. (2004). Extinction risk from climate change. Nature, 427(6970), 145–148. https://doi.org/10.1038/nature02121

Welch, J. R., Brondízio, E. S., Hetrick, S. S., & Coimbra, C. E. A. (2013). Indigenous burning as conservation practice: Neotropical savanna recovery amid agribusiness deforestation in Central Brazil. PLoS ONE, 8(12), e81226. https://doi.org/10.1371/journal.pone.0081226

Vale, M. M., Arias, P. A., Ortega, G., Cardoso, M., Oliveira, B. F. A., Loyola, R., & Scarano, F. R. (2021). Climate change and biodiversity in the Atlantic Forest: Best climatic models, predicted changes and impacts, and adaptation options. In M. C. M. Marques & C. E. V. Grelle (Eds.), The Atlantic Forest: History, biodiversity, threats and opportunities of the mega-diverse forest (pp. 253–267). Springer International Publishing.

Vancine, M. H., Muylaert, R. L., Niebuhr, B. B., Oshima, J. E. F., Tonetti, V., Bernardo, R., De Angelo, C., Rosa, M. R., Grohmann, C. H., & Ribeiro, M. C. (2024). The Atlantic Forest of South America: Spatiotemporal dynamics of the vegetation and implications for conservation. Biological Conservation, 291, 110499. https://doi.org/10.1016/j.biocon.2024.110499

2. Chapter 2 - Paleoclimatic Dynamics and Biogeographic Shifts of South American Tropical Forests from the Late Pleistocene to the Holocene

ABSTRACT

This study investigates the variation in climatic suitability of South American Tropical and Subtropical Moist Broadleaf Forests (TSMBF) over the past 21,000 years using species distribution models (SDMs) based on the MaxEnt algorithm. The analysis integrates modern occurrence data (1.085 occurrence records from 145 taxa) obtained from GBIF and pollen-based palaeoecological records from twelve sites distributed across the Amazon and Atlantic Forest biomes. Six bioclimatic variables (BIO2, BIO3, BIO8, BIO15, BIO18, and BIO19) were selected based on low multicollinearity (VIF < 5) and used as predictors in models trained under current climate conditions (1979–2013) and projected onto seven paleoclimatic intervals (LGM, HS1, BA, YDS, EH, MH, LH), totaling eight temporal slices. Model performance was validated using the AUC metric (0.745), with an ensemble weighted by model accuracy and a suitability threshold defined by the MaxSSS criterion (0.45997). For the present scenario, the variable importance analysis indicated BIO3 (isothermality) as the most influential predictor, followed by BIO19 (precipitation of the coldest quarter) and BIO8 (mean temperature of the wettest quarter). The projections reveal a non-linear trajectory of expansion and contraction of TSMBF suitability. During the Last Glacial Maximum (LGM), suitable areas were restricted to western Amazonia, reflecting cold and dry conditions with high diurnal temperature range (BIO2). A slight westward expansion is observed during Heinrich Stadial 1 (HS1). The Bølling-Allerød (BA) represents a key turning point, marked by extensive forest expansion and increased connectivity between Amazonia and the Atlantic Forest. This trend was partially reversed during the Younger Dryas (YDS), which induced renewed fragmentation. The Early and Mid-Holocene periods show substantial recovery and climatic stabilization. In contrast, the Late Holocene reveals a modest decline and increasing precipitation seasonality (BIO15), influenced by growing anthropogenic disturbances. Statistical analyses indicate significant differences across climatic periods, especially between the LGM and the present for BIO2 and BIO8, underscoring trends of warming and increased seasonal precipitation. Temporal boxplots highlight a progressive increase in wet-season temperature (BIO8), a decrease in diurnal thermal amplitude (BIO2), enhanced winter precipitation (BIO19), and rising isothermality (BIO3) throughout the Holocene. These findings are consistent with palaeoecological evidence and provide quantitative and spatially explicit insights into the response of TSMBF to climatic oscillations. Western Amazonia emerged as a persistent nucleus of climatic suitability, while historical forest connectivity was modulated by thermal and hydrological regimes. The study emphasizes the resilience of tropical forests to natural variability, but warns thatcontemporary climate change differs in magnitude, pace, and anthropogenic influence requiring conservation strategies informed by long-term bioclimatic patterns.

Keywords: Tropical Forests; Paleoclimate; Species Distribution Models (SDMs); MaxEnt; Bioclimatic Variables; Climate Change; Late Quaternary; Amazon; Atlantic Forest; Environmental Suitability

1.INTRODUCTION

South American tropical forests play a fundamental role in global climate regulation, acting as carbon sinks and influencing precipitation and temperature patterns (Hubau et al., 2020; Artaxo et al., 2022). Beyond their climatic importance, these forests harbor rich biodiversity and provide essential ecosystem services, such as maintaining the hydrological cycle and preserving soil fertility (Borma et al., 2022). However, anthropogenic pressures, such as deforestation and climate change, threaten their resilience and the continuity of these ecosystem services (Artaxo et al., 2022; Borma et al., 2022).

The Atlantic Forest and the Amazon are two highly threatened tropical biomes. The former, recognized as one of the world's main biodiversity hotspots (Rezende et al., 2018), faces challenges such as fragmentation and land conversion, which reduce its ecological connectivity (Vancine et al., 2024). The latter, although still vast, is undergoing increasing degradation due to deforestation and changes in the carbon balance, which directly affect its ecological structure and functioning (Hubau et al., 2020).

The historical dynamics of these forests have been deeply influenced by climate change over time. Palaeoecological studies indicate that variations in temperature and precipitation have shaped the distribution of tropical forests from the Last Glacial Maximum (LGM, ~21 ka) to the Holocene (Flantua et al., 2015; Brown et al., 2018). During the LGM (~21 ka) and Heinrich Stadial 1 (HS1, ~17–14.7 ka), conditions were colder across the region (Justino et al., 2008; Bush et al., 2004; Colinvaux et al., 2000; Tierney et al., 2020; Maksic et al., 2022; Pinaya et al., 2024), although moisture conditions varied geographically. For instance, some areas experienced cold and wet conditions that favored the expansion of montane forest taxa, such as during Heinrich Stadial 1 in southern and southeastern Brazil (Pinaya et al., 2024). Despite this variability, closed tropical forest appears to have persisted in some lowland areas of the Amazon during the LGM (Colinvaux et al., 2000; Bush et al., 2004; Häggi et al., 2017), suggesting resilience to widespread aridity (Colinvaux et al., 2000; Bush et al., 2004; Häggi et al., 2017).

To assess how past climate changes, especially those associated with glacial periods can inform future global warming scenarios, it is essential to understand the mechanisms that regulate the climate system, including the effects of both natural and anthropogenic forcings. Understanding climate feedback improves our interpretation

of the Earth system's responses and helps reduce uncertainties in future projections (Justino et al., 2008; Pancost, 2017; Tierney et al., 2020).

Increasingly detailed and reliable paleoclimatic records provide valuable insights into past climatic and environmental variability (Bradley, 2000; Hegerl, 2014; Tierney et al., 2020). According to Tierney et al. (2020), in-depth knowledge of past climates is essential for tuning and calibrating climate models, allowing the identification of processes that may still be underrepresented in current simulations. In this context, reconstructing past climates through models and proxy indicators such as fossil pollen and charcoal has proven to be an effective approach to understanding environmental responses to climate change (Pancost, 2017).

In addition to climate change, the current configuration of tropical biomes has also been shaped by anthropogenic factors over time. Growing evidence suggests that pre-Columbian human populations modified the composition of tropical forests by promoting the dispersal of useful species and altering vegetation structure (Kelly et al., 2017; Maezumi et al., 2018a, 2018b). In the Atlantic Forest, forest fragmentation resulting from historical land use highlights the importance of functional connectivity between remnants for maintaining biodiversity (Vancine et al., 2024).

Despite advances in the reconstruction of paleoclimatic scenarios, uncertainties remain regarding how different climatic and anthropogenic events have influenced the distribution of tropical vegetation over time. Many studies based on pollen and charcoal records (Urrego et al., 2011; Flantua et al., 2015; Rodríguez-Zorro et al., 2018) reveal trends in forest dynamics but are limited in spatial and temporal resolution.

In this context, ecological niche modeling (ENM) emerges as an appropriate tool to understand the dynamics of tropical vegetation in response to climate changes throughout the Late Quaternary, which is the focus of this study. Species Distribution Models (SDMs) (Naimi & Araújo, 2016), also known as Ecological Niche Models (ENMs) or Habitat Suitability Models, are fundamental tools for quantifying the relationship between species occurrence records and the environmental variables of their habitats (Elith et al., 2006; Guisan & Zimmermann, 2000; Peterson et al., 2011; Valavi et al., 2022). These models have been widely applied in biogeography, conservation, and in predicting the impacts of climate change on biodiversity (Elith & Leathwick, 2009; Aiello-Lammens et al., 2015; Hirata, 2024). Among the available algorithms, MaxEnt stands out for its robust predictive performance in estimating

environmental suitability, operating under the principle of maximum entropy (Phillips & Dudík, 2008; Merow et al., 2013; Valavi et al., 2022). It is important to emphasize that MaxEnt does not estimate the realized distribution, but rather environmental suitability, often associated with the species climatic or fundamental niche (Merow et al., 2013; Jiménez et al., 2020). Although the literature often broadly uses the term SDM, in the context of modeling based solely on presence-only data and environmental variables, the concept of ENM is more precise (Soberón & Peterson, 2005; Esser et al., 2024). The literature also highlights that integrative analyses combining SDMs/ENMs with palaeoecological data, environmental proxies, dispersal information, biotic interactions, and anthropogenic impacts are essential to improve our understanding of vegetation dynamics and biodiversity distribution over time (Flantua et al., 2015; Maksic et al., 20220; Esser et al., 2024; Vasconcellos et al., 2024).

Colinvaux et al. (2000) argue that closed forest covered most of the Amazon Basin during glacial times. Maksic et al. (2022) model the persistence of forest in the western and central Amazon during the LGM, due to negative temperature anomalies, while a decrease in past precipitation was responsible for changes in the eastern sector. Häggi et al. (2017) interpret their data as indicative that the forest remained covered and resistant to glacial drought, although more open or seasonal vegetation expanded in northern areas during the Heinrich Stadials. Pinaya et al. (2024) discuss the existence of ecological corridors during the LGM that connected different regions, allowing the migration of taxa adapted to cold and humid conditions.

In this context, the present study investigates the dynamics of Tropical and Subtropical Moist Broadleaf Forests (TSMBF) in South America over the past 21,000 years. Using predictive modeling in conjunction with palaeoecological records, we aim to address the following questions:

1.How have climatic oscillations since the Last Glacial Maximum influenced the potential distribution patterns of South American tropical forests?

2.Which periods showed the greatest expansion and contraction in climatic suitability for tropical forests, and what climatic factors contributed to these dynamics?

3.What are the implications of historical distribution patterns for the conservation of tropical forests in the face of contemporary climate change?

4.What patterns and contrasts emerge from the comparison between different paleoclimatic scenarios in terms of the climatic suitability of tropical forests?

This study integrates multiple data sources species occurrence records, paleoecological proxies, paleoclimatic simulations, ecological niche models (ENMs), and climate projections from global climate models (GCMs) to improve the understanding of how climatic variability and anthropogenic drivers have shaped the dynamics of South American tropical biomes over time. Furthermore, this approach allows the identification of regions with high climatic vulnerability such as northern Amazonia and the Atlantic Forest and reinforces the role of protected areas and forest restoration in promoting ecosystem resilience under future climate scenarios.

2. MATERIALS AND METHODS

2.1 Study Area

Precise definition of study areas is crucial for understanding biodiversity patterns, species distributions, and the impacts of climate and anthropogenic changes on ecosystems. Although classical biome categorization is widely used in ecological and conservation studies, this approach has limitations when dealing with internal ecosystem variability or historical environments without direct modern analogs (Flantua et al., 2015). To address these limitations, this study adopted the Ecoregions2017 database (Dinerstein et al., 2017), which classifies the planet into 846 ecoregions and provides a more detailed representation of environmental heterogeneity within biomes.

In this study, the term "Amazonia" is used in an ecologically expanded sense (Supplementary Material 1), extending beyond the Amazon River Basin. As shown in Figure 1, the region encompasses the lowland rainforests, the Guiana Shield, and the Andean foothills, which form a cohesive biogeographic entity (Malhi et al., 2008; Gatti et al., 2021). We also consider ecologically connected areas and transitional forests that share historical migration routes and floristic affinities with the core basin (Colinvaux et al., 2000; Wang et al., 2004; Pinaya et al., 2019, 2024; Kelley et al., 2024). Although geographically separated by the Andes, the Colombian Chocó is included in this expanded context due to its structural and climatic similarities with Amazonian rainforests (Flantua et al., 2015). The map illustrates the extent of the Tropical & Subtropical Moist Broadleaf Forests (TSMBF) biome in South America, highlighting in dark green the ecoregions classified as Amazonian according to the delimitation proposed by the Global Ecoregions dataset (Dinerstein et al., 2017), while other TSMBF regions, such as the Atlantic Forest, are represented in light green.

This spatial delimitation provides the geographic framework for the ecological modeling developed in this research.

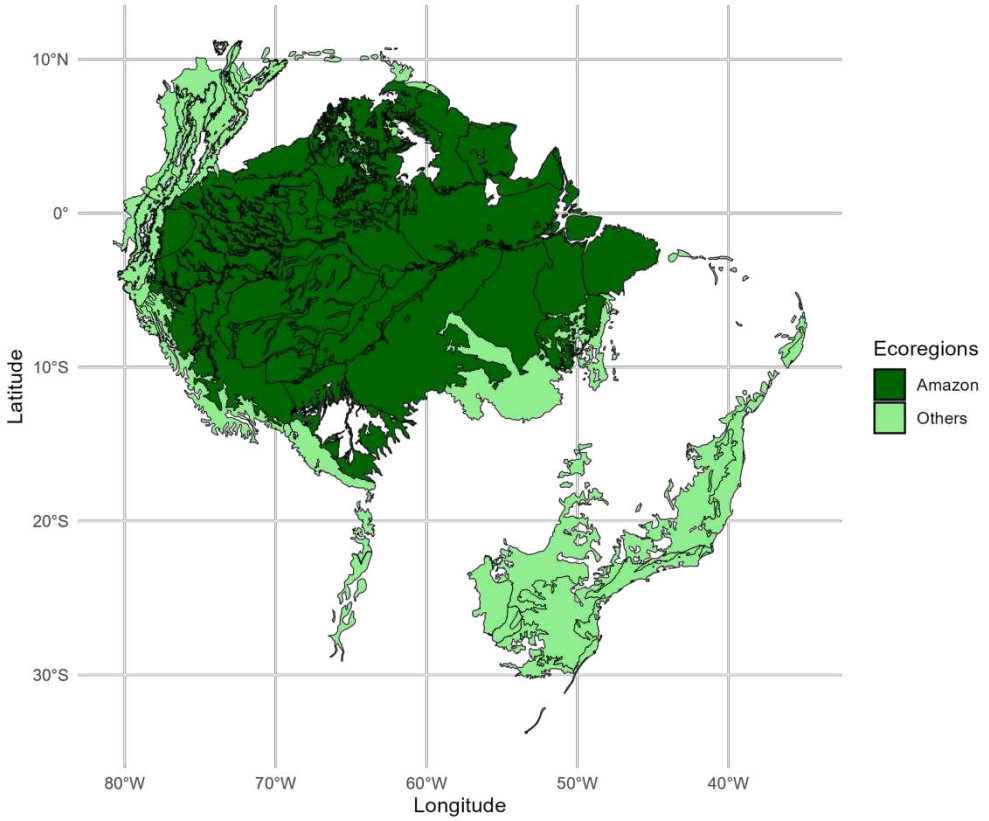

Figure 1. Geographic extent of the Tropical and Subtropical Moist Broadleaf Forests (TSMBF) biome in South America.

The Amazon, located in northern South America, is characterized by high humidity and elevated temperatures, playing a crucial role in regulating hydrological cycles (Borma et al., 2022). It harbors remarkable biodiversity, including over 15.000 tree species (ter Steege et al., 2015), and is recognized as one of the most biodiverse regions on Earth (Cheng et al., 2013), potentially hosting up to one-quarter of the planet's terrestrial species (Malhi et al., 2008).

The Amazon Rainforest is vital for moisture distribution across South America (Borma et al., 2022; Malhi et al., 2008), with approximately 32% of the basin's rainfall originating from the forest's own evapotranspiration (Staal et al., 2018; Maksic et al., 2022). This process is driven by air masses that, after crossing the Amazon Basin, are redirected by the Andes toward the southwest, contributing to the formation of the South Atlantic Convergence Zone (SACZ) (Montade et al., 2019; Borma et al., 2022; Reboita, 2022). Currently, forest degradation has become a major

concern, already surpassing direct deforestation in terms of affected area (Qin et al., 2019; Matricardi et al., 2020; Flores et al., 2024) and contribution to aboveground biomass loss (Qin et al., 2019). This results in significant carbon emissions, particularly through fires, which are exacerbated by intensified dry seasons and increased deforestation (Maezumi et al., 2018a; Gatti et al., 2021; Artaxo et al., 2022).

The Atlantic Forest, in turn, is a biome comprising ecosystems that range from seasonally dry to permanently wet forests, including ombrophilous and semideciduous formations (Borma et al., 2022; Esser et al., 2024). It extends from northeastern to southern Brazil along the Atlantic coast (Joly, Metzger, & Tabarelli, 2014; Vancine, 2024). This biome presents significant climatic variability, with humid summers and dry winters, particularly in southeastern Brazil (Ledru et al., 2009; Montade et al., 2019). Although it is currently highly fragmented forming an archipelago of small forest remnants that compromises ecological connectivity and the provision of ecosystem services (Joly, Metzger, & Tabarelli, 2014; Arroyo-Rodríguez et al., 2017; Rezende et al., 2018; Borma et al., 2022; Vancine, 2024). the Atlantic Forest remains crucial for biodiversity conservation (Rezende et al., 2018; Borma et al., 2022; Esser et al., 2024; Vancine, 2024). and regional climate stability. It plays a key role in climate regulation and rainfall generation (Joly, Metzger, & Tabarelli, 2014; Borma et al., 2022), especially in areas that have demonstrated climatic stability over time and have functioned as climatic refugia (Ledru et al., 2009; Sobral-Souza et al., 2018; Esser et al., 2024).

2.2 Database used

2.2.1 Taxa selection

The analysis was carried out using ten previous pollen based palaeoecological studies spread all over the study area found on Neotoma Paleoecology Database (Williams et al., 2018) (Figure 2 and Table 1). These sites were selected once they cover most of periods here studied.

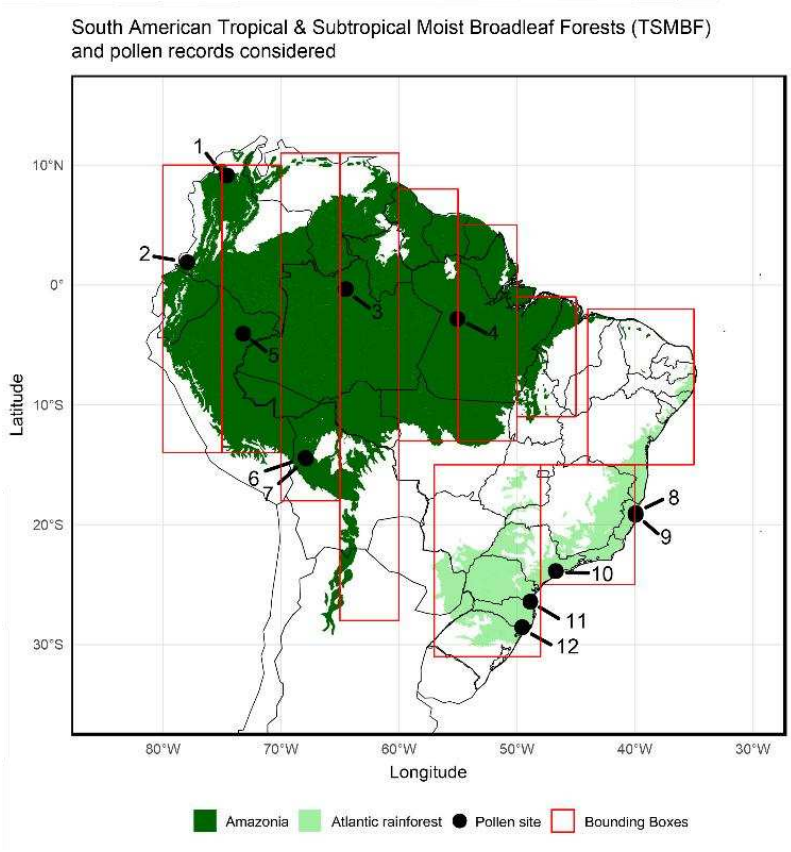

Figure 2. Representation of the Tropical & Subtropical Moist Broadleaf Forests (TSMBF) and related biomes Amazonia and the Atlantic Rainforest ecoregions in South America. Black dots indicate pollen samples used to build the datasets. Red bounding boxes represent the selected areas for local occurrence data.

Table1: List of sites analyzed and further information ordered from north to south.

Number	Site	Neotoma Id	Lon	Lat	Period covered (cal BP)	Authors
1	Boquillas	14011	-74.5	9.1	11420 to 1690	Berrío et al. (2001, 2002)
2	Laguna Piusbi	13993	-77.9	1.9	4930 to 130 5630 to 60	Behling et al. (1998), Urrego e Berrio (2011)
3	Lake Acarabixi	27010	-64.5	-0.3	10790 to 652	Rodríguez-Zorro et al. (2018)
4	Lake Caranã	26166	-55.0	-2.8	8615 to -70	Maezumi et al. (2018a, 2018b)
5	San Jorge	18835	-73.2	-4.0	2298 to -64	Kelly et al. (2017)
6	Lake Santa	13976	-67.9	-14.5	16110 to 0	Urrego et al. (2013)

	Rosa					
7	Lake Chalalán	13964	-67.9	-14.3	16520 to -60	Urrego et al. (2013)
8	Lagoa do Macuco	28343	-39.9	-19.0	7750 to 20	Buso Jr et al. (2013a, 2013b)
9	Nativo do Flamengo	27008	-39.9	-19.1	6130 to -60	Buso Jr et al. (2019)
10	Colônia CO3	27369	-46.7	-23.7	108500 to 150	Ledru (2009), Rodríguez-Zorro et al. (2020)
11	Poço Grande	1828	-48.9	-26.4	4840 to -40	Behling (1993, 1995)
12	Serra do Rio Rastro	2509	-49.5	-28.5	11180 to 800	Behling (1993, 1995)

2.2.2 Occurrence data

Taxa occurrences were filtered for those that coordinates overlaid onto ecoregion boundaries of TSMBF. Thus, only occurrences within the delimited areas were retained, ensuring analyses were restricted to regions of interest. Later, the occurrences were treated following some approaches for balancing the spatial distribution of taxa, avoiding higher concentration over short areas.

Occurrence records for the 145 taxa were compiled from the Global Biodiversity Information Facility (GBIF, 2023) and processed through a multi-step filtering protocol to ensure data quality and minimize spatial sampling bias.

First, occurrences were filtered to retain only records whose geographic coordinates fell within the ecoregion boundaries of the Tropical & Subtropical Moist Broadleaf Forests (TSMBF), according to the World Ecoregions dataset (Dinerstein et al., 2017). This ensured that the analyses were restricted to the target biomes, specifically the Amazon and Atlantic Forest regions.

Second, a bounding box filter was applied. Ten bounding boxes were delineated to geographically constrain the search for occurrence records, ensuring that only records within ecologically relevant areas were retained. This step avoided the inclusion of disjunct or ecologically irrelevant records.

Third, to reduce the disproportionate influence of taxa with a high number of records, a maximum limit of 1.000 occurrences per taxon in each bounding box was imposed. This subsampling strategy aims to minimize sampling bias and the risk of

overfitting critical issues in ecological niche modeling discussed by Phillips et al. (2006), Kramer-Schadt et al. (2013), and Boria et al. (2014).

Fourth, a data cleaning process was performed to remove duplicated records, georeferencing errors (e.g., coordinates with zero values, country centroids, and marine locations), and records falling outside the study area. After this step, the dataset was reduced to 234.965 occurrences.

Finally, to address spatial autocorrelation and further mitigate spatial sampling bias, a spatial thinning procedure was applied using the spThin package in R (Aiello-Lammens et al., 2015). A minimum distance of 100 km between occurrence points was set, ensuring that no two points for the same taxon were closer than this threshold. The thinning process is inherently stochastic, as it randomly selects among possible spatial configurations that satisfy the distance constraint. Therefore, the thinning was replicated five times (reps = 5), generating five alternative spatially filtered datasets for each taxon.

Consistently, the first replicate was selected for all taxa. This approach follows the finding that different spatial configurations retaining the same maximum number of occurrences yield similar model results (Aiello-Lammens et al., 2015). This choice ensures both methodological consistency and reproducibility. The thin() function employs a randomization algorithm that retains the maximum possible number of points while respecting the specified minimum distance between nearest neighbors, effectively reducing spatial autocorrelation (Veloz, 2009) and preventing the artificial inflation of environmental suitability in densely sampled areas.

The final dataset comprised 1.085 spatially filtered occurrences, representing 145 families, 487 genera, and 863 species, providing a taxonomically and geographically representative sample of tropical and subtropical moist broadleaf forests in South America (Supplementary Material 2).

2.2.3 Climate data

This study utilized 19 bioclimatic variables (BIO1–BIO19), which are extensively employed in ecological and biogeographical research due to their importance for species distribution modeling (Brown et al., 2018; Fordham et al., 2017; Karger et al., 2017). These variables are computed from monthly climate data specifically temperature (mean, minimum, and maximum, when available) and precipitation capturing essential climate characteristics such as long-term annual

trends (e.g., mean annual temperature and precipitation), seasonal variability (e.g., annual temperature and precipitation range), and extreme climatic events (e.g., temperature or precipitation during the driest/wettest or coldest/warmest month or quarter) (Brown et al., 2018; Karger et al., 2017). The term “quarter” refers to any consecutive three-month period (Brown et al., 2018; Karger et al., 2017). Detailed definitions, descriptions, and units for all variables are presented in Table 2.

Table 2 – List of bioclimatic variables

Variable	Description	Unit
BIO1	Annual Mean Temperature	°C
BIO2	Mean Diurnal Range (Mean of monthly [max temp - min temp])	°C
BIO3	Isothermality (BIO2/BIO7 × 100)	%
BIO4	Temperature Seasonality (standard deviation × 100)	°C × 100
BIO5	Max Temperature of Warmest Month	°C
BIO6	Min Temperature of Coldest Month	°C
BIO7	Temperature Annual Range (BIO5 - BIO6)	°C
BIO8	Mean Temperature of Wettest Quarter	°C
BIO9	Mean Temperature of Driest Quarter	°C
BIO10	Mean Temperature of Warmest Quarter	°C
BIO11	Mean Temperature of Coldest Quarter	°C
BIO12	Annual Precipitation	mm
BIO13	Precipitation of Wettest Month	mm
BIO14	Precipitation of Driest Month	mm
BIO15	Precipitation Seasonality (Coefficient of Variation)	%
BIO16	Precipitation of Wettest Quarter	mm
BIO17	Precipitation of Driest Quarter	mm
BIO18	Precipitation of Warmest Quarter	mm
BIO19	Precipitation of Coldest Quarter	mm

The derivation of these variables followed established protocols from WorldClim (Hijmans et al., 2005) and ANUCLIM (Xu & Hutchinson, 2013), implemented via the biovars function in the R package dismo (Brown et al., 2018). Similarly, CHELSA climatologies were generated under equivalent methodological frameworks (Karger et al., 2017). All climatic layers were standardized to a spatial resolution of 10 arc-minutes (~18 km), which ensures consistency between present-day and paleoclimatic datasets. This resolution provides a balance between computational efficiency and the ability to capture relevant climatic gradients, making

it widely adopted in biogeographical modeling (Fordham et al., 2017; Brown et al., 2018).

Bioclimatic variables for past climates were obtained from the PaleoClim database (Brown et al., 2018). For current climate conditions (1979–2013), we used high-resolution climatologies from CHELSA (Karger et al., 2017). Paleoclimatic reconstructions for the Late Pleistocene and Holocene, including the Younger Dryas (12.9–11.7 ka), Bølling Allerød (14.7–12.9 ka), and Heinrich Stadial 1 (17.0–14.7 ka), were derived from the PaleoView framework (Fordham et al., 2017), based on the TRaCE-21ka transient simulation using the CCSM3 (Community Climate System Model, version 3). CCSM3 has been extensively validated for its ability to reproduce major atmospheric and oceanic circulation patterns during the last deglaciation, as well as present-day climate dynamics (Fordham et al., 2017).

Variable selection is a key step in conducting ecological niche suitability modeling. It reduces model complexity and operational cost, and helps to avoid collinearity among predictors, which can compromise the accuracy and interpretability of regression coefficient estimates (Dormann et al., 2012; Merow et al., 2013). To address this issue, the Variance Inflation Factor (VIF) was applied. The use of VIF is recommended to ensure that statistical models produce robust, reliable, and interpretable estimates (Dormann et al., 2012). Early detection of multicollinearity allows for appropriate adjustments in the set of variables, improving the quality of inferences drawn from the developed model (Boria et al., 2014). The calculation of VIF is straightforward: for each independent variable, a linear regression model is fitted using it as the dependent variable and all other variables as predictors. From the resulting coefficient of determination (R^2), the VIF is then calculated as:
($VIF = 1/ (1 - R^2)$) (Dormann et al., 2012).

2.4 Ecological Niche Models (ENMs)

The ecological niche models (ENMs) for all 7 palaeo time slices were carried out based on responses achieved from Maximum Entropy algorithm (MaxEnt) (Phillips et al., 2006; Elith et al., 2011) applied to present (1979-2013) once we assumed ecological niche preferences remained stable through time (Peterson et al., 1999; Wiens & Graham, 2005), principle widely used in palaeoecological studies (Esser et al., 2024).

Presence data from GBIF and bioclimatic variables were imported for modeling using MaxEnt. The process begins with the input of presence-only records (i.e., locations where the species has been observed) and environmental predictors, such as bioclimatic variables (Phillips et al., 2006, 2017; Phillips & Dudík, 2008; Guillera-Arroita et al., 2015). The objective is to train the model and estimate a probability distribution or environmental suitability based on these presence data, while minimizing the need for explicit assumptions about absences (Phillips et al., 2006; Phillips & Dudík, 2008; Guillera-Arroita et al., 2015). Fundamentally, MaxEnt estimates the distribution of environmental suitability (or potential distribution, although the authors note that the output often reflects realized distribution, relative suitability, or probability of observation, depending on the data and context) (Phillips et al., 2006, 2017; Phillips & Dudík, 2008; Guillera-Arroita et al., 2015).

This is achieved by contrasting the environmental conditions at known presence locations with the range of environmental conditions across the study area, represented by background data (Phillips & Dudík, 2008; Guillera-Arroita et al., 2015). The theoretical foundation of the maximum entropy method is detailed in Dudík et al. (2004) and applied to ecology by Phillips et al. (2006) and Phillips & Dudík (2008). Thus, the potential distribution of each taxon is identified by the probability distribution of maximum entropy (least biased distribution) subject to environmental constraints derived from the known occurrence data (Phillips et al., 2006). To do this, the algorithm starts by assigning a weight to each feature derived from environmental variables, based on how strongly that feature is associated with the species' presence. These weights reflect the relative influence of each feature in shaping the species' ecological niche. For every grid cell in the study area, MaxEnt multiplies the value of each feature by its corresponding weight and adds the results together. This total is then exponentiated, generating a raw suitability score for that location (Phillips et al., 2006; Phillips & Dudík, 2008).

Aiming to reduce sampling bias, 10.000 pseudo-absence points were randomly generated within the study area (Phillips & Dudík, 2008) avoiding overlap with occurrence points - points too close to recorded observations were removed - ensuring a more balanced and representative spatial distribution.

The total number of records (presences + background), consisting of 11.085 points, was divided into five equal parts. In each iteration, the model was trained with 80% of the data (8.868 points) and tested with the remaining 20% (2.217 points). To

ensure prediction reliability, cross-validation (k = 5, with 5 replicates) was used to reduce the risk of overfitting by testing the model on different data subsets (Phillips & Dudík, 2008). This procedure was repeated five times per replicate, ensuring that all data were used as test data at least once. As five replicates were performed (n = 5), the 5-fold cross-validation was run five times with different random partitions, increasing the robustness of model evaluation. Model performance was assessed using the Area Under the Curve (AUC) metric, which is widely used to estimate the predictive capacity of ecological models (Fielding & Bell, 1997; Phillips et al., 2006).

To make these scores easier to interpret, the algorithm scales them so that the final values fall between 0 and 1 where zero indicates completely unsuitable conditions, and one represents the highest predicted suitability within the modeled area. To convert these predictions into binary presence/absence maps, threshold selection criteria were applied a critical step for interpreting results. Among available methods, we chose the Maximization of Sensitivity and Specificity (Max SSS) as proposed by Liu et al. (2013), which is widely used to transform continuous suitability outputs into binary maps. This method balances omission and commission errors by selecting the threshold that maximizes the sum of sensitivity and specificity. It has been commonly adopted in recent ecological modeling studies (e.g., Brzozowski, Pełechaty, & Bogawski, 2022). This criterion balances correct presence detection and absence exclusion, minimizing omission and commission errors. It also showed greater visual congruence with the Ecoregions2017 base, enhancing reliability in delineating suitable areas. Alternative methods, such as the Least Presence Threshold (LPT) (Pearson et al., 2007), were tested but proved more sensitive to outliers, reinforcing the choice of Max SSS. This standardization ensures consistency in identifying suitable areas for tropical vegetation across paleoclimatic periods.

Model performance was evaluated using the Area Under the ROC Curve (AUC), a threshold-independent metric that estimates the model's ability to discriminate between presence areas and background or absence areas (Fielding & Bell, 1997; Allouche et al., 2006). To increase result reliability, k-fold cross-validation was adopted, partitioning the data into training and testing subsets, thereby reducing the bias associated with a single data split (Fielding & Bell, 1997; Phillips & Dudík, 2008). Additionally, the importance of environmental variables was analyzed to understand each predictor's contribution to model structure (Brzozowski et al., 2022). For projection accuracy, models may be combined into an ensemble, a strategy

used to address uncertainty in individual predictions and stabilize results (Elith et al., 2010; Brzozowski et al., 2022). Finally, continuous environmental suitability values were converted into binary maps using the threshold that maximizes the sum of sensitivity and specificity (Max SSS), an objective criterion recommended for presence-only data (Liu et al., 2013; Brzozowski et al., 2022)

Although the Area Under the Curve (AUC) is widely used to evaluate species distribution models, it presents important limitations, especially in presence-only contexts (Valavi et al., 2022; Jiménez et al., 2020; Phillips & Dudík, 2008). In the absence of reliable true absence data, the theoretical and probabilistic interpretation of the AUC becomes problematic (Jiménez et al., 2020). Furthermore, the selection and number of background points directly influence both the predictive accuracy and the distribution of estimated suitability values (Phillips & Dudík, 2008; Barbet-Massin et al., 2012; Merow et al., 2013; Jiménez et al., 2020).

Therefore, combining multiple methodological approaches can improve the robustness of model evaluations. The joint use of AUC (to assess predictive performance) (Jiménez et al., 2020; Valavi et al., 2022), cross-validation (to ensure generality and consistency) (Baldwin, 2009; Merow et al., 2013; Valavi et al., 2022), and ensemble modeling (to reduce uncertainties associated with a single model) (Valavi et al., 2022) represents a valuable strategy. However, these tools do not inherently guarantee that results are ecologically interpretable in all scenarios. Proper interpretation still requires ecological justification and context-specific evaluation (Merow et al., 2013; Jiménez et al., 2020; Valavi et al., 2022).

The MaxEnt algorithm, in particular, is well-suited for palaeoecological applications (Pinaya et al., 2019; 2024) due to its ability to handle sparse or incomplete data a common feature of palaeoecological records (Phillips & Dudík, 2008; Baldwin, 2009; Merow et al., 2013). Additionally, MaxEnt can capture complex relationships between environmental variables and species occurrences by applying several types of feature transformations (Phillips & Dudík, 2008; Merow et al., 2013). The core of the method relies on comparing presence points with background points, which represent environmental availability within the study area (Merow et al., 2013).

3. RESULTS

3.1 Model Performance and Validation – Present Scenario

To ensure reliable model performance under present climatic conditions, we first evaluated the collinearity structure among the bioclimatic predictors. The Variance Inflation Factor (VIF) analysis reduced the original set of 19 variables to six predictors with VIF values below the adopted threshold (VIF < 5), indicating low multicollinearity and statistical independence. The retained variables were: BIO2 – Mean Diurnal Range (VIF = 2.05); BIO3 – Isothermality (VIF = 1.51); BIO8 – Mean Temperature of the Wettest Quarter (VIF = 1.43); BIO15 – Precipitation Seasonality (VIF = 1.48); BIO18 – Precipitation of the Warmest Quarter (VIF = 1.36), and BIO19 – Precipitation of the Coldest Quarter (VIF = 1.35).

Figure 3 shows the spatial patterns of these variables across the domain of Tropical and Subtropical Moist Broadleaf Forests (TSMBF). The temperature-related variables (Figs. 3a–c) reveal strong latitudinal and altitudinal variation. BIO2 (Figure 3a) displays lower diurnal temperature range in humid tropical areas (such as the Amazon Basin) and higher values in mountainous regions like the Andes, as well as in areas with combined high altitude and latitude such as along the Serra do Mar in southern and southeastern Brazil. BIO3 (Figure 3b), which represents isothermality, shows the highest values mainly in the northern portion encompassing the Amazon region and neighboring biomes, as well as in coastal fragments in the northern Atlantic Forest, indicating greater relative thermal stability throughout the year compared to the southeastern parts of the TSMBF. BIO8 (Figure 3c) reveals a pattern across the entire TSMBF domain, with higher temperatures during the wettest quarter in most of its range and lower temperatures along the Andes and the southern Brazilian plateau, suggesting that these regions experience elevated temperatures even during the wettest part of the year.

The precipitation-related variables (Figures 3d–f) indicate strong contrasts between humid and seasonal regions. In the present study, BIO15 values were higher in the peripheral zones of the biomes that comprise the TSMBF, reflecting strong precipitation seasonality in these areas (Figure3d). In contrast, Amazonian, coastal, and southern plateau regions exhibited lower values, indicating consistent rainfall throughout the year.

The lowest values of BIO18 were recorded in areas near the central region of the continent, characterized by strong seasonality and a semi-arid climate where

summer coincides with the dry season (Figure 3e). However, moving from eastern Amazonia toward southern Brazil and the eastern Atlantic Forest, the precipitation of the warmest quarter increases, indicating that these regions receive most of their rainfall during summer.

Complementarily, BIO19 highlights that the coldest quarter experiences higher precipitation in the central and southern parts of northern South America, particularly in northwestern Brazil, southern Venezuela, Colombia, and parts of Peru. In contrast, within the Atlantic Forest domain, southern and southeastern Brazil show significantly lower values, below 400 mm, revealing drier winter conditions.

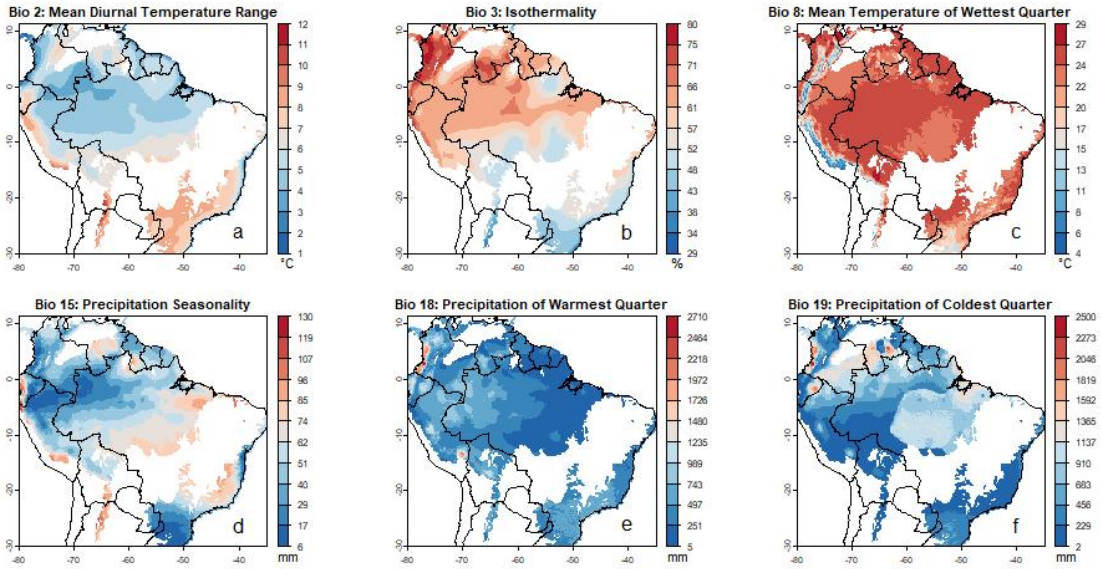

Figure 3. Spatial variation of the main bioclimatic variables used in the modeling of the distribution of Tropical and Subtropical Moist Broadleaf Forests (TSMBF) in South America under the current climate scenario (1979–2013).

3.1.2 Importance of Environmental Variables in the Present Model

The relative importance of the six bioclimatic variables used in the model for the period 1979–2013 was assessed through permutation, considering two complementary metrics: Pearson correlation and AUC, as shown in Figure 4. The values correspond to the mean of the 25 replications of the weighted ensemble

model.

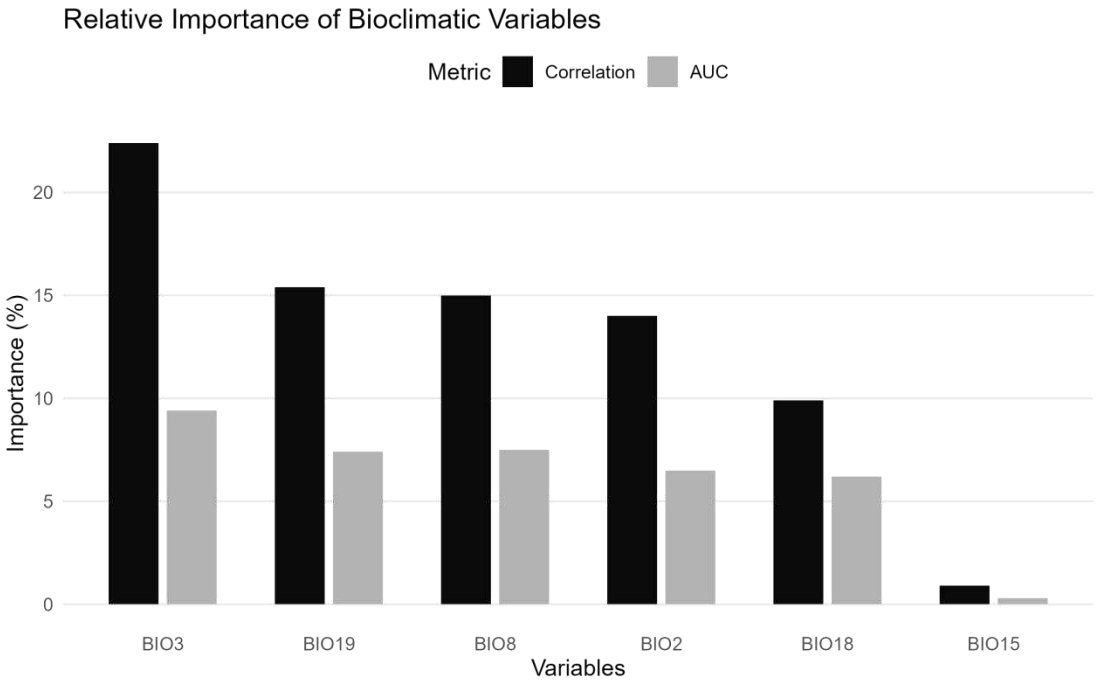

Figure 4. Relative importance of the bioclimatic variables used in the current distribution model (1979–2013), based on two evaluation metrics: Pearson correlation and AUC. BIO3 (Isothermality) showed the highest contribution in both metrics, followed by BIO19 (Precipitation of Coldest Quarter), BIO8 (Mean Temperature of Wettest Quarter), and BIO2 (Mean Diurnal Temperature Range). BIO15 (Precipitation Seasonality) was the least influential variable.

Based on the Pearson correlation metric, the variables with the highest contribution to model performance were BIO3 (Isothermality, 22.4%), BIO19 (Precipitation of the Coldest Quarter, 15.4%), BIO8 (Mean Temperature of the Wettest Quarter, 15.0%), and BIO2 (Mean Diurnal Temperature Range, 14.0%). The lowest contributions were observed for BIO18 (Precipitation of the Warmest Quarter, 9.9%) and, especially, for BIO15 (Precipitation Seasonality, 0.9%).

According to the AUC metric, the most important variable was again BIO3 (9.4%), followed by BIO8 (7.5%), BIO19 (7.4%), BIO2 (6.5%), and BIO18 (6.2%), while BIO15 once again showed the lowest relative importance (0.3%).

Importantly, these importance values (percent contribution and permutation importance) are expressed in relative terms, meaning that the algorithm distributes a total of 100% importance across all environmental predictors used in the model. In this framework, higher percentages indicate variables that contributed more to

improving model gain, whereas lower values reflect minimal or negligible influence on model performance.

These results help to interpret the patterns observed in the climatic suitability maps (Figure 3). The strong influence of thermal variables (BIO2, BIO3, BIO8) and precipitation during critical quarters (BIO19 and BIO18) is reflected in the high suitability recorded in the Amazon Basin, along the Andean foothills, and in humid regions of the Atlantic Forest, where thermal stability and hydrological regularity prevail. On the other hand, the low importance of precipitation seasonality (BIO15) is consistent with the reduced suitability in semi-arid and highly seasonal areas, such as northeastern Brazil and portions of the Cerrado.

3.1.3 Climatic Suitability of TSMBF under Present Conditions

Figure 5-A shows the spatial pattern of continuous climatic suitability for TSMBF across South America. Suitability values range from 0 (unsuitable) to 1 (highly suitable), as indicated by the color scale.

The highest climatic suitability is concentrated in the northern portion of the continent, especially in the Amazon Basin, along the Andean foothills, and in humid coastal areas of northeastern and southeastern Brazil. Parts of the Araucaria Plateau in southern Brazil also stand out, suggesting that these regions offer favorable climatic conditions for the establishment and persistence of tropical moist vegetation.

In contrast, high-altitude regions (central Andes), semi-arid zones (such as northeastern Brazil), areas of the Cerrado, and higher southern latitudes show low climatic suitability, reflecting thermal and water-related constraints that limit the occurrence of TSMBF in these environments.

The performance of the climatic suitability model under present conditions was evaluated using the AUC (Area Under the ROC Curve) metric, based on validation with 1.085 actual occurrence records and 10,000 background points. The mean AUC value was 0.745, indicating good discriminative ability of the model in distinguishing between areas of high and low climatic suitability. This performance supports the use of the model for spatial projection of the potential distribution of Tropical and Subtropical Moist Broadleaf Forests (TSMBF) under current climate conditions.

Based on the maximization of the sum of sensitivity and specificity (max (se + sp) criterion), a climatic suitability threshold of 0.45997 was determined. This value

was used to binarize the continuous suitability raster, classifying all cells with values equal to or greater than the threshold as potential presence (1), and those with lower values as potential absence (0). The result of this process is shown in Figure 5-B, which displays the spatial distribution of areas with higher climatic suitability for the occurrence of TSMBF under current climate conditions.

A concentration of areas classified as potential presence is observed in the Amazon region, extending northward and northwestward into the Andean páramo ecosystems and the Chocó zone, as well as in fragments of the Atlantic Forest and portions of southern Brazil. This distribution aligns with the patterns of high suitability shown in the continuous suitability map (Figure 5-A).

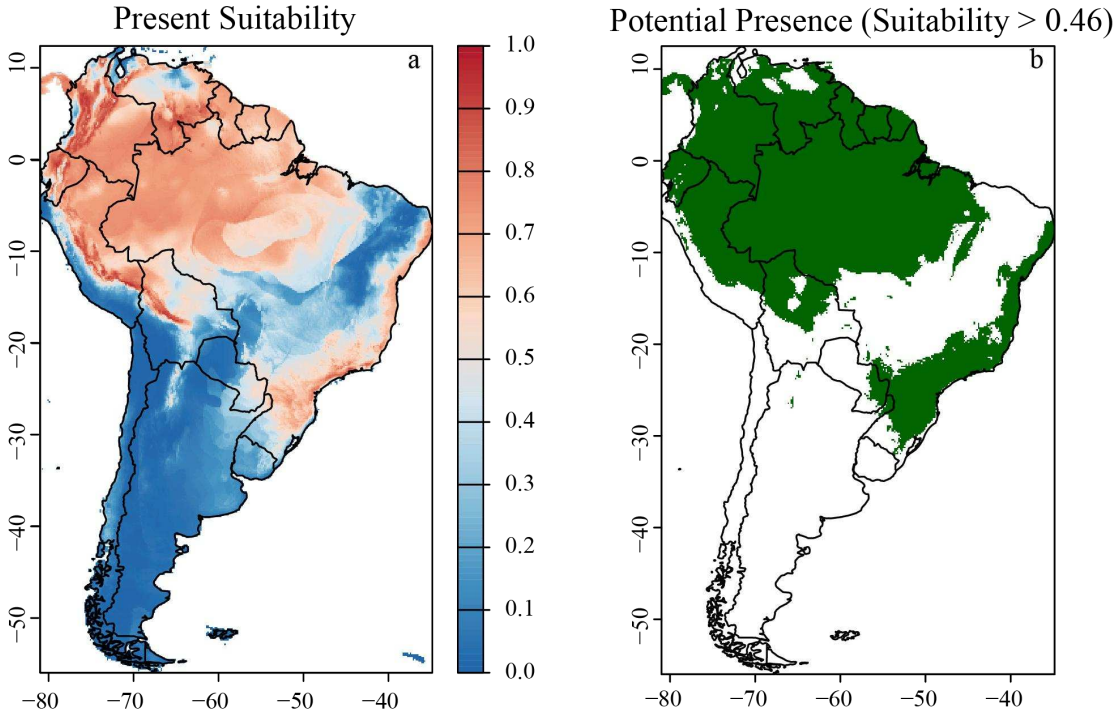

Figure 5. Modeling of the potential distribution of TSMBF under the present climate scenario (1979–2013). (A) Continuous map of climatic suitability generated by the ensemble model. (B) Binary map of potential presence.

3.2 Temporal Variation in Climatic Suitability of TSMBF Over the Last 21,000 Years

Figures 6 (A - N) provide complementary insights into the paleoenvironmental conditions and the climatic suitability for Tropical and Subtropical Moist Broadleaf Forests (TSMBF) over the last 21.000 years. The models were calibrated using

present-day occurrence data and projected onto seven key paleoclimatic intervals to assess how climatic fluctuations influenced the spatial dynamics of suitable habitats.

Figure 6 shows the continuous climatic suitability maps (top panel: A - G) and the corresponding binary presence-absence maps (bottom panel: H - N) for TSMBF across the paleoclimatic time slices: Last Glacial Maximum (LGM), Heinrich Stadial 1 (HS1), Bølling-Allerød (BA), Younger Dryas (YDS), Early Holocene (EH), Mid-Holocene (MH), and Late Holocene (LH). Higher values in the continuous maps indicate greater climatic suitability, while the binary maps display areas classified as suitable (green) or unsuitable (white) based on an ecologically optimized threshold.

Together, these figures offer a comprehensive understanding of how climatic drivers have shaped the historical distribution of TSMBF in South America, highlighting the interactions between climatic variability and tropical forest dynamics throughout the Late Quaternary.

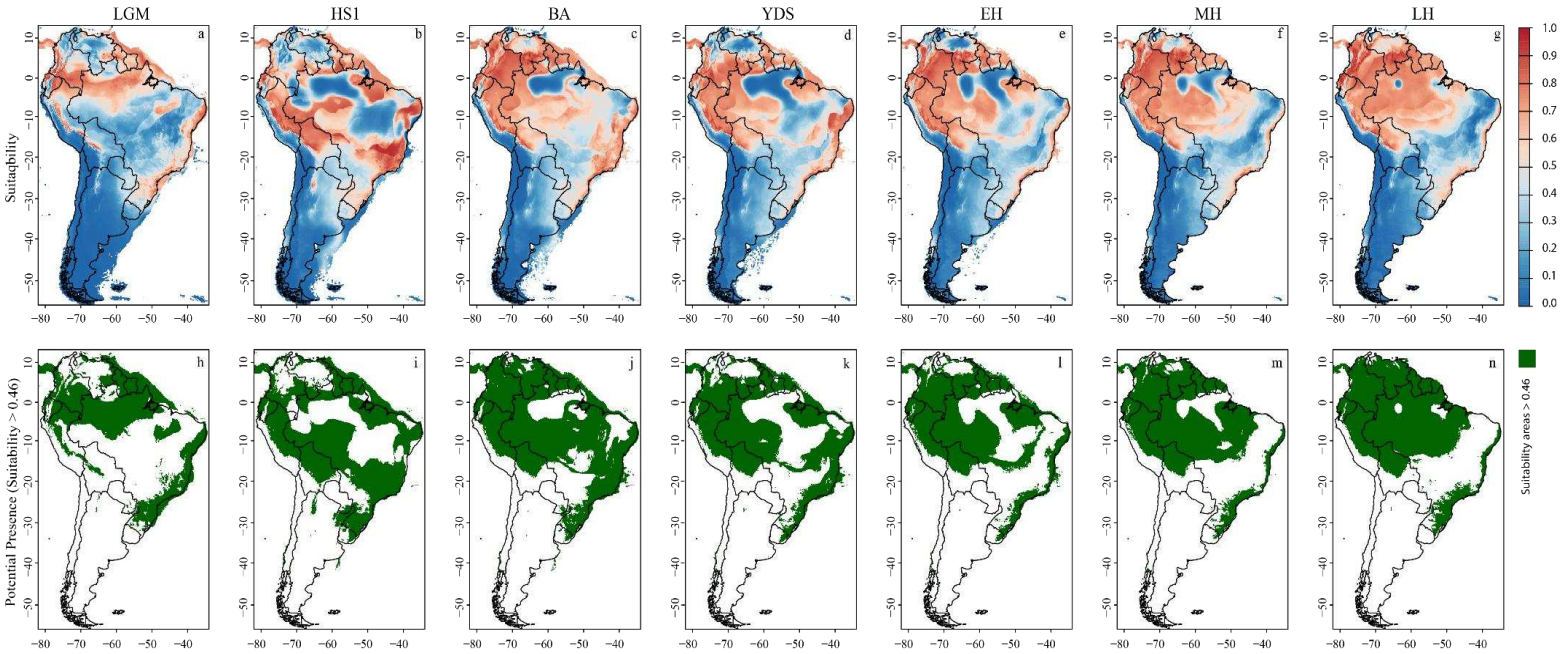

Figure 6. Climatic suitability and binary potential presence maps of TSMBF in South America over the past 21.000 years. The suitability maps (a–g) indicate the probability of TSMBF occurrence based on continuous climatic suitability, ranging from 0 (unsuitable) to 1 (high suitability), according to species distribution models (SDMs) calibrated using MaxEnt. The binary maps (h–n) represent areas above the potential presence threshold (threshold = 0.46), indicating regions with climatic conditions favorable for the occurrence of TSMBF in each period.

During the Last Glacial Maximum (LGM, ca. 21 ka), the projections indicate that areas with the highest climatic suitability for the occurrence of TSMBF were mainly concentrated in central Amazonia, including northwestern Brazil, southern Colombia, western and eastern Ecuador, northern Peru extending southward into Bolivia, as well as a broad coastal strip along northeastern to southern Brazil (Figure 6A). In contrast, large portions of eastern Amazonia, southeastern Brazil, and the southern plateau exhibited low suitability levels, suggesting unfavorable environmental conditions for the maintenance of these forest formations.

The binary map (Figure 6H), generated from the model's threshold, reveals a fragmented distribution of suitable areas, with restricted core zones primarily in central Amazonia and along the Andean foothills, indicating potential ecological persistence zones during the glacial period. In the Atlantic Forest, suitable areas were limited to humid enclaves and elevated regions, along the Serra do Mar and southern Brazil, highlighting a marked retraction and fragmentation of subtropical moist vegetation under colder and drier climate conditions.

During Heinrich Stadial 1 (HS1, ca. 17.0–14.7 ka), a subtle reconfiguration of high-suitability zones is observed, with favorable core areas maintained along the Andean foothills and reduced extent in central Amazonia (Figure 6B). However, there was an increase in connectivity between Andean areas and western Amazonia, suggesting a partial recovery of climatic conditions compared to the LGM. Suitability also increased along the northeastern Brazilian Atlantic coast and in the southeastern region, which retained suitable zones, though now more fragmented in distribution, while central Amazonia and southern Brazil continued to show reduced values.

The binary panel (Figure 6I) confirms an expansion of potential presence areas compared to the previous period, with highlights in western Amazonia and isolated portions of eastern Brazil. The Atlantic Forest shows an increase in suitable zones, with the emergence of new cores in inland areas and humid transitional zones. These patterns indicate a climatic transition context, with partial mitigation of the extreme environmental constraints of the LGM.

During the Bølling-Allerød (BA, ca. 14.7–12.9 ka), the process of climatic recovery initiated during HS1 intensified, particularly in southern, northwestern, and northern Amazonia (Figure 6C). Highly suitable areas became more extensive and continuous, reflecting a significant expansion of conditions favorable to TSMBF. Central and southern Amazonia began to exhibit greater climatic homogeneity, while

the western portion remained a stable core. On the other hand, northern Amazonia showed a decrease in suitability levels, indicating persistent regional limitations.

The Atlantic coast of northeastern Brazil and the eastern interior displayed broad zones of high suitability, suggesting a warmer and wetter regime. The binary map (Figure 6J) reinforces this scenario, showing a marked increase in the potential presence of TSMBF, particularly with enhanced connectivity between Amazonia, eastern Brazil, and the Atlantic Forest. The formation of intermittent ecological corridors and the continued expansion of humid areas from the northeast to the south of the country suggest that the BA was a key moment for forest re-expansion.

The brief but significant climatic reversal represented by the Younger Dryas Stadial (YDS, ca. 12.9–11.7 ka) interrupted this expansion trend. As illustrated in Figure 6D, zones of high suitability became more restricted and localized, especially in central and western Amazonia, with persistence in parts of northwestern Brazil, Peru, Ecuador, Bolivia, and Colombia. In contrast, southeastern and south-central Brazil once again presented unfavorable conditions.

The binary map (Figure 6K) shows strong fragmentation of potential presence areas, with a loss of connectivity both within the Amazon and between Amazonia and the Atlantic Forest. Distribution in eastern Brazil became sparse and discontinuous, limited to humid enclaves and elevated areas. These results suggest that the YDS temporarily reshaped the boundaries of climatic suitability, highlighting the crucial role of ecologically stable zones in maintaining tropical biodiversity during abrupt cooling events.

In the Early Holocene (EH, ca. 11.7–8.326 ka), there is a more pronounced recovery of favorable conditions for TSMBF, consolidating the transition to the current interglacial period (Figure 6E). Highly suitable areas expand again, especially in central and western Amazonia, although a slight contraction is observed along parts of the Atlantic coast. Compared to the YDS, there is a substantial increase in connectivity between regions of high suitability, indicating the reestablishment of a warm and humid climatic regime.

Figure 6L confirms this trend, with an expanded potential presence in central Amazonia and increased integration among previously isolated core areas. Connections with peripheral zones, including the Atlantic Forest, become more evident, although with a relative reduction in area within that region. Still, suitable corridors extending from northeastern to southern Brazil are maintained.

The Mid-Holocene (MH, ca. 8.326–4.2 ka), shown in Figure 6F, displays broad and homogeneous suitability across Amazonia, especially in its central, southern, and western portions. The Atlantic coast continues to exhibit continuous suitability belts, particularly from the northeast to the south of Brazil. This climatic homogeneity reflects a period of elevated temperatures and high-water availability.

The binary panel (Figure 6M) reinforces this stability, with potential presence broadly distributed and strong connectivity between major Amazonian and Atlantic Forest cores. The Atlantic Forest areas appear integrated into cohesive bands, both along the coast and in some inland regions of southeastern and southern Brazil.

In the Late Holocene (LH, ca. 4.2–0.3 ka), climatic conditions remain favorable, although slight changes are observed in the southern Amazon. Figure 6G indicates continued high suitability in central and western Amazonia, with localized increases associated with shifts in seasonal precipitation and temperature patterns. The Atlantic coast shows an expansion of suitability into interior regions, with punctual increases in southeastern and southern Brazil. Climatic conditions remained favorable, although slight changes are observed in the southern Amazon region. Figure 6G indicates the persistence of high suitability levels in central and western Amazonia, with possible localized increases associated with shifts in seasonal precipitation and temperature patterns. The Atlantic coast experienced an expansion of suitability into interior areas, with punctual increases in southeastern and southern Brazil.

The binary map (Figure 6N) reveals this growth of potential presence zones, especially along the southern edges of the Amazon and in parts of the Atlantic Forest. These adjustments may be related to both climatic variations and the onset of more intense anthropogenic pressures, such as fire use, forest resource management, and increased human occupation. Nevertheless, Amazonia retained extensive suitable areas, functioning as a major forest continuum up to recent times. This period marks a transition between the ecological stability of the Mid-Holocene and the growing impacts of human activities on tropical ecosystems.

3.3 Statistical Analysis of Bioclimatic Variables Across Periods

3.3.1 Climatic Differences Between Periods

The application of Dunn’s test with Bonferroni correction revealed highly significant statistical contrasts among the different paleoclimatic periods (Table 3),

with particular emphasis on comparisons involving the Last Glacial Maximum (LGM) and the present-day scenario.

Table 3 summarizes, for each bioclimatic variable analyzed, the comparison between periods that showed the lowest adjusted significance value (P.adj), highlighting the intervals of greatest climatic instability over the past 21.000 years.

Table 3. Summary of the most significant contrasts (lowest adjusted p-values) between paleoclimatic periods for each bioclimatic variable, based on Dunn's test with Bonferroni correction.

Variable	Comparison Between Periods	Most Significant Comparison	Adjusted P-value (P.adj)	Interpretation
BIO2 – Mean Diurnal Range	13	LGM vs. Present	5.62×10^{-235}	Highest contrast in daily temperature range
BIO8 – Mean Temp of Wettest Quarter	24	LGM vs. Present	5.44×10^{-211}	Progressive warming in the wet season
BIO19 – Precip. of Coldest Quarter	13	LGM vs. LH	1.64×10^{-80}	Major difference in cold-season precipitation
BIO3 – Isothermality	17	HS1 vs. LGM	2.71×10^{-72}	Sharp thermal reorganization between glacial phases
BIO18 – Precip. of Warmest Quarter	8	HS1 vs. Present	2.03×10^{-15}	Climatic reversal impact on summer rainfall
BIO15 – Precipitation Seasonality	1	LH vs. YDS	2.14×10^{-3}	Increase in rainfall seasonality

Among the ten comparisons, the most pronounced contrasts were observed for the variable BIO2 (Mean Diurnal Temperature Range), particularly between the Last Glacial Maximum (LGM) and the present scenario, which exhibited the lowest adjusted significance value (P.adj = 5.62×10^{-235}). This result indicates a sharp thermal shift over time, reflecting the substantial difference in temperature ranges between glacial and current climatic conditions.

The variable BIO8 (Mean Temperature of the Wettest Quarter) also showed substantial changes, with the most notable contrast again occurring between the LGM and the present (P.adj = 5.44×10^{-211}). This contrast reinforces the trend of

progressive warming during the wet seasons, accompanying the transition from glacial to interglacial and contemporary climate conditions.

BIO19 (Precipitation of the Coldest Quarter) exhibited significant differences across several periods, with the most pronounced contrast observed between the Last Glacial Maximum (LGM) and the Late Holocene (LH) ($P.adj = 1.64 \times 10^{-80}$). This result suggests a substantial increase in precipitation during the coldest months of the year, reflecting significant changes in hydrological regimes from the late Pleistocene to the Late Holocene.

The variable BIO3 (Isothermality) showed its most significant contrast between Heinrich Stadial 1 (HS1) and the LGM ($P.adj = 2.71 \times 10^{-72}$). This difference points to major changes in the relationship between diurnal and seasonal temperature variation, indicating important thermal reorganizations during the transition between two glacial phases.

For the variable BIO18 (Precipitation of the Warmest Quarter), the most significant contrast was between Heinrich Stadial 1 (HS1) and the present-day scenario, with a P.adj value of 2.03×10^{-15}. This result indicates substantial changes in precipitation volumes during the wettest part of the year, reflecting an intensification of the seasonal hydrological regime during the transition from the late Pleistocene to the recent Holocene.

The variable BIO15 (Precipitation Seasonality) showed only one statistically significant comparison, between the Late Holocene (LH) and the Younger Dryas Stadial (YDS), with a P.adj value of 2.14×10^{-3}. This difference points to a more localized variation in the seasonal distribution of rainfall, suggesting that this variable remained stable across most of the periods analyzed, with isolated changes linked to abrupt climatic events.

3.3.2 Visualization of Temporal Variations: Boxplots of Bioclimatic Variables

Figure 7 presents boxplots of the six selected bioclimatic variables, highlighting temporal trends across the eight climatic periods and revealing consistent patterns of climatic transition over the past 21.000 years. These plots emphasize the contrast between glacial and interglacial periods.

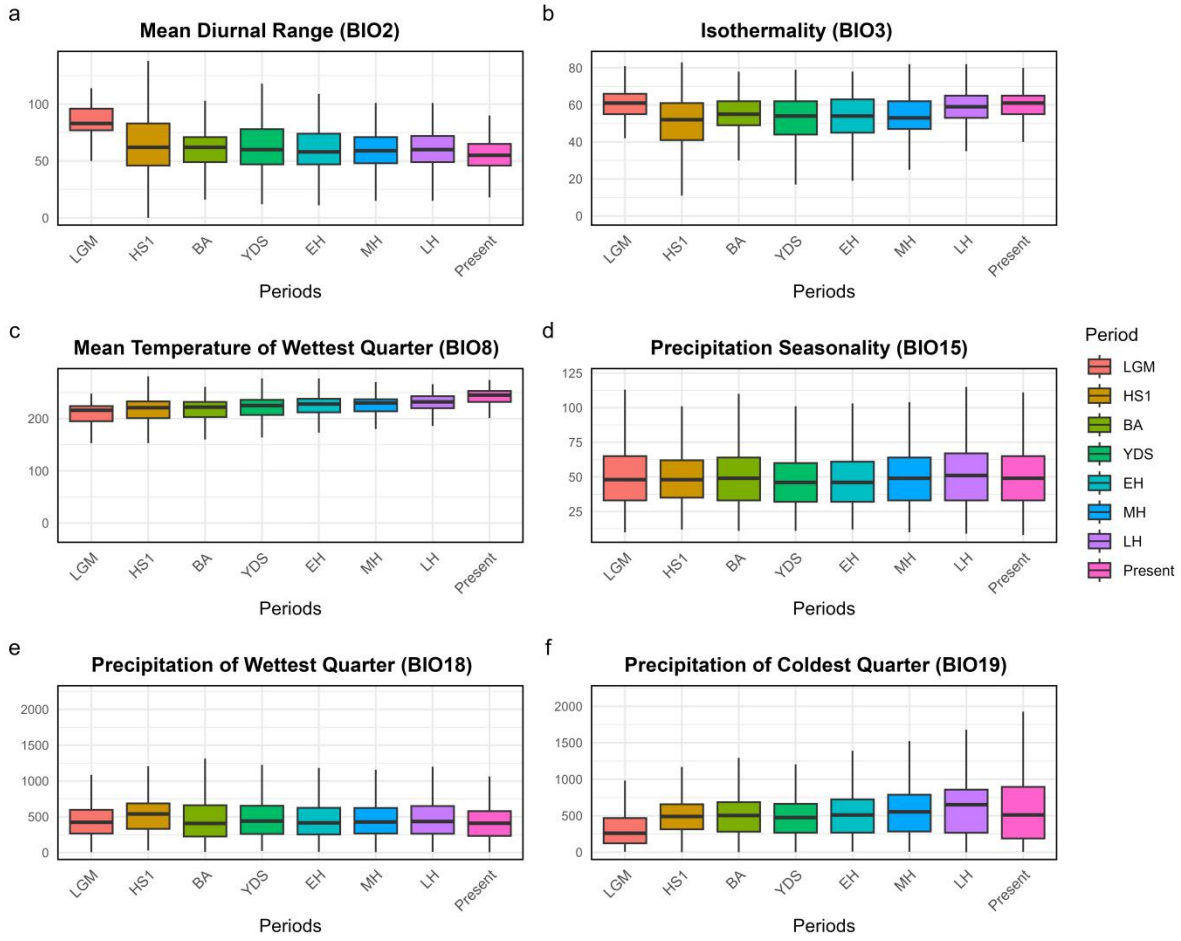

Figure 7 – Temporal variation of bioclimatic variables. Boxplots show the distribution of six bioclimatic variables across eight periods: LGM, HS1, BA, YDS, EH, MH, LH, and Present (1979–2013). (a) BIO2 – Mean Diurnal Range; (b) BIO3 – Isothermality; (c) BIO8 – Mean Temperature of Wettest Quarter; (d) BIO15 – Precipitation Seasonality; (e) BIO18 – Precipitation of Wettest Quarter; (f) BIO19 – Precipitation of Coldest Quarter. Colors represent the periods according to the legend.

Regarding temperature, the variable BIO2 (Figure 7a) exhibits an inverse trend compared to other thermal variables, with the highest values recorded during the Last Glacial Maximum (LGM) and a progressive decline toward the present. This indicates a reduction in the difference between daytime and nighttime temperatures, consistent with the expansion of vegetation cover, increased atmospheric moisture, and greater cloudiness during interglacial periods. The decrease in diurnal temperature range reflects a shift from the dry, continental climate typical of glacial periods to a more buffered, humid, and thermally stable environment in more recent intervals, especially throughout the Holocene. Lower thermal amplitude favors the stability of tropical

ecosystems by reducing thermal stress on vegetation and promoting more favorable conditions for biodiversity maintenance.

The variable BIO3 (Figure 7b), which expresses isothermality (the percentage ratio between the mean diurnal temperature range and the annual temperature range), shows higher median values during the LGM. Given the elevated BIO2 values, it can be inferred that diurnal thermal oscillation during the LGM was proportionally high compared to the annual range, a feature typical of arid, open environments with sparse vegetation cover. However, there is a sharp decline during the Heinrich Stadial 1 (HS1), suggesting a period of instability between diurnal and seasonal temperature variations. Starting in the Bølling-Allerød (BA), a progressive recovery of isothermality is observed, with stable values throughout the Holocene and a return to near-LGM levels under present-day conditions. This pattern may reflect a reorganization of diurnal and seasonal thermal gradients over time, resulting in a more balanced climate in recent periods. The current high isothermality indicates a climatic environment in which differences between daily and seasonal temperature extremes are smaller, favoring greater ecological stability.

Finally, the variable BIO8 (Figure 7c) reveals a clear trend of continuous increase from the LGM to the present, reflecting the gradual warming of the wettest seasons over the past 21.000 years. This pattern reinforces the narrative of a transition from a glacial to an increasingly warmer interglacial climate, with significant ecological implications. Higher temperatures during the wettest quarters may alter fundamental physiological and ecosystem processes such as evapotranspiration and the distribution of tropical species. The current scenario characterized by warmer rainy seasons tends to be particularly favorable for the maintenance and expansion of tropical rainforests, especially in regions with lower thermal seasonality.

The variable BIO15 (Figure 7d), which represents precipitation seasonality, exhibits low variability across the periods but shows a slight increasing trend starting from the Mid-Holocene, reaching slightly higher values in the Late Holocene and the present. This shift suggests a growing irregularity in intra-annual rainfall distribution, linked to the intensification of modern atmospheric patterns such as Atlantic and Pacific modes of variability.

The variable BIO18 (Figure 7e) shows higher median values during the Bølling-Allerød (BA) and Heinrich Stadial 1 (HS1), indicating that rainy seasons were more intense during these climatic intervals. In contrast, the lowest values are

recorded both during the Last Glacial Maximum (LGM) and the present, suggesting a relative reduction in the intensity of the wet season under extreme glacial conditions and, surprisingly, also in the current climatic context. This pattern highlights that there has not been a continuous increase in precipitation during the wettest quarters over time, but rather a non-linear variation, related to changes in tropical atmospheric circulation and shifts in the position of the Intertropical Convergence Zone (ITCZ) throughout the different paleoclimatic periods.

The variable BIO19 (Figure 7f) displays a clearly increasing pattern over the past 21,000 years. The lowest values are recorded during the LGM, reflecting the aridity and cooling characteristic of that period. From the HS1 onward, a progressive increase in precipitation during the coldest quarters is observed, reaching peak values in the Late Holocene (LH) and the present. This behavior suggests an intensification of the hydrological cycle throughout the Holocene, associated with increased atmospheric moisture, expansion of vegetation cover, and a reduction in thermal seasonality. The fact that the coldest quarters today are also wetter points to a transition toward less seasonal climatic regimes, with higher water availability throughout the year, including traditionally dry seasons.

4. DISCUSSION

4.1 Climate dynamics and environmental variations throughout the Late Quaternary

The climate dynamics of the Late Quaternary played a decisive role in shaping the patterns of environmental suitability for South American tropical forests. The data obtained in this study reveal statistically significant changes in bioclimatic variables over the past 21.000 years, supporting a climatic narrative characterized by the transition from a cold and predominantly dry regime with low atmospheric CO_2 concentrations and restricted refuge areas, particularly in western Amazonia during the Last Glacial Maximum (Ledru et al., 2009; Akabane et al., 2024). This regime gradually shifted toward warmer and generally wetter conditions throughout the Holocene, punctuated by significant fluctuations during the deglaciation, such as the Heinrich Stadial 1 and Younger Dryas events, which triggered complex atmospheric and hydrological reorganizations (Akabane et al., 2024). These processes shaped the heterogeneous expansion and consolidation of tropical and subtropical forests in the

region, a pattern widely corroborated by paleoclimatic and paleoecological studies (Ledru et al., 2009; Maezumi et al., 2018a; Akabane et al., 2024).

In our investigation, we observed that the variable BIO8 corresponding to the mean temperature of the wettest quarter exhibited a continuous upward trajectory from the Last Glacial Maximum (LGM) to the present. This pattern reflects a global warming trend associated with post-LGM deglaciation, as described by Clark et al. (2009). According to these authors, the retreat of polar ice sheets and increased insolation in the Northern Hemisphere triggered amplification feedback mechanisms such as rising atmospheric CO_2 and ocean warming that promoted global climate warming, including in the Southern Hemisphere.

Regional evidence supports this dynamic. A study conducted by Bush et al. (2004) in an area near the Amazon Basin documented an estimated temperature increase of approximately 1°C per millennium during the transition from the Pleistocene to the Holocene. This warming trend is consistent with the magnitude of temperature change recorded in other proxies, such as the ~8–12°C cooling during the LGM observed in the Huascarán ice core in Peru (Thompson et al., 1995) and the ~5.4°C cooling derived from noble gas records in groundwater in eastern Brazil (Stute et al., 1995).

However, hydroclimatic regimes in the Amazon during this interval exhibited strong spatial heterogeneity. Speleothem data analyzed by Cheng et al. (2013) reveal the existence of an orbital-scale precipitation dipole, in which the eastern portion of the Amazon became progressively wetter after the LGM, while the western portion showed a tendency toward slightly drier conditions. These patterns are linked to changes in the South American Monsoon (SAM) and Southern Hemisphere summer insolation (ASI), as discussed by Cheng et al. (2013) and Urrego et al. (2012).

Despite these spatial differences in thermal and rainfall regimes, palaeoecological records demonstrate the persistence of humid forests in parts of adjacent and southwestern Amazonia throughout the Holocene, highlighting the resilience or adaptive capacity of these vegetation formations to environmental changes (Bush et al., 2004; Urrego et al., 2012).

In contrast, BIO2 — Mean Diurnal Range (monthly mean of daily temperature range) showed the highest values during the LGM, with a progressive decline in subsequent periods. Although the HS1 already indicates a reduction in the median thermal amplitude, it still maintained high variability, reflecting residual thermal

instabilities from the glacial phase. This transition points to a shift from dry, sparsely vegetated continental climates to more regulated conditions, marked by greater forest cover and humidity features typical of stabilized tropical systems (Behling, 1995).

The reduction in thermal amplitude can also be interpreted as an indirect signal of the development of a forest microclimate, as the vertical structure of the vegetation helps buffer extreme temperature variations (Scheffers et al., 2017; Jucker et al., 2018; De Frenne et al., 2019).

BIO3, which relates diurnal temperature range to annual temperature range (isothermality), displayed a non-linear pattern throughout the Late Quaternary. The highest values were observed at present and during the LGM, followed by a significant decrease during the HS1 and YDS. These periods of low BIO3 values were characterized by high dispersion and thermal instability, a pattern consistent with evidence of increased climate variability and reorganization of tropical atmospheric systems during these intervals (Bush & Silman, 2004; Ledru et al., 2009; Akabane et al., 2024).

From the Early Holocene onward, the results indicate a recovery and subsequent stabilization of isothermality. This upward trend from the Late Holocene aligns with the transition to an interglacial regime that favored the expansion of vegetation cover compared to glacial periods (Behling, 1995; Ledru et al., 2009).

The presence of dense vegetation during the Holocene contributed to a thermal buffering effect at local scales, mitigating temperature extremes and reducing microclimatic thermal seasonality (Bush & Silman, 2004; Scheffers et al., 2016; Jucker et al., 2018; De Frenne et al., 2019). This relative thermal stability, particularly in contrast to the more volatile glacial periods is crucial for the maintenance of highly specialized tropical biological communities that are sensitive to abrupt climatic variations (Colwell et al., 2008; Deutsch et al., 2008).

BIO15 — Precipitation Seasonality — did not exhibit a clear trend of increase or decrease over the past 21.000 years. Although the medians remained stable across the periods, greater dispersion of values was observed during the LGM, BA, and LH, suggesting increased intra-annual variability in precipitation under transitional or regionally unstable climatic conditions.

The slight rise in the median during the Late Holocene and the present may reflect changes in seasonal patterns associated with the reorganization of the South

American monsoon system, as suggested by Wang et al. (2004) and Cheng et al. (2013), though without indicating an abrupt transformation in the hydrological regime. From an ecological perspective, these oscillations may have affected the phenology of species sensitive to water deficits, favoring those with adaptive strategies suited to more seasonal regimes (Borchert et al., 2005; Markesteijn & Poorter, 2009).

The variable BIO18 (precipitation during the warmest quarter) reached its highest value during Heinrich Stadial 1 (HS1), reflecting a climatic episode marked by atmospheric circulation anomalies and an intensification of the South American Summer Monsoon (SASM) linked to the displacement of the Intertropical Convergence Zone (ITCZ) (Pinaya et al., 2019).

Although the Mid-Holocene (MH) did not exhibit the highest absolute values of this variable, it was characterized by regionally variable hydrological regimes. For instance, palaeoecological records indicate the expansion and consolidation of dense forests in the Atlantic Forest of southern Brazil, consistent with wetter conditions (Behling & Negrelle, 2001), while other records from the Atlantic Forest (Ledru et al., 2009) and the Amazon (Maezumi et al., 2018a) suggest drier conditions or distinct wet periods during parts of the MH.

In our results, the variable BIO19 (precipitation of the coldest quarter) exhibited lower values during the Last Glacial Maximum (LGM) (Bush & Silman, 2004; Akabane et al., 2024). The LGM in the Amazon was characterized by colder and, in some regions, drier conditions (Akabane et al., 2024; Bush & Silman, 2004). During the Holocene, precipitation generally increased compared to the LGM (Akabane et al., 2024), but the hydrological history of the South American tropics was marked by significant variability rather than a consistent upward trend in seasonal precipitation across all regions up to the present (Akabane et al., 2024). Palaeoecological records indicate the occurrence of drier phases in different regions and time periods throughout the Holocene (Akabane et al., 2024). For example, studies in eastern Amazonia report drier conditions after ~2.500 cal yr B.P. (Maezumi et al., 2018a). Peat accumulation records, such as at the San Jorge site, also show significant fluctuations in moisture, including periods of slow or no accumulation between c. 1300 and 400 cal yr BP, due to drier climate (Kelly et al., 2017).

In the present period, our results for BIO19 reveal a high dispersion of values, reflecting more pronounced spatial and interannual variability in winter (cold season) precipitation (Gatti et al., 2021). This observation is consistent with contemporary

trends reported by Gatti et al. (2021), which show warming and declining precipitation during the dry season (ASO – August, September, October), especially in eastern and southeastern Amazonia, intensifying the dry season (Gatti et al., 2021).

The IPCC (2023) panel confirms that human influence has warmed the climate and increased the likelihood of compound extreme events, including heatwaves and droughts (IPCC, 2023). The water cycle has intensified, increasing both variability and the frequency of extremely wet and extremely dry events, linked to contemporary climate forcings driven by human activity (IPCC, 2023).

Collectively, these results reinforce the view that the Late Quaternary climatic trajectory in South America was marked by a transition from a cold climate regime (Behling & Negrelle, 2001; Bush, 2004; Akabane et al., 2024), dry in several regions (Behling & Negrelle, 2001; Akabane et al., 2024), and highly seasonal (Bush & Silman, 2004; Akabane et al., 2024) with implications for the contraction of tropical vegetation (Behling & Negrelle, 2001; Akabane et al., 2024) to progressively warmer conditions (Bush, 2004; Akabane et al., 2024), with a general increase in humidity following the Last Glacial Maximum (LGM) and the transitional period (Akabane et al., 2024), and greater thermal stability (Bush & Silman, 2004), which supported the expansion and consolidation of tropical forests (Behling et al., 1995; Behling & Negrelle, 2001; Akabane et al., 2024).

It is important to note, however, that Holocene precipitation records exhibit complex spatial and temporal variability rather than a continuous linear progression toward increased moisture (Bush & Silman, 2004; Cheng et al., 2013; Maezumi et al., 2018a; Maezumi et al., 2018b). These conclusions are supported by sedimentary, palynological, and isotopic evidence from multiple paleoenvironmental records across the region (Behling et al., 1995; Behling & Negrelle, 2001; Bush & Silman, 2004; Bush, 2004; Wang et al., 2004; Urrego et al., 2012; Cheng et al., 2013; Kelly et al., 2016; Maezumi et al., 2018a; Maezumi et al., 2018b; Akabane et al., 2024).

4.2 Expansions and Contractions of Suitable Areas

The paleoclimatic reconstruction based on potential distribution modeling reveals a non-linear trajectory of expansion and contraction of South American tropical forests from the LGM to the present. These variations reflect direct responses to changes in climatic conditions, particularly in seasonal temperature and

precipitation dimensions, as demonstrated by the binary suitability maps and statistical results obtained in this study.

During the Last Glacial Maximum (LGM, ca. 21 ka), areas with high climatic suitability for tropical rainforests were restricted to the western portion of the Amazon, notably in northwestern Brazil, southern Colombia, eastern Peru, and parts of Bolivia. This pattern reflects a climatic scenario characterized by lower temperatures, high diurnal temperature range, and limited precipitation, as evidenced by high average values of BIO2 and low values of BIO8 and BIO19 observed for that period.

Recent modeling studies also indicate that climatically favorable areas during the LGM were concentrated in the western Amazon, reinforcing the idea that this region functioned as a zone of relative stability (Pinaya et al., 2019, 2024). This spatial pattern is consistent with paleoclimatic evidence indicating a sharp reduction in precipitation in the eastern and central portions of the basin, while the west maintained higher rainfall levels (Cheng et al., 2013; Colinvaux et al., 1996; Pinaya et al., 2024).

In addition, recent studies suggest that northwestern Amazonia was less affected by climatic oscillations over time and by anthropogenic pressures during the Holocene, compared to eastern and southeastern regions (Maezumi et al., 2018a, 2018b; Gatti et al., 2021), which may have favored the persistence of humid forests in that sector.

The pattern observed in the models is embedded in an ongoing scientific debate regarding precipitation patterns in the Amazon during the LGM, as highlighted by Sylvestre (2009) and synthesized by Heine (2024). Three main hypotheses have been proposed based on pollen records: (i) partial replacement of tropical forests by savannas; (ii) maintenance of tropical forest even under glacial climate; or (iii) contraction of forest only at the margins of the basin (Hermanowski et al., 2012).

Large-scale fluctuations in Amazon forest extent during the Quaternary have been discussed by various authors (Behling, 1997; Heine, 1994b), while the group led by Colinvaux (1996, 2000) rejected the hypothesis of significant forest retraction during glacial phases.

Isotopic and speleothem studies confirm that Western Amazonia functioned as a zone of long-term hydroclimatic stability (Cheng et al., 2013). Unlike Eastern Amazonia, which faced significant drying during glacial periods, the western sector maintained or even modestly increased its precipitation levels (Cheng et al., 2013).

Furthermore, even during drier intervals such as the Early-Mid Holocene, the region retained stable forest cover, contrasting with the high variability observed in the east (Cheng et al., 2013). The results of this study, by indicating nuclei of high climatic suitability in western Amazonia, align with this view of relative stability in the western portion of the basin.

Records indicate a significant reduction in precipitation in the eastern and central portions of the basin (Häggi et al., 2017; Wang et al., 2017), while the western sector remained humid, maintaining high rainfall levels (Cheng et al., 2013). In the same context, average annual temperatures in the Amazon region were approximately 4 to 6 °C lower than pre-industrial Holocene levels (Maksic et al., 2022; Colinvaux et al., 1996). This drier climate scenario, combined with decreased atmospheric carbon dioxide concentrations (Petit et al., 1999), drove physiological changes in vegetation (Maksic et al., 2022). While the western Amazon remained largely resilient, these conditions led to the contraction of evergreen rainforests and their replacement by seasonal forests or open vegetation types, particularly in the eastern and marginal portions of the basin (Häggi et al., 2017; Maksic et al., 2022).

The subsequent phase, Heinrich Stadial 1 (HS1), shows an expansion of climatic suitability, although still concentrated in the western Amazon and the Andean foothills. This pattern may be related to increased regional humidity associated with the southward displacement of the Intertropical Convergence Zone (ITCZ), as indicated by paleoclimatic records (Wang et al., 2004; Cheng et al., 2013) and simulated by Akabane et al. (2024), who demonstrated the tropical rainfall belt's response to the slowdown of the Atlantic Meridional Overturning Circulation (AMOC) during this interval. Despite this shift, the expansion of suitable areas remained modest, reflecting the persistence of a prolonged dry season and residual thermal instabilities, especially in northern Amazonia (Colinvaux et al., 1996; Akabane et al., 2024).

Palynological data indicate that, at the beginning of HS1, cold-adapted taxa such as Podocarpus and Hedyosmum were replaced by seasonal and savanna vegetation elements, suggesting a local loss of suitability for late-glacial humid forests (Akabane et al., 2024).

This pattern is consistent with paleoclimatic modeling results based on simulations with a 50% weakened AMOC under LGM conditions, which point to reduced suitability in the northern regions of the basin (Akabane et al., 2024).

During the Bølling-Allerød (BA), a globally recognized interstadial period following Heinrich Stadial 1 (HS1) (Maksic et al., 2022; Häggi et al., 2017; Akabane et al., 2024), we observe a phase marked by rising temperatures (Colinvaux et al., 2000; Bush, 2004; Wang et al., 2017; Maksic et al., 2022) and the reorganization of atmospheric and hydrological circulation patterns, associated with the collapse of ice sheets and Southern Hemisphere warming (Clark et al., 2009; Häggi et al., 2017). These conditions favored the recolonization or improved climatic suitability of areas that had previously been physiologically and climatically less favorable for certain taxa, especially those adapted to warmer climates, as temperatures (Clark et al., 2009; Häggi et al., 2017; Maksic et al., 2022).

During the deglaciation, which includes the Bølling-Allerød (BA), tropical forest in the Amazon Basin largely persisted, even under the colder and regionally drier conditions of the LGM and HS1 (Colinvaux et al., 2000; Bush & Silman, 2004; Wang et al., 2017; Häggi et al., 2017; Maksic et al., 2022; Pinaya et al., 2024).

In the context of gradual post-HS1 warming that characterizes the BA (Bush, 2004; Bush & Silman, 2004), a significant reorganization of floristic composition occurred within the existing forest (Colinvaux et al., 2000; Bush, 2004). Cold-adapted and montane taxa that had expanded into lower altitudes during glacial periods (Colinvaux et al., 2000; Akabane et al., 2024; Pinaya et al., 2024) retreated with the post-HS1 warming (Colinvaux et al., 2000; Akabane et al., 2024). Akabane et al. (2024) indicate that post-LGM climate warming and increased atmospheric CO_2 levels were the primary drivers of long-term floristic changes in the Amazon Basin. Bush (2004) observed a continuous species turnover during the transition, although the rates of change did not differ from those of the preceding period.

There were significant regional variations in climatic responses (Bush & Silman, 2004; Cheng et al., 2013; Maksic et al., 2022). For example, eastern Amazonia experienced an increase in precipitation during deglaciation compared to the LGM (Wang et al., 2017). In contrast, palaeoecological records from southern Brazil indicate the predominance of open vegetation or limited forest recovery during the period encompassing the BA (Behling et al., 1995; Behling & Negrelle, 2001; Ledru et al., 2009). In the southern Brazilian lowlands, grasslands and cold-adapted forests dominated during the LGM, with impoverished tropical forest developing only after ca. 12.300 ^{14}C years BP (Behling & Negrelle, 2001). On the southern Brazilian plateaus, grasslands prevailed during the Late Pleistocene, with forest expansion

occurring only at the beginning of the Holocene (Behling et al., 1995). Ledru et al. (2009) reported a drastic reduction in biodiversity and dominance of open vegetation between ca. 23 and 12 cal kyr, a period encompassing the LGM and the BA, in southern Brazil.

During the Younger Dryas (YD), the trend of increasing climatic suitability and forest connectivity is temporarily interrupted. Simulations for cold periods, such as the Last Glacial Maximum (LGM), suggest rearrangements in biome distribution (Clark et al., 2009; Maksic et al., 2022). Palaeoecological records indicate a renewed contraction of suitable areas and vegetation stress in certain regions during the Late Glacial period, which includes the YD (Maksic et al., 2022). This was especially observed at the southern and eastern margins of the Amazon (Mayle et al., 2000; Behling, 2002; Maksic et al., 2022) and in sections of the Atlantic Forest (Behling, 1995; Behling & Negrelle, 2001; Ledru et al., 2009).

For example, in southern Brazil (Atlantic Forest), the end of the Pleistocene was characterized by cooler and drier conditions, with the predominance of grasslands and low forest biodiversity (Behling et al., 1995; Behling & Negrelle, 2001; Ledru et al., 2009). In eastern Amazonia, speleothem evidence (such as from Paraíso Cave) indicates drier conditions during events like the Younger Dryas and Heinrich Stadial 1 (Häggi et al., 2017; Wang et al., 2017), although the South American climatic response to cold events in the Northern Hemisphere is complex and regionally variable (Bush & Silman, 2004; Cheng et al., 2013; Maksic et al., 2022). In some cases, it even resulted in increased humidity in northeastern Brazil during HS1 (Wang et al., 2004; Häggi et al., 2017).

Such a reversal in forest expansion trends in some areas aligns with the intensification of Northern Hemisphere cold events (such as Heinrich events and the YD itself) and the consequent reorganization of tropical circulation (Häggi et al., 2017; Pinaya et al., 2019; Akabane et al., 2024). This reorganization notably includes shifts in the Intertropical Convergence Zone (ITCZ) (Bush & Silman, 2004; Ledru et al., 2009; Häggi et al., 2017; Akabane et al., 2024) and changes in the South American monsoon system (Ledru et al., 2009; Häggi et al., 2017; Akabane et al., 2024).

Although continental pollen records specifically focused on the YD are scarce or suffer from dating uncertainties in some key regions, such as southeastern Brazil (Behling & Negrelle, 2001; Ledru et al., 2009), making detailed vegetation reconstructions for this interval challenging, evidence from other periods and

locations indicates that tropical forests can respond rapidly to abrupt climatic oscillations (Hughen et al., 2004; Pinaya et al., 2019), reinforcing their high sensitivity to short-term disturbances (Akabane et al., 2024).

With the onset of the Holocene (~11.7 ka), a cycle of forest expansion was observed across several regions of South America (Ledru et al., 2009), associated with progressively wetter conditions (Cheng et al., 2013). However, thermal stability and the pace of this expansion varied regionally, with some areas experiencing significant warming (Behling & Negrelle, 2001).

During the Early Holocene, climatic suitability changed across different regions of South America, influenced by the reorganization of tropical atmospheric circulation. According to records from southern Brazil, the South American Monsoon (SAM) was weak during the early to mid-Holocene (Cheng et al., 2013).

Palaeoecological records support varied vegetation responses during this period. While forest cover may have been maintained or expanded in some areas, others experienced a more gradual re-establishment with lower biodiversity. For example, in the southern Atlantic Forest, this initial period (starting around ~12.300 ^{14}C years BP) was marked by low biodiversity (Behling & Negrelle, 2001), with the full development of mature tropical forest occurring significantly later in the Holocene (after ~9000 ^{14}C years BP) (Behling & Negrelle, 2001; Ledru et al., 2009).

During the approximate period of the Mid-Holocene referenced in the literature with intervals such as ~6 ka or ~9–5 ka / 6–4 ka cal BP (Cheng et al., 2013; Maezumi et al., 2018b), climatic and vegetational conditions in tropical South America exhibited complex and regionally variable patterns. In contrast to the idea of a generalized increase in climatic suitability, the sources indicate significant heterogeneity (Cheng et al., 2013; Häggi et al., 2017; Maksic et al., 2022). While a speleothem record from eastern Amazonia (Paraíso) suggests that precipitation was around 142% of modern levels approximately 6.000 years ago (Wang et al., 2017), indicating wetter conditions in this region during part of the period, records from western Amazonia show the highest δ^{18}O values in the entire ~250,000-year record (Cheng et al., 2013), suggesting the driest conditions of the last two glacial-interglacial cycles during the Mid-Holocene (~10–5 ka BP) (Cheng et al., 2013).

Palaeoecological studies in the eastern Andes and western Amazon also document dry conditions during this period (Whitney et al., 2011; Urrego et al., 2012; Häggi et al., 2017). Locally, in eastern Amazonia (Lago Caranã), regional climate

data show a gradual transition toward drier conditions starting around 4.500 cal yr BP (Maezumi et al., 2018a). Despite this heterogeneity and dryness in some regions, a modeling study analyzing the transition from the Last Glacial Maximum (LGM) to the present considers the synergistic effect of rising temperature and CO_2 levels since the LGM (Maksic et al., 2022).

In the Atlantic Forest, the situation also showed regional variability (Behling & Negrelle, 2001; Pinaya et al., 2019; Maksic et al., 2022). While a palynological record in southeastern Brazil shows that a dense Atlantic Forest developed after around 6.100 ^{14}C years BP (Behling & Negrelle, 2001), associated with a successional sequence following an initial phase of weakened forest (after ~12.300 ^{14}C years BP) and marine disturbances (Behling & Negrelle, 2001), other records from southern Brazil indicate dry phases during the Holocene (Pinaya et al., 2019) or forest regression linked to much drier conditions in specific sites such as the Colônia Crater over longer timescales (Ledru et al., 2009; Pinaya et al., 2024).

Factors such as regional seasonality and edaphic constraints are relevant to vegetation distribution (Tuomisto & Ruokolainen, 1994; Oliveira-Filho & Fontes, 2000; Behling & Negrelle, 2001; Ledru et al., 2009), but the cited sources do not explicitly identify them as primary limiting factors for the expansion of the Atlantic Forest during the Mid-Holocene when compared directly to Amazonia, focusing more on climatic variations to explain the observed changes (Behling & Negrelle, 2001; Ledru et al., 2009; Maksic et al., 2022).

Temperatures during the Holocene may have become stable in some areas (Cheng et al., 2013). However, precipitation exhibited contrasting patterns between eastern and western Amazonia, with drier conditions in the west and in parts of the southern/southeastern Atlantic Forest (Behling & Negrelle, 2001; Cheng et al., 2013; Häggi et al., 2017; Pinaya et al., 2019). The idea of a strengthened South American Monsoon (SAM) as a driver of uniformly wetter conditions is not directly supported by the available data, which show heterogeneous precipitation patterns (Cheng et al., 2013; Häggi et al., 2017).

The reorganization of convergence zones (ITCZ/SACZ) is a relevant climatic factor (Wang et al., 2004; Ledru et al., 2009; Häggi et al., 2017), but its influence during the Mid-Holocene, as described in the sources, does not align with a scenario of uniformly high humidity across tropical South America (Cheng et al., 2013; Häggi et al., 2017).

Palaeoecological evidence from the cited sources reflects this regional variability (Behling & Negrelle, 2001; Ledru et al., 2009; Whitney et al., 2011; Urrego et al., 2012; Häggi et al., 2017; Maezumi et al., 2018a). Pollen records from the Amazon show the persistence of tropical forests in some areas (Colinvaux et al., 1996, 2000; Häggi et al., 2017) throughout glacial cycles (Colinvaux et al., 1996a, 2000).

However, data also document drier conditions in parts of western Amazonia and in the southern/southeastern Atlantic Forest during the Mid-Holocene (Behling & Negrelle, 2001; Urrego et al., 2012; Cheng et al., 2013; Häggi et al., 2017), leading to forest regressions or more open formations (Behling & Negrelle, 2001; Urrego et al., 2012). Vegetation composition also exhibited regional changes over time (Ledru et al., 2009), and there is evidence of fire activity and human cultivation beginning around ~4.500 cal yr BP at sites such as Lake Caranã, which locally altered vegetation (Maezumi et al., 2018a).

Although some records indicate persistent forests in certain areas (Colinvaux et al., 1996, 2000; Häggi et al., 2017), the depiction of uniformly "mature, biodiverse, and climatically stable" forests across all regions of South America throughout the Mid-Holocene is not fully supported by the available data (Behling & Negrelle, 2001; Ledru et al., 2009; Urrego et al., 2012; Maezumi et al., 2018a), which highlight regional contrasts and periods of localized aridity (Behling & Negrelle, 2001; Cheng et al., 2013; Häggi et al., 2017).

From ~4.500 cal yr BP onward (Maezumi et al., 2018b), a gradual transition toward drier climatic conditions was observed in some regions of tropical South America, such as eastern Amazonia (Wang et al., 2017; Maezumi et al., 2018a). In contrast, the earlier Mid-Holocene (~6,000 years ago) in eastern Amazonia showed precipitation levels around 142% of present-day values (Wang et al., 2017), suggesting a climatic shift to drier conditions in that region.

The sources indicate that precipitation in eastern Amazonia became the lowest of the entire Holocene after ~2.000 cal yr BP (Wang et al., 2017; Maezumi et al., 2018a). Although this did not constitute a widespread collapse of tropical forests, these drier conditions in certain peripheral areas contrast with the wetter conditions of earlier periods in the same locations (Wang et al., 2017).

The occurrence of periodic droughts in the Amazon, particularly in the eastern and central regions, is associated with positive sea surface temperature anomalies in

the tropical Pacific (Malhi et al., 2008), and a possible strengthening of El Niño–Southern Oscillation (ENSO) activity after the Mid-Holocene may have exacerbated the decline in precipitation and increased water $\delta^{18}O$ values (Wang et al., 2017).

This localized climatic contraction coincides temporally with the intensification of anthropogenic influence on forest ecosystems in some areas, particularly in eastern Amazonia. At sites such as Lake Caranã, charcoal data indicate that fire management, characterized by low-severity burning, was the primary driver of both local and regional fire activity during pre-Columbian times, beginning around ~4.500 cal yr BP with the onset of fire management and polyculture practices (Maezumi et al., 2018a, 2018b). Agroforestry polyculture and the enrichment of forest composition with edible plants increased from ~2.500 cal yr BP onward (Maezumi et al., 2018a, 2018b), driven by species such as Mauritia/Mauritiella, Agavaceae, Caryocar, Byrsonima, Lecythidaceae, and Theobroma (Maezumi et al., 2018a).

The palaeoecological evidence provided by the sources, particularly palynological records from eastern Amazonia (Lake Caranã), documents the persistence of tropical forest taxa (>50% initially, later ~30–45%) despite increasing pre-Columbian activity and fire management (Maezumi et al., 2018b). While the sources support structural changes in vegetation communities and greater fire susceptibility in managed areas of eastern Amazonia (Maezumi et al., 2018a), records from the Rio Negro (Lake Acarabixi) indicate forest stability during the Late Holocene (1600–650 cal yr BP), with high forest pollen dominance (77–89%) and no drastic vegetation changes, despite evidence of human disturbance such as fire and pioneer taxa (Rodríguez-Zorro et al., 2018).

Potential vegetation distribution modeling for the present climate reveals a wide distribution of favorable conditions for tropical forests in South America (Sobral-Souza et al., 2018; Maksic et al., 2022; Akabane et al., 2024). The Amazon Basin maintains a climate that supports the largest tropical forest on Earth. Potential vegetation models under current climatic conditions accurately reproduce the main South American biomes, including tropical forests in Amazonia and the Atlantic coastal region (Sobral-Souza et al., 2018; Maksic et al., 2022; Akabane et al., 2024).

Studies using ecological niche modeling for the present also simulate the delimitation of the Amazon and Atlantic Forests in close agreement with known biogeographic boundaries (Sobral-Souza et al., 2018).

However, actual forest presence is influenced by additional factors beyond climate. Maps of current and potential vegetation distribution indicate fragmentation along the edges of these biomes particularly in the southern and eastern Amazon and in the Atlantic Forest (Sobral-Souza et al., 2018; Gatti et al., 2021). This fragmentation reflects the predominant role of non-climatic anthropogenic factors. In the Amazon, forest degradation caused by logging and fire has spatially surpassed deforestation (Matricardi et al., 2020), while extensive land conversion for agriculture continues to drive carbon losses in the southeast (Gatti et al., 2021). The Atlantic Forest represents an extreme case of this historical impact: 97% of its remaining vegetation fragments are smaller than 50 ha (Vancine et al., 2024), severely impacting connectivity and ecosystem integrity (Sobral-Souza et al., 2018; Grantham et al., 2020).

5.CONCLUSION

In summary, this study elucidates the complex and non-linear trajectory of Tropical and Subtropical Moist Broadleaf Forests (TSMBF) in South America over the past 21.000 years, revealing how climatic oscillations since the Last Glacial Maximum (LGM) have profoundly shaped their potential distribution. We demonstrate that western Amazonia functioned as a crucial refuge during cold and dry glacial periods, whereas widespread expansions occurred during warmer and wetter interglacial phases.

The detailed analysis of bioclimatic variables and species distribution models revealed that TSMBF suitability reached its lowest and most fragmented levels during the LGM and Heinrich Stadial 1 (HS1). The transition toward warmer, wetter, and more thermally stable conditions initiated during the Bølling-Allerød (BA) and consolidated throughout the Holocene (Early, Middle, and Late) enabled progressive expansion and increased connectivity, culminating in the current patterns of maximum extent, especially across the Amazon Basin, the Southeast Atlantic coast, and southern Brazil. This pattern is primarily driven by higher wet-season temperatures (BIO8), greater cold-season precipitation (BIO19), and reduced mean diurnal temperature range (BIO2).

However, regional and temporal heterogeneity in precipitation regimes during the Holocene, coupled with escalating anthropogenic pressures over the past millennia, adds complexity to these patterns. This study highlights that although tropical forests

have demonstrated remarkable resilience to past natural climatic variability, contemporary climate change differs in magnitude, rate, and the unprecedented influence of human activities. Therefore, a deep understanding of these historical dynamics grounded in paleoenvironmental records and ecological modeling is essential to inform effective conservation strategies and to foster the resilience of these vital ecosystems in the face of the unprecedented challenges posed by the current global scenario.

6. REFERÊNCIAS

Aiello-Lammens, M.E., Boria, R.A., Radosavljevic, A., Vilela, B. and Anderson, R.P. (2015), spThin: an R package for spatial thinning of species occurrence records for use in ecological niche models. Ecography, 38: 541-545. https://doi.org/10.1111/ecog.01132

Akabane, T.K., Chiessi, C.M., Hirota, M. et al. Weaker Atlantic overturning circulation increases the vulnerability of northern Amazon forests. Nat. Geosci. 17, 1284–1290 (2024). https://doi.org/10.1038/s41561-024-01578-z

Allouche, O., Tsoar, A., & Karni, O. (2006). Assessing the accuracy of species distribution models: Prevalence, kappa and the true skill statistic (TSS). Journal of Applied Ecology, 43(6), 1223–1232. https://doi.org/10.1111/j.1365-2664.2006.01214.x

Almazroui, M., Ashfaq, M., Islam, M.N. et al. Assessment of CMIP6 Performance and Projected Temperature and Precipitation Changes Over South America. Earth Syst Environ 5, 155–183 (2021). https://doi.org/10.1007/s41748-021-00233-6

Arroyo-Rodríguez, V., Melo, F.P.L., Martínez-Ramos, M., Bongers, F., Chazdon, R.L., Meave, J.A., Norden, N., Santos, B.A., Leal, I.R. and Tabarelli, M. (2017), Multiple successional pathways in human-modified tropical landscapes: new insights from forest succession, forest fragmentation and landscape ecology research. Biol Rev, 92: 326-340. https://doi.org/10.1111/brv.12231

Artaxo, P, et al. 2022. Tropical and Boreal Forest – Atmosphere Interactions: A Review. Tellus B: Chemical and Physical Meteorology, 74(2022), 24–163. DOI: https:// doi.org/10.16993/tellusb.34

Baldwin, R. A. (2009). Use of Maximum Entropy Modeling in Wildlife Research. Entropy, 11(4), 854-866. https://doi.org/10.3390/e11040854

Barbet-Massin, M., Jiguet, F., Albert, C.H. and Thuiller, W. (2012), Selecting pseudo-absences for species distribution models: how, where and how many?. Methods in Ecology and Evolution, 3: 327-338. https://doi.org/10.1111/j.2041-210X.2011.00172.x

Behling, H. 1993. Untersuchungen zur spätpleistozänen und holozänen Vegetations- und Klimageschichte der tropischen Küstenwälder und der Araukarienwälder in Santa Catarina (Südbrasilien). Dissertationes Botanicae 206. J Cramer, Berlin Stuttgart, Germany.

Behling, H. 1995. Investigations into the Late Pleistocene and Holocene history of vegetation and climate in Santa Catarina (S Brazil). Vegetation History and Archaeobotany 4:127-152.

Behling, H., H. Hooghiemstra, and A.J. Negret. 1998. Holocene history of the Chocó rain forest from Laguna Piusbi, southern Pacific Lowlands of Colombia. Quaternary Research 50(3):300-308. [DOI: https://doi.org/10.1006/qres.1998.1998]

Behling, H., & Negrelle, R. R. B. (2001). Tropical rain forest and climate dynamics of the Atlantic lowland, southern Brazil, during the Late Quaternary. Quaternary Research, 56(3), 383–389. https://doi.org/10.1006/qres.2001.2264

Behling, H. (2002). Late Quaternary vegetation and climate dynamics in southeastern Amazonia inferred from Lagoa da Confusão, Tocantins State, northern Brazil. Amazoniana, 17(1), 27–39.

Berrío Mogollón, J.C. 2002. Doctoral dissertation. Amsterdam, The Netherlands.

Berrío, J.C., A. Boom, P.J. Botero, L.F. Herrera, H. Hooghiemstra, F. Romero, and G. Sarmiento. 2001. Multi-disciplinary evidence of the Holocene history of a cultivated floodplain area in the wetlands of northern Colombia. Vegetation history and archaeobotany 10(3):161-174.

Borchert, R., Robertson, K., Schwartz, M. D., & Williams-Linera, G. (2005). Phenology of temperate trees in tropical climates. International Journal of Biometeorology, 50(1), 57–65. https://doi.org/10.1007/s00484-005-0261-7

Boria, R. A., Olson, L. E., Goodman, S. M., & Anderson, R. P. (2014). Spatial filtering to reduce sampling bias can improve the performance of ecological niche models. Ecological Modelling, 275, 73–77. https://doi.org/10.1016/j.ecolmodel.2013.12.012

Borma, L. S., Costa, M. H., da Rocha, H. R., Arieira, J., Nascimento, N. C. C., Jaramillo-Giraldo, C., et al. (2022). Beyond carbon: The contributions of South American tropical humid and subhumid forests to ecosystem services. Reviews of Geophysics, 60, e2021RG000766. https://doi. org/10.1029/2021RG000766

Bradley, R. S. (2000). Past global changes and their significance for the future. Quaternary Science Reviews, 19(1–5), 391–402. https://doi.org/10.1016/S0277-3791(99)00071-2

Brown, J., Hill, D., Dolan, A. et al. PaleoClim, high spatial resolution paleoclimate surfaces for global land areas. Sci Data 5, 180254 (2018). https://doi.org/10.1038/sdata.2018.254

Brzozowski, M., Pełechaty, M., & Bogawski, P. (2022). A winner or a loser in climate change? Modelling the past, current, and future potential distributions of a rare charophyte species. Global Ecology and Conservation, 34, e02038. https://doi.org/10.1016/j.gecco.2022.e02038

Burbridge, R. E., Mayle, F. E., & Killeen, T. J. (2004). Fifty-thousand-year vegetation and climate history of Noel Kempff Mercado National Park, Bolivian Amazon. Quaternary Research, 61(2), 215–230. https://doi.org/10.1016/j.yqres.2003.12.004

Bush, M. B., De Oliveira, P. E., Colinvaux, P. A., Miller, M. C., & Moreno, J. E. (2004). Amazonian paleoecological histories: one hill, three watersheds. Palaeogeography, Palaeoclimatology, Palaeoecology, 214, 359–393

Bush, M. B., & Silman, M. R. (2004). Observations on Late Pleistocene cooling and precipitation in the lowland Neotropics. Journal of Quaternary Science, 19(7), 677–684. https://doi.org/10.1002/jqs.883

Buso Jr, A. A., Pessenda, L. C. R., Mayle, F. E., Lorente, F. L., Volkmer-Ribeiro, C., Schiavo, J. A., Pereira, M. G., Bendassolli, J. A., Macario, K. C. D., & Siqueira, G. S. (2019). Paleovegetation and paleoclimate dynamics during the last 7000 years in the Atlantic forest of Southeastern Brazil based on palynology of a waterlogged sandy soil. Review of Palaeobotany and Palynology, 264, 1–10. https://doi.org/10.1016/j.revpalbo.2019.02.002

Buso Jr, A. A., Pessenda, L. C. R., de Oliveira, P. E., Giannini, P. C. F., Cohen, M. C. L., Volkmer-Ribeiro, C., Barros de Oliveira, S. M., Favaro, D. I. T., Rossetti, D., Lorente, F. L., Borotti Filho, M. A., Schiavo, J. A., Bendassolli, J. A., Franca, M. C., Guimarães, J. T. F., & Siqueira, G. S. (2013a). From an estuary to a freshwater lake: A paleo-estuary evolution in the context of Holocene sea-level fluctuations, SE Brazil. Radiocarbon, 55(2–3), 1735–1746. https://doi.org/10.2458/azu_js_rc.55.16210

Buso Jr, A. A., Pessenda, L. C. R., de Oliveira, P. E., Giannini, P. C. F., Cohen, M. C. L., Volkmer-Ribeiro, C., Barros de Oliveira, S. M., Rossetti, D., Lorente, F. L., Borotti Filho, M. A., Schiavo, J. A., Bendassolli, J. A., Franca, M. C., Guimarães, J. T. F., & Siqueira, G. S. (2013b). Late Pleistocene and Holocene vegetation, climate dynamics, and Amazonian taxa in the Atlantic Forest, Linhares, SE Brazil. Radiocarbon, 55(2–3), 1747–1756. https://doi.org/10.2458/azu_js_rc.55.16211

Cheng, H., Sinha, A., Cruz, F. et al. Climate change patterns in Amazonia and biodiversity. Nat Commun 4, 1411 (2013). https://doi.org/10.1038/ncomms2415

Colinvaux, P. A., De Oliveira, P. E., Moreno, J. E., Miller, M. C., & Bush, M. B. (1996). A long pollen record from lowland Amazonia: Forest and cooling in glacial times. Science, 274(5284), 85–88. https://doi.org/10.1126/science.274.5284.85

Colinvaux, P. A., De Oliveira, P. E., & Bush, M. B. (2000). Amazonian and neotropical plant communities on glacial time-scales: The failure of the aridity and refuge hypotheses. Quaternary Science Reviews, 19(1–5), 141–169

Colwell, R. K., Brehm, G., Cardelús, C. L., Gilman, A. C., & Longino, J. T. (2008). Global warming, elevational range shifts, and lowland biotic attrition in the wet tropics. Science, 322(5899), 258–261. https://doi.org/10.1126/science.1162547

Clark, P. U., Dyke, A. S., Shakun, J. D., Carlson, A. E., Clark, J., Wohlfarth, B., Mitrovica, J. X., Hostetler, S. W., & McCabe, A. M. (2009). The Last Glacial Maximum. Science, 325(5941), 710–714. https://doi.org/10.1126/science.1172873

De Frenne, P., Zellweger, F., Rodríguez-Sánchez, F., Scheffers, B. R., Hylander, K., Luoto, M., Vellend, M., Verheyen, K., & Lenoir, J. (2019). Global buffering of temperatures under forest canopies. Nature Ecology & Evolution, 3(5), 744–749. https://doi.org/10.1038/s41559-019-0842-1

Deutsch, C. A., Tewksbury, J. J., Huey, R. B., Sheldon, K. S., Ghalambor, C. K., Haak, D. C., & Martin, P. R. (2008). Impacts of climate warming on terrestrial ectotherms across latitude. Proceedings of the National Academy of Sciences of the United States of America, 105(18), 6668–6672. https://doi.org/10.1073/pnas.0709472105

Dinerstein, E., Olson, D., Joshi, A., Vynne, C., Burgess, N. D., Wikramanayake, E., Hahn, N., Palminteri, S., Hedao, P., Noss, R., Hansen, M., Locke, H., Ellis, E. C., Jones, B., Barber, C. V., Hayes, R., Kormos, C., Martin, V., Crist, E., Sechrest, W., Price, L., Baillie, J. E. M., Weeden, D., Suckling, K., Davis, C., Sizer, N., Moore, R., Thau, D., Birch, T., Potapov, P., Turubanova, S., Tyukavina, A., de Souza, N., Pintea, L., Brito, J. C., Llewellyn, O. A., Miller, A. G., Patzelt, A., Ghazanfar, S. A., Timberlake, J., Klöser, H., Shennan-Farpón, Y., Kindt, R., Barnekow Lillesø, J. P., van Breugel, P., Graudal, L., Voge, M., Al-Shammari, K. F., & Saleem, M. (2017). An ecoregion-based approach to protecting half the terrestrial realm. BioScience, 67(6), 534–545. https://doi.org/10.1093/biosci/bix014

Elith, J., & Leathwick, J. R. (2009). Species distribution models: Ecological explanation and prediction across space and time. Annual Review of Ecology, Evolution, and Systematics, 40, 677–697. https://doi.org/10.1146/annurev.ecolsys.110308.120159

Elith, J., Graham, C. H., Anderson, R. P., Dudík, M., Ferrier, S., Guisan, A., Hijmans, R. J., Huettmann, F., Leathwick, J. R., Lehmann, A., Li, J., Lohmann, L. G., Loiselle, B. A., Manion, G., Moritz, C., Nakamura, M., Nakazawa, Y., Overton, J. M. C., Peterson, A. T., Phillips, S. J., Richardson, K., Scachetti-Pereira, R., Schapire, R. E., Soberón, J., Williams, S., Wisz, M. S., & Zimmermann, N. E. (2006). Novel methods improve prediction of species' distributions from occurrence data. Ecography, 29(2), 129–151. https://doi.org/10.1111/j.2006.0906-7590.04596.x

Elith, J., Phillips, S.J., Hastie, T., Dudík, M., Chee, Y.E. and Yates, C.J. (2011), A statistical explanation of MaxEnt for ecologists. Diversity and Distributions, 17: 43-57. https://doi.org/10.1111/j.1472-4642.2010.00725.x

Esser, L. F., Neves, D., & Jarenkow, J. A. (2024). Species persistence and climatic stability have shaped plant communities of the Atlantic forest biodiversity hotspot. Plant Ecology and Diversity. https://doi.org/10.1080/17550874.2024.2396285

Flantua, S. G. A., Hooghiemstra, H., Grimm, E. C., Behling, H., Bush, M. B., González-Arango, C., Gosling, W. D., Ledru, M.-P., Lozano-García, S., Maldonado, A., Prieto, A. R., Rull, V., & Van Boxel, J. H. (2015). Updated site compilation of the Latin American Pollen Database. Review of Palaeobotany and Palynology, 223, 104–115. http://dx.doi.org/10.1016/j.revpalbo.2015.09.008

Flores, B.M., Montoya, E., Sakschewski, B. et al. Critical transitions in the Amazon forest system. Nature 626, 555–564 (2024). https://doi.org/10.1038/s41586-023-06970-0

Fordham, D. A., Saltré, F., Haythorne, S., Wigley, T. M. L., Otto-Bliesner, B. L., Chan, K. C., & Brook, B. W. (2017). PaleoView: A tool for generating continuous climate projections spanning the last 21,000 years at regional and global scales. Ecography, 40(11), 1348–1358. https://doi.org/10.1111/ecog.03031

GBIF. Global Biodiversity Information Facility. Disponível em: <https://www.gbif.org>. Acesso em: 5 dez. 2024.

Gatti, L.V., Basso, L.S., Miller, J.B. et al. Amazonia as a carbon source linked to deforestation and climate change. Nature 595, 388–393 (2021). https://doi.org/10.1038/s41586-021-03629-6

Guillera-Arroita, G., Lahoz-Monfort, J. J., Elith, J., Gordon, A., Kujala, H., Lentini, P. E., McCarthy, M. A., Tingley, R., & Wintle, B. A. (2015). Matching distribution models to applications. Global Ecology and Biogeography, 24(3), 276–292. https://doi.org/10.1111/geb.12268

Guisan, A., & Zimmermann, N. E. (2000). Predictive habitat distribution models in ecology. Ecological Modelling, 135(2–3), 147–186

Häggi, C., Chiessi, C. M., Merkel, U., Mulitza, S., Prange, M., Schulz, M., & Schefuß, E. (2017). Response of the Amazon rainforest to late Pleistocene climate variability. Earth and Planetary Science Letters, 479, 50–59. https://doi.org/10.1016/j.epsl.2017.09.013

Heine, K. (2024). The Quaternary in the Tropics: A Reconstruction of the Palaeoclimate. Springer Cham. https://doi.org/10.1007/978-3-031-31921-1

Hegerl, G., & Stott, P. (2014). Atmospheric science: From past to future warming. Science, 343(6173), 844–845. https://doi.org/10.1126/science.1249368

Hermanowski, B., da Costa, M. L., & Behling, H. (2012). Environmental changes in southeastern Amazonia during the last 25,000 yr revealed from a paleoecological record. Quaternary Research, 77(1), 138–148. https://doi.org/10.1016/j.yqres.2011.10.009

Hijmans, R. J., Cameron, S. E., Parra, J. L., Jones, P. G., & Jarvis, A. (2005). Very high resolution interpolated climate surfaces for global land areas. International Journal of Climatology, 25(15), 1965–1978. https://doi.org/10.1002/joc.1276

Hijmans, R. J., Phillips, S. J., Leathwick, J., & Elith, J. (2018). dismo: Species distribution modeling (R package version). https://CRAN.R-project.org/package=dismo

Hirata, A., Ohashi, H., Hasegawa, T. et al. The choice of land-based climate change mitigation measures influences future global biodiversity loss. Commun Earth Environ 5, 259 (2024). https://doi.org/10.1038/s43247-024-01433-4

Hubau, W., Lewis, S.L., Phillips, O.L. et al. Asynchronous carbon sink saturation in African and Amazonian tropical forests. Nature 579, 80–87 (2020). https://doi.org/10.1038/s41586-020-2035-0

IPCC. (2023). Summary for Policymakers. In H. Lee & J. Romero (Eds.), Climate Change 2023: Synthesis Report. Contribution of Working Groups I, II and III to the Sixth Assessment Report of the Intergovernmental Panel on Climate Change (pp. 1–34). IPCC. https://doi.org/10.59327/IPCC/AR6-9789291691647.001

Jaeschke, A., Rühlemann, C., Arz, H., Heil, G., & Lohmann, G. (2007). Coupling of millennial-scale changes in sea surface temperature and precipitation off northeastern Brazil with high-latitude climate shifts during the last glacial period. Paleoceanography, 22(4), PA4206. https://doi.org/10.1029/2006PA001391

Jiménez, L., & Soberón, J. (2020). Leaving the area under the receiving operating characteristic curve behind: An evaluation method for species distribution modelling applications based on presence-only data. Methods in Ecology and Evolution, 11(12), 1571–1586. https://doi.org/10.1111/2041-210X.13479

Joly, C.A., Metzger, J.P. and Tabarelli, M. (2014), Experiences from the Brazilian Atlantic Forest: ecological findings and conservation initiatives. New Phytol, 204: 459-473. https://doi.org/10.1111/nph.12989

Jucker, T., Hardwick, S. R., Both, S., Elias, D. M. O., Ewers, R. M., Milodowski, D. T., Swinfield, T., & Coomes, D. A. (2018). Canopy structure and topography jointly constrain the microclimate of human-modified tropical landscapes. Global Change Biology, 24(11), 5243–5258. https://doi.org/10.1111/gcb.14415

Justino, F., Stordal, F., Kucharski, F., & Pezzi, L. P. (2008). Influence of boundary conditions on the Southern Hemisphere atmospheric circulation during the Last Glacial Maximum. Revista Brasileira de Meteorologia, 23(4), 490–500. https://doi.org/10.1590/S0102-77862008000400008

Karger, D., Conrad, O., Böhner, J. et al. Climatologies at high resolution for the earth's land surface areas. Sci Data 4, 170122 (2017). https://doi.org/10.1038/sdata.2017.122

Kelley, D.I., Sato, H., Ecker, M. et al. Niche-dependent forest and savanna fragmentation in Tropical South America during the Last Glacial Maximum. npj biodivers 3, 23 (2024). https://doi.org/10.1038/s44185-024-00056-4

Kelly, T. J., Lawson, I. T., Roucoux, K. H., Baker, T. R., Jones, T. D., & Sanderson, N. K. (2017). The vegetation history of an Amazonian domed peatland. Palaeogeography, Palaeoclimatology, Palaeoecology, 468, 129–141. https://doi.org/10.1016/j.palaeo.2016.11.039

Kramer-Schadt, S., Niedballa, J., Pilgrim, J. D., Schröder, B., Lindenborn, J., Reinfelder, V., Stillfried, M., Heckmann, I., Scharf, A. K., Augeri, D. M., Cheyne, S. M., Hearn, A. J., Ross, J., Macdonald, D. W., Mathai, J., Eaton, J., Marshall, A. J., Semiadi, G., & Wilting, A. (2013). The importance of correcting for sampling bias in MaxEnt species distribution models. Diversity and Distributions, 19(11), 1366–1379. https://doi.org/10.1111/ddi.12096

Ledru, M.-P., Mourguiart, P., & Riccomini, C. (2009). Related changes in biodiversity, insolation and climate in the Atlantic rainforest since the last interglacial. Palaeogeography, Palaeoclimatology, Palaeoecology, 271(1-2), 140–152. https://doi.org/10.1016/j.palaeo.2008.10.008

Liu, C., White, M., & Newell, G. (2013). Selecting thresholds for the prediction of species occurrence with presence-only data. Journal of Biogeography, 40(4), 778–789. https://doi.org/10.1111/jbi.12058

Maezumi, S.Y., D. Alves, M. Robinson, J.G. de Souza, C. Levis, R.L. Barnett, E.A. de Oliveira, D. Urrego, D. Schaan, and J. Iriarte. 2018a. The legacy of 4,500 years of polyculture agroforestry in the eastern Amazon. Nature Plants 4(8):540-547. [DOI: 10.1038/s41477-018-0205-y]

Maezumi, S.Y., M. Robinson, J. de Souza, D.H. Urrego, D. Schaan, D. Alves, and J. Iriarte. 2018b. New insights from pre-Columbian land use and fire management in Amazonian dark earth forests. Frontiers in Ecology and Evolution 6:111. [DOI: 10.3389/fevo.2018.00111]

Maksic, J., Venancio, M., Shimizu, M. H., Chiessi, C. M., Piacsek, P., Sampaio, G., Cruz, F. W., & Alexandre, F. F. (2022). Brazilian biomes distribution: Past and future. Palaeogeography, Palaeoclimatology, Palaeoecology, 585, 110717. https://doi.org/10.1016/j.palaeo.2021.110717

Malhi, Y., Roberts, J. T., Betts, R. A., Killeen, T. J., Li, W., & Nobre, C. A. (2008). Climate change, deforestation, and the fate of the Amazon. Science, 319(5860), 169–172. https://doi.org/10.1126/science.1146961

Markesteijn, L., & Poorter, L. (2009). Seedling root morphology and biomass allocation of 62 tropical tree species in relation to drought- and shade-tolerance. Journal of Ecology, 97(2), 311–325. https://doi.org/10.1111/j.1365-2745.2008.01466.x

Matricardi, E. A. T., Skole, D. L., Costa, O., Pedlowski, M. A., Samek, J. H., & Miguel, E. P. (2020). Long-term forest degradation surpasses deforestation in the Brazilian Amazon. Science, 369(6509), 1378–1382. https://doi.org/10.1126/science.abb3021

Merow, C., Smith, M.J. and Silander, J.A., Jr (2013), A practical guide to MaxEnt for modeling species' distributions: what it does, and why inputs and settings matter. Ecography, 36: 1058-1069. https://doi.org/10.1111/j.1600-0587.2013.07872.x

Montade, V., Ledru, M.-P., Giesecke, T., Flantua, S. G., Behling, H., & Peyron, O. (2019). A new modern pollen dataset describing the Brazilian Atlantic Forest. The Holocene, 29(8), 1253-1262. https://doi.org/10.1177/0959683619846981

Mulitza, S., Zhang, Y., Regenberg, M., Butzin, M., Prange, M., Nuernberg, D., Steph, S., Tjallingii, R., Batenburg, S. J., Rühlemann, C., & Lohmann, G. (2017). Synchronous and proportional deglacial changes in Atlantic meridional overturning and northeast Brazilian precipitation. Paleoceanography, 32(6), 622–633. https://doi.org/10.1002/2017PA003084

Naimi, B. and Araújo, M.B. (2016), sdm: a reproducible and extensible R platform for species distribution modelling. Ecography, 39: 368-375. https://doi.org/10.1111/ecog.01881

Oliveira-Filho, A. T., & Fontes, M. A. L. (2000). Patterns of floristic differentiation among Atlantic forests in southeastern Brazil and the influence of climate. Biotropica, 32(4), 793–810. https://doi.org/10.1646/0006-3606(2000)032[0793:POFDAA]2.0.CO;2

Pancost, R. (2017). Climate change narratives. Nature Geoscience, 10(7), 466–468. https://doi.org/10.1038/ngeo2981

Pearson, R. G., Raxworthy, C. J., Nakamura, M., & Peterson, A. T. (2007). Predicting species distributions from small numbers of occurrence records: A test case using cryptic geckos in Madagascar. Journal of Biogeography, 34(1), 102–117. https://doi.org/10.1111/j.1365-2699.2006.01594.x

Peterson, A. T., Soberón, J., Pearson, R. G., Anderson, R. P., Martínez-Meyer, E., Nakamura, M., & Araújo, M. B. (2011). Ecological Niches and Geographic Distributions. Princeton University Press

Peterson, A. T., Soberón, J., & Sánchez-Cordero, V. (1999). Conservatism of ecological niches in evolutionary time. Science, 285(5431), 1265–1267. https://doi.org/10.1126/science.285.5431.1265

Petit, J. R., Jouzel, J., Raynaud, D., Barkov, N. I., Barnola, J. M., Basile, I., Bender, M., Chappellaz, J., Davis, M., Delaygue, G., Delmotte, M., Kotlyakov, V. M., Legrand, M., Lipenkov, V. Y., Lorius, C., Pépin, L., Ritz, C., Saltzman, E., & Stievenard, M. (1999). Climate and atmospheric history of the past 420,000 years from the Vostok ice core, Antarctica. Nature, 399(6735), 429–436. https://doi.org/10.1038/20859

Phillips, S. J., Anderson, R. P., & Schapire, R. E. (2006). Maximum entropy modeling of species geographic distributions. Ecological Modelling, 190(3–4), 231–259. https://doi.org/10.1016/j.ecolmodel.2005.03.026

Phillips, S.J. and Dudík, M. (2008), Modeling of species distributions with Maxent: new extensions and a comprehensive evaluation. Ecography, 31: 161-175. https://doi.org/10.1111/j.0906-7590.2008.5203.x

Phillips, S. J., Anderson, R. P., Dudík, M., Schapire, R. E., & Blair, M. E. (2017). Opening the black box: An open-source release of Maxent. Ecography, 40(7), 887–893. https://doi.org/10.1111/ecog.03049

Pinaya, J. L. D., Cruz, F. W., Ceccantini, G. C. T., Corrêa, P. L. P., Pitman, N., Vemado, F., Lopez, M. S., Pereira Filho, A. J., Grohmann, C. H., Chiessi, C. M., Stríkis, N. M., & De Oliveira, P. E. (2019). Brazilian montane rainforest expansion induced by Heinrich Stadial 1 event. Scientific Reports, 9(17912). (2019) 9:17912 | https://doi.org/10.1038/s41598-019-53036-1

Pinaya, J. L. D., Pitman, N. C. A., Cruz, F. W., Akabane, T. K., Sanz Lopez, M. C., Pereira-Filho, A. J., Grohmann, C. H., Reis, L. S., Rodrigues, E. S. F., Ceccantini, G. C. T., & De Oliveira, P. E. (2024). Humid and cold forest connections in South America between the eastern Andes and the southern Atlantic coast during the LGM. Scientific Reports, 14(2080). https://doi.org/10.1038/s41598-024-51763-8

Qin, Y., Xiao, X., Dong, J. et al. Improved estimates of forest cover and loss in the Brazilian Amazon in 2000–2017. Nat Sustain 2, 764–772 (2019). https://doi.org/10.1038/s41893-019-0336-9

Reboita, M.S., Kuki, C.A.C., Marrafon, V.H. et al. South America climate change revealed through climate indices projected by GCMs and Eta-RCM ensembles. Clim Dyn 58, 459–485 (2022). https://doi.org/10.1007/s00382-021-05918-2

Rezende, C. L., Scarano, F. R., Assad, E. D., Joly, C. A., Metzger, J. P., Strassburg, B. B. N., et al. (2018). From hotspot to hopespot: An opportunity for the Brazilian Atlantic Forest. Perspectives in Ecology and Conservation, 16(4), 208–214. https://doi.org/10.1016/j.pecon.2018.10.002

Rodríguez-Zorro, P.A., B. Turcq, R.C. Cordeiro, L.S. Moreira, R.L. Costa, C.H. McMichael, and H. Behling. 2018. Forest stability during the early and late Holocene in the igapó floodplains of the Rio Negro, northwestern Brazil. Quaternary Research 89(1):75-89. [DOI: doi:10.1017/qua.2017.99]

Rodríguez-Zorro, P.A., M.-P. Ledru, E. Bard, O. Aquino-Alfonso, A. Camejo, A.-L. Daniau, C. Favier, M. Garcia, T.D. Mineli, F. Rostek, F. Ricardi-Branco, A.O. Sawakuchi, Q. Simon, K. Tachikawa, and N. Thouveny. 2020. Shut down of the South American summer monsoon during the penultimate glacial. Scientific Reports 10(6275). [DOI: https://doi.org/10.1038/s41598-020-62888-x 2]

Staal, A., Tuinenburg, O.A., Bosmans, J.H.C. et al. Forest-rainfall cascades buffer against drought across the Amazon. Nature Clim Change 8, 539–543 (2018). https://doi.org/10.1038/s41558-018-0177-y

Scheffers, B. R., Edwards, D. P., Macdonald, S. L., Senior, R. A., Andriamahohatra, L. R., Roslan, N., Rogers, A. M., Haugaasen, T., Wright, P., & Williams, S. E. (2017).

Extreme thermal heterogeneity in structurally complex tropical rain forests. Biotropica, 49(1), 35–44. https://doi.org/10.1111/btp.12355

Sifeddine, A., Martin, L., Turcq, B., Volkmer-Ribeiro, C., Soubies, F., Cordeiro, R.C. and Suguio, K. (2001) Variations of the Amazonian Rainforest Environment: A Sedimentological Record Covering 30,000 Years. Palaeogeography, Palaeoclimatology, Palaeoecology, 168, 221-235.

Soberón, J., & Peterson, A. T. (2005). Interpretation of models of fundamental ecological niches and species distributional areas. Biodiversity Informatics, 2, 1–10. https://doi.org/10.17161/bi.v2i0.4

Sobral-Souza, T., Vancine, M. H., Ribeiro, M. C., & Lima-Ribeiro, M. S. (2018). Efficiency of protected areas in Amazon and Atlantic Forest conservation: A spatio-temporal view. Acta Oecologica, 87, 1–7. https://doi.org/10.1016/j.actao.2018.01.001

Stute, M., Forster, M., Frischkorn, H., Serejo, A., Clark, J. F., Schlosser, P., Broecker, W. S., & Bonani, G. (1995). Cooling of tropical Brazil (5°C) during the Last Glacial Maximum. Science, 269(5222), 379–383. https://doi.org/10.1126/science.269.5222.379

Sylvestre, F. (2009). Moisture pattern during the Last Glacial Maximum in South America. In F. Vimeux, F. Sylvestre, & M. Khodri (Eds.), Past Climate Variability in South America and Surrounding Regions (pp. 3–27). Developments in Paleoenvironmental Research, 14. https://doi.org/10.1007/978-90-481-2672-9_1

ter Steege, H., Pitman, N. C. A., Killeen, T. J., Laurance, W. F., Peres, C. A., Guevara, J. E., ... & Silman, M. R. (2015). Estimating the global conservation status of more than 15,000 Amazonian tree species. Science Advances, 1(10), e1500936. https://doi.org/10.1126/sciadv.1500936

Tierney, J. E., Poulsen, C. J., Montañez, I. P., Bhattacharya, T., Feng, R., Ford, H. L., Hönisch, B., Inglis, G. N., Petersen, S. V., Sagoo, N., Tabor, C. R., Thirumalai, K., Zhu, J., & Zhang, Y. G. (2020). Past climates inform our future. Science, 370(6517), eaay3701. https://doi.org/10.1126/science.aay3701

Thompson, L. G., Mosley-Thompson, E., Davis, M. E., Lin, P.-N., Henderson, K. A., Cole-Dai, J., Bolzan, J. F., & Liu, K.-B. (1995). Late Glacial Stage and Holocene tropical ice core records from Huascarán, Peru. Science, 269(5220), 46–50. https://doi.org/10.1126/science.269.5220.46

Tuomisto, H. and Ruokolainen, K. (1994), Distribution of Pteridophyta and Melastomataceae along an edaphic gradient in an Amazonian rain forest. Journal of Vegetation Science, 5: 25-34. https://doi.org/10.2307/3235634

Urrego, D.H., Bush, M.B., Silman, M.R., Niccum, B.A., De La Rosa, P., McMichael, C.H., Hagen, S. e Palace, M. (2012). "Holocene fires, forest stability and human occupation in south-western Amazonia." Journal of Biogeography, 39(3), 521-533

Urrego, L.E., and J.C. Berrio. 2011. Los estudios paleoecológicos en el Chocó biogeográfico durante el Holoceno medio y reciente. Pages 23-38 in J.O. Rangel, editor. Colombia Diversidad Biótica IV, El Chocó biogeográfico/Costa Pacífica. Universidad Nacional de Colombia, Conservación Internacional, Bogotá D.C., Colombia.

Valavi, R., G. Guillera-Arroita, J. J. Lahoz-Monfort, and J. Elith. 2022. Predictive performance of presence-only species distribution models: a benchmark study with reproducible code. Ecological Monographs 92(1):e01486. 10.1002/ecm.1486

Vancine, M. H., Muylaert, R. L., Niebuhr, B. B., Oshima, J. E. F., Tonetti, V., Bernardo, R., De Angelo, C., Rosa, M. R., Grohmann, C. H., & Ribeiro, M. C. (2024). The Atlantic Forest of South America: Spatiotemporal dynamics of the vegetation and implications for conservation. Biological Conservation, 291, 110499. https://doi.org/10.1016/j.biocon.2024.110499

Vasconcellos, M. M., Varela, S., Reginato, M., Gehara, M., Carnaval, A. C., & Michelangeli, F. A. (2024). Evaluating the impact of historical climate and early human groups in the Araucaria Forest of eastern South America. Ecography, 47, e06756. doi: 10.1111/ecog.06756

Veloz, S. D. (2009). Spatially autocorrelated sampling falsely inflates measures of accuracy for presence-only niche models. Journal of Biogeography, 36(12), 2290–2299. https://doi.org/10.1111/j.1365-2699.2009.02174.x

Wang, X., Auler, A. S., Edwards, R. L., Cheng, H., Cristalli, P. S., Smart, P. L., Richards, D. A., & Shen, C.-C. (2004). Wet periods in northeastern Brazil over the past 210 kyr linked to distant climate anomalies. Nature, 432(7018), 740–743. https://doi.org/10.1038/nature03067

Whitney, B. S., Mayle, F. E., Punyasena, S. W., Fitzpatrick, K. A., Burn, M. J., Guillen, R., Chavez, E., Mann, D., Pennington, R. T., & Metcalfe, S. E. (2011). A 45kyr palaeoclimate record from the lowland interior of tropical South America. Palaeogeography, Palaeoclimatology, Palaeoecology, 307(1), 177–192. https://doi.org/10.1016/j.palaeo.2011.05.012

Wiens, J. J., & Graham, C. H. (2005). Niche conservatism: Integrating evolution, ecology, and conservation biology. Annual Review of Ecology, Evolution, and Systematics, 36, 519–539. https://doi.org/10.1146/annurev.ecolsys.36.102803.095431

Williams, J.W., Grimm, E.G., Blois, J., Charles, D.F., Davis, E., Goring, S.J., Graham, R., Smith, A.J., Anderson, M., Arroyo-Cabrales, J., Ashworth, A.C., Betancourt, J.L., Bills, B.W., Booth, R.K., Buckland, P., Curry, B., Giesecke, T., Hausmann, S., Jackson, S.T., Latorre, C., Nichols, J., Purdum, T., Roth, R.E., Stryker, M., Takahara, H., 2018. The Neotoma Paleoecology Database: A multi-proxy, international community-curated data resource. Quaternary Research 89, 156-177.

Xu, T., & Hutchinson, M. F. (2013). New developments and applications in the ANUCLIM spatial climatic and bioclimatic modelling package. Environmental Modelling & Software, 40, 267–279. https://doi.org/10.1016/j.envsoft.2012.08.002

3. Chapter 3 - Climatic Suitability Projections and Potential Distribution of Tropical and Subtropical Moist Broadleaf Forests in South America under Future Socioeconomic Scenarios (2021–2100)

Abstract

Tropical and Subtropical Moist Broadleaf Forests (TSMBF) in South America play a crucial role in biodiversity conservation and continental climate regulation. This study investigated the potential distribution of these forest formations under contemporary climate conditions (1970–2000) and future projections (2021–2100), using ecological niche modeling with the MaxEnt algorithm and CMIP6 climate scenarios (SSP1–2.6, SSP2–4.5, SSP3–7.0, and SSP5–8.5). Results indicate that current areas of highest climatic suitability are concentrated in central and western Amazonia and in fragments of the Atlantic Forest. The most influential variables in the models were isothermality (BIO3), and temperature and precipitation during critical quarters (BIO2, BIO8, BIO18, and BIO19). Projections reveal a pattern of increasing contraction and fragmentation of TSMBF throughout the 21st century, with high-emission scenarios (SSP3–7.0 and SSP5–8.5) leading to substantial losses in climatic suitability, especially along the eastern and southern Amazon margins and across most of the Atlantic Forest. These patterns imply a high risk to ecological resilience, connectivity, and the maintenance of ecosystem services. The persistence of suitable core areas in more conservative scenarios (SSP1–2.6) underscores the importance of ambitious climate policies, ecological restoration, and the expansion of protected areas to mitigate the impacts of climate change on South American tropical forests.

Keywords: Climate change; ecological niche modeling; MaxEnt; tropical forest; Amazon; Atlantic Forest; SSP scenarios; climatic suitability; fragmentation; conservation.

1. INTRODUCTION

Tropical and subtropical broadleaf forests are globally recognized for their biodiversity and their crucial role in regulating the Earth's climate (Borma et al., 2022; Marques et al., 2021; Anjos et al., 2021; Koch & Kaplan, 2022). In South America, the main representatives of this biome, the vast Amazon Rainforest and the remnants

of the Atlantic Forest, cover extensive areas and host a significant portion of the planet's biological richness (Vancine et al., 2024; Marques et al., 2021; Anjos et al., 2021). The Atlantic Forest, for example, is considered one of the most threatened biodiversity hotspots in the world (Myers et al., 2000; Rezende et al., 2018; Ribeiro et al., 2009; Vancine et al., 2024).

However, these vital ecosystems are increasingly threatened by environmental changes, including rising surface temperatures and altered precipitation patterns observed over the past century (Almazroui et al., 2021; Anjos et al., 2021; Reboita et al., 2022). Future climate projections indicate a continuing trend of widespread warming and reduced moisture across much of tropical South America, with potentially severe impacts on forest biomes (Anjos et al., 2021). Such climatic changes, manifested through extreme events such as more frequent and intense droughts, floods, and wildfires (Almazroui et al., 2021; Filho, 2024; Reboita et al., 2022), may fundamentally alter the environmental conditions that define the potential distribution of biomes and species (Anjos et al., 2021).

Ecological niche modeling (also known as species distribution modeling – SDMs) is a well-established tool for assessing environmental suitability for species or biomes based on their relationships with climatic and environmental variables (Miranda et al., 2019; Sales et al., 2021; Tonetti et al., 2024). By projecting these relationships onto future climate scenarios, it is possible to estimate potential changes in the distribution and extent of suitable habitats under different greenhouse gas emission trajectories (Miranda et al., 2019; Sales et al., 2021; Tonetti et al., 2024). The Shared Socioeconomic Pathways (SSPs) from the CMIP6 project (Eyring et al., 2016; O'Neill et al., 2016, 2017) offer a spectrum of climate futures, ranging from low mitigation (SSP1–2.6) to high emissions and limited mitigation (SSP5–8.5) (O'Neill et al., 2017; Moss et al., 2010; Van Vuuren et al., 2011), allowing for the analysis of ecosystem sensitivity to varying degrees of global warming (Anjos et al., 2021; Almazroui et al., 2021).

Understanding how future climate change will affect the potential distribution of TSMBF in South America is essential for informing conservation and adaptation strategies (Miranda et al., 2019), given their importance for biodiversity, ecosystem services, and climate regulation on both continental and global scales (Borma et al., 2022; Marques et al., 2021; Anjos et al., 2021; Koch & Kaplan, 2022). Projected drier

conditions and rising temperatures are critical factors that may lead to the contraction and fragmentation of these forests (Anjos et al., 2021; Almazroui et al., 2021).

In this context, the present study aimed to model the potential distribution of Tropical and Subtropical Moist Broadleaf Forests (TSMBF) in South America under contemporary (1970–2000) and future climatic conditions (2021–2040, 2041–2060, 2061–2080, and 2081–2100), using ecological niche modeling (MaxEnt) and climate projections from multiple emission scenarios (SSP1–2.6, SSP2–4.5, SSP3–7.0, and SSP5–8.5). We analyzed the influence of bioclimatic variables on the current distribution and assessed the magnitude and spatial patterns of projected changes throughout the 21st century, focusing on implications for the extent, climatic suitability, and connectivity of these forests under different climate futures.

2. MATERIALS AND METHODS

2.1 Study Area

Accurate delineation of study areas is essential for analyzing biodiversity patterns, species distributions, and the effects of climatic and anthropogenic changes on ecosystems. While traditional biome classifications are commonly used in ecological and conservation research, they present limitations when addressing internal ecosystem variability or historical environments without direct modern analogs (Flantua et al., 2015).

To overcome these constraints, this study employed the Ecoregions2017 database (Dinerstein et al., 2017), which divides the planet into 846 ecoregions, offering a more detailed depiction of environmental heterogeneity within biomes.

The focus of this research was the Tropical and Subtropical Moist Broadleaf Forests (TSMBF) ecoregion in South America, encompassing the Amazon and Atlantic rainforest biomes (Dinerstein et al., 2017). These biomes are vital for regional and global climate regulation (Staal et al., 2018; Vancine et al., 2024), are recognized as biodiversity hotspots (Myers et al., 2000), and are increasingly threatened by climate change and deforestation (Hubau et al., 2020; Artaxo et al., 2022). (Refer to Figure 2 on page 25)

The Amazon, situated in northern South America, is marked by high humidity and warm temperatures, playing a vital role in regulating the region’s hydrological cycles (Borma et al., 2022). It harbors exceptional biodiversity, with around 16,000 tree species and approximately 10% (Mittermeier et al., 2003) of the world’s

vertebrate and vascular plant species (ter Steege et al., 2020). The Amazon contributes to up to 50% of local rainfall and is key to the distribution of moisture across South America, as air masses are diverted by the Andes toward the southwest, supporting the formation of the South Atlantic Convergence Zone (Staal et al., 2018; Flantua et al., 2016). Notably, the ongoing degradation of its forests now surpasses the impact of direct deforestation in terms of carbon emissions (Qin et al., 2021; Flores et al., 2024).

The Atlantic Forest, in contrast, comprises a range of ecosystems, from seasonally dry to evergreen forests, stretching along Brazil's coastline from the northeast to the south. It experiences notable climatic variation, with humid summers and dry winters influenced by shifts in the Intertropical Convergence Zone (ITCZ) that drive the South American monsoon system (Ledru et al., 2009; Montade et al., 2019). Despite being heavily fragmented today, undermining ecological connectivity and the delivery of ecosystem services (Vancine et al., 2024), it remains critically important for biodiversity conservation and climate regulation, especially in areas with pronounced seasonality (Rezende et al., 2018; Grantham et al., 2020).

2.2 Taxa Selection

This analysis was based on ten previously published pollen-based paleoecological studies distributed across the study area, all retrieved from the Neotoma Paleoecology Database (Williams et al., 2018) (Refer to Figure 2 and Table 1 on page 25). These sites were selected because they span the majority of the temporal intervals addressed in this study.

A total of 1.500 taxa were initially compiled from the selected studies, excluding aquatic species, ferns, and non-native taxa. The dataset was then standardized to a consistent taxonomic level and nomenclature to allow reliable comparison and further analyses.

Assuming that the structural composition of both biomes has remained relatively stable over time, we retained 145 taxa that best represent the local vegetation richness throughout the studied periods.

The current spatial occurrences of these 145 taxa were then compiled and downloaded from the Global Biodiversity Information Facility (GBIF, 2024) (see Supplementary Material 2).

2.2.1 Occurrence Data and Processing

Taxa occurrences were filtered to retain only those whose coordinates fell within the boundaries of the Tropical and Subtropical Moist Broadleaf Forests (TSMBF) ecoregions. This ensured that all analyses remained focused on the target region. Subsequently, a series of spatial filtering steps were applied to balance the geographic distribution of records and minimize clustering in over-sampled areas.

Ten bounding boxes were defined to geographically constrain the search for modern records of the 145 selected taxa in GBIF, allowing only occurrences within predefined regions to be included.

Within each bounding box, a maximum of 1.000 occurrence records per taxon was retrieved, resulting in a total of 1.092.678 initial records. This approach helps reduce taxonomic overrepresentation, limits spatial bias, and aligns with best practices in species distribution modeling (Boria et al., 2014; Kramer-Schadt et al., 2013; Phillips et al., 2006).

A data cleaning step was then performed to remove duplicates, georeferencing errors, and records outside the study area, which reduced the dataset to 234.65 occurrences.

To further minimize spatial autocorrelation and ensure data independence, a minimum distance of 100 km between occurrence points was applied using the thinning procedure from the SpThin package in R (Aiello-Lammens et al., 2015). This threshold was empirically chosen to preserve the ecological integrity of the dataset while reducing redundancy, in accordance with recommendations from Veloz (2009), Boria et al. (2014), and Aiello-Lammens et al. (2015). Thinning is widely used in ecological modeling to eliminate spatial bias by removing closely spaced records, thereby preventing overestimation of environmental suitability in heavily sampled regions. The thin() function applies a randomization algorithm that retains the maximum number of records while ensuring the specified minimum distance between neighboring points.

The final dataset consisted of 1.085 spatially filtered occurrences (Supplementary Material 2), representing 145 families, 487 genera, and 863 species, providing a comprehensive taxonomic representation of tropical and subtropical forest flora.

2.2.2 Climate data

In this study, 19 bioclimatic variables (BIO1–BIO19) were used, which are widely applied in ecological research as they represent annual trends, seasonality, and extreme climatic conditions relevant to species distribution (Table 2). These variables were derived from monthly data on minimum, mean, and maximum temperature, as well as precipitation, provided by WorldClim version 2.1, a set of interpolated climate layers for global land areas, representing the average conditions for the period 1970–2000, at a spatial resolution of 10 arc-minutes (~340 km²) (Fick & Hijmans, 2017).

The bioclimatic variables were generated using the biovars() function from the dismo package in R (Hijmans et al., 2018), based on monthly climate series. These variables are considered biologically meaningful, as they reflect environmental conditions that directly influence species physiology, tolerance, and potential distribution.

Table 2 – List of bioclimatic variables (Fick & Hijmans, 2017).

Variable	Description	Unit
BIO1	Annual Mean Temperature	°C
BIO2	Mean Diurnal Range (Mean of monthly [max temp - min temp])	°C
BIO3	Isothermality (BIO2/BIO7 × 100)	%
BIO4	Temperature Seasonality (standard deviation × 100)	°C × 100
BIO5	Max Temperature of Warmest Month	°C
BIO6	Min Temperature of Coldest Month	°C
BIO7	Temperature Annual Range (BIO5 - BIO6)	°C
BIO8	Mean Temperature of Wettest Quarter	°C
BIO9	Mean Temperature of Driest Quarter	°C
BIO10	Mean Temperature of Warmest Quarter	°C
BIO11	Mean Temperature of Coldest Quarter	°C
BIO12	Annual Precipitation	mm
BIO13	Precipitation of Wettest Month	mm
BIO14	Precipitation of Driest Month	mm
BIO15	Precipitation Seasonality (Coefficient of Variation)	%
BIO16	Precipitation of Wettest Quarter	mm

BIO17	Precipitation of Driest Quarter	mm
BIO18	Precipitation of Warmest Quarter	mm
BIO19	Precipitation of Coldest Quarter	mm

Future climate conditions were derived from five General Circulation Models (GCMs) from the Coupled Model Intercomparison Project Phase 6 (CMIP6): IPSL-CM6A-LR, ACCESS-CM2, EC-Earth3-Veg, MIROC6, and MPI-ESM1-2-HR. These models were selected for their relevance in simulating climate dynamics over South America and for providing consistent downscaled projections in the WorldClim 2.1 framework (Fick & Hijmans, 2017). The projections were carried out using an ensemble approach, combining these five GCMs across four emission scenarios (SSP1-2.6, SSP2-4.5, SSP3-7.0, and SSP5-8.5), allowing for a more robust assessment of future climatic conditions.

Each GCM was assessed under four Shared Socioeconomic Pathways (SSPs), representing distinct trajectories of greenhouse gas emissions and socioeconomic development. Projections were conducted for four future time slices spanning the 21st century: 2021–2040, 2041–2060, 2061–2080, and 2081–2100.

All bioclimatic variables for future scenarios were directly obtained from the WorldClim 2.1 database, ensuring consistency with CMIP6 models and compatibility with the spatial resolution used throughout this study. The model trained with present-day climatic conditions was projected across the four future time periods using each of the five selected GCMs and the four emission scenarios, allowing assessment of potential shifts in environmental suitability for the target vegetation types.

2.3 Ecological Niche Modeling Under Future Climate Scenarios

The potential distribution of Tropical and Subtropical Moist Broadleaf Forests (TSMBF) under future climate conditions was modeled using the Maximum Entropy algorithm (MaxEnt) (Phillips et al., 2006; Elith et al., 2011), which is widely used in ecological studies due to its effectiveness with presence-only data. The model was trained using present-day occurrences (1979–2013), based on the assumption of niche conservatism, i.e., that species ecological preferences remain stable through time (Peterson et al., 1999; Wiens & Graham, 2005).

Species occurrence records were obtained from the Global Biodiversity Information Facility (GBIF) and spatially filtered to reduce sampling bias and spatial autocorrelation. Bioclimatic variables were sourced from WorldClim version 2.1 (Fick & Hijmans, 2017), which provides high-resolution climate surfaces for the baseline period. Modeling was conducted using presence data along with 10.000 pseudo-absence points, randomly generated within the study area while avoiding overlap with known presence locations, as recommended by Phillips & Dudík (2008).

Model evaluation followed a 5-fold cross-validation approach, repeated five times with different random partitions to ensure generality and minimize overfitting. A total of five replicates was used, and model performance was assessed using the Area Under the Receiver Operating Characteristic Curve (AUC-ROC) (Fielding & Bell, 1997; Allouche et al., 2006), a widely adopted metric for predictive accuracy in species distribution modeling.

To enhance projection reliability, an ensemble model weighted by AUC values was generated using the best-performing replicates (ensemble(method = 'weighted', stat = 'auc')) (Valavi et al., 2022). Continuous suitability outputs were then converted into binary presence/absence maps using the Maximization of Sensitivity and Specificity (Max SSS) threshold (Liu et al., 2013), which balances omission and commission errors and showed higher spatial coherence with the Ecoregions2017 classification. Alternative thresholds, such as the Lowest Presence Threshold (LPT) (Pearson et al., 2007), were tested but proved more sensitive to outliers.

Although AUC is a standard metric in species distribution modeling, it has known limitations in presence-only contexts, especially in the absence of true absence data (Jiménez et al., 2020; Valavi et al., 2022). Therefore, the modeling strategy incorporated multiple complementary approaches, including AUC-based evaluation, cross-validation, and ensemble forecasting, to improve the robustness of predictions. However, ecological interpretation still requires careful contextual analysis and should not rely solely on statistical performance (Merow et al., 2013; Valavi et al., 2022).

MaxEnt is particularly suitable for paleoecological and future projections because of its capacity to handle sparse, incomplete, or biased data (Baldwin, 2009; Merow et al., 2013; Phillips & Dudík, 2008). It can model complex, nonlinear relationships between environmental variables and species occurrences by using a variety of feature transformations. Importantly, the method relies on comparing

environmental conditions at presence locations with those sampled across the background environment. However, spatial sampling bias may persist if background points are not adjusted accordingly. Strategies such as Target Group Sampling or the use of biased background priors may help align background data with known biases in occurrence records (Phillips & Dudík, 2008; Merow et al., 2013).

3. RESULTS

3.1 Models and Climatic Suitability (1970–2000)

The potential distribution modeling of the Tropical and Subtropical Moist Broadleaf Forests (TSMBF) under contemporary climatic conditions was performed using the MaxEnt algorithm, with five-fold cross-validation (k = 5) and an ensemble weighted by AUC values. The bioclimatic variables were obtained from the WorldClim 2 dataset (Fick & Hijmans, 2017), which provides high-resolution climate averages for the period 1970 to 2000.

Figure 2 presents the modeling results for the present-day scenario. The continuous suitability map (Figure 2-A) shows values ranging from 0 (unsuitable) to 1 (highly suitable). Areas of highest suitability are concentrated in central and western Amazonia, in stretches of northern South America, and in fragmented portions of the Atlantic Forest, especially in eastern Brazil, along the Atlantic coast, and in the southeastern region.

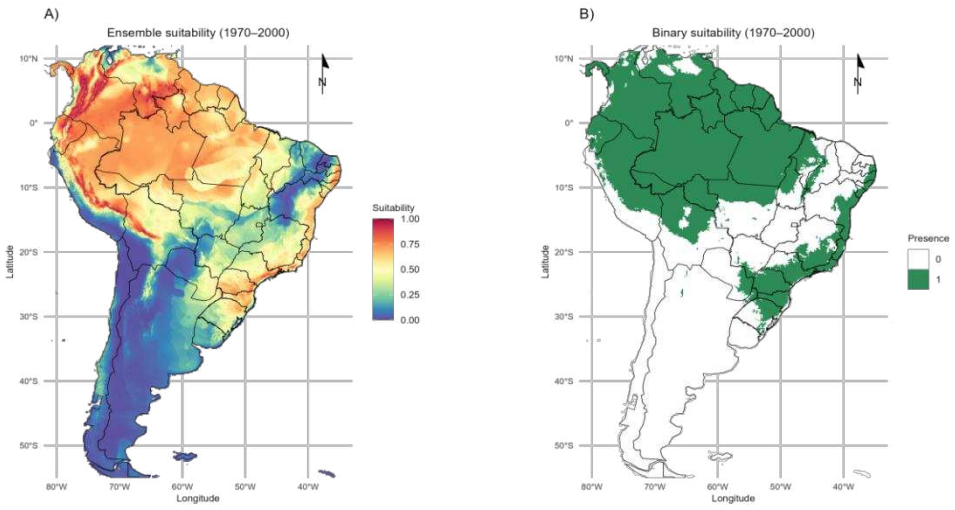

Figure 2. Climatic suitability distribution for the Tropical and Subtropical Moist Broadleaf Forests (TSMBF) in South America under the contemporary scenario (1970–2000).

In Figure 2-B, the binary map resulting from the application of the optimal threshold (threshold = 0.447) highlights areas of potential climatic presence of the vegetation. A broad continuous zone can be observed across the Amazon Basin, along with fragmented areas in southeastern and southern Brazil, corresponding to the remaining portions of the Atlantic Forest and southern moist forest formations.

The model yielded an AUC of 0.754, indicating good predictive performance. The analysis of the relative importance of bioclimatic variables (based on permutation using AUC) revealed that isothermality (BIO3) was the most influential variable, contributing 10.4%. This was followed by the mean temperature of the wettest quarter (BIO8) at 8.4%, precipitation of the coldest quarter (BIO19) at 7.3%, mean diurnal temperature range (BIO2) at 7.6%, and precipitation of the warmest quarter (BIO18) at 6.1%. Precipitation seasonality (BIO15) showed a marginal contribution of only 0.5%, indicating a lower relevance of this factor in the current model.

These results suggest that thermal stability and water availability during critical periods are the main climatic drivers of the current distribution of TSMBF, reflecting the ecological requirements for constant moisture and low thermal variability in these forest formations.

3.2 Future Climatic Patterns (2021–2040)

Future projections for the period 2021 to 2040 (Figure 3) reveal contrasting patterns of climatic suitability and potential presence in central Amazonia under different socioeconomic emission scenarios (SSP1-2.6, SSP2-4.5, SSP3-7.0, and SSP5-8.5), as illustrated in the following figure.

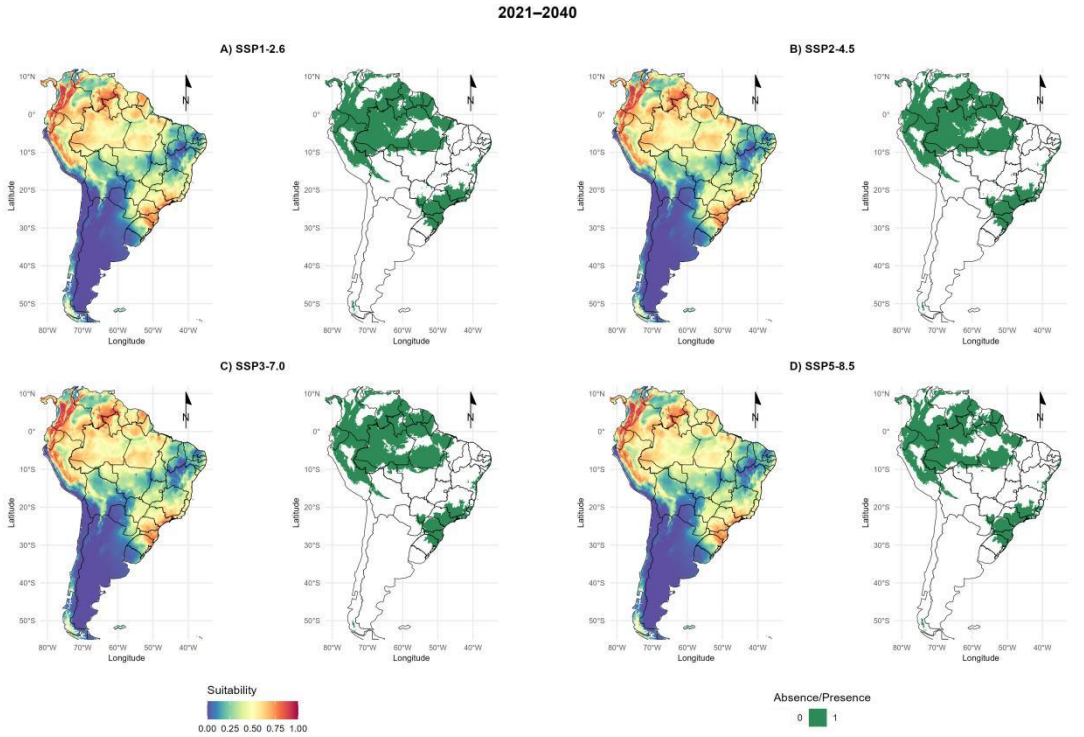

Figure 3. Projections of continuous climatic suitability (left) and binary potential presence (right) of the Tropical and Subtropical Moist Broadleaf Forests (TSMBF) in South America for the period 2021–2040, under four socioeconomic scenarios (SSPs): (A) SSP1-2.6, (B) SSP2-4.5, (C) SSP3-7.0, and (D) SSP5-8.5.

3.2.1 General Patterns of Suitability (2021–2040)

In the continuous maps, the largest areas of high climatic suitability are primarily concentrated in central Amazonia and in lowland regions along the Amazon Basin. Under all scenarios, a consistent pattern is also observed in the Atlantic Forest region. These areas appear in reddish tones, indicating environmental conditions more favorable for the persistence of TSMBF. In contrast, areas of lower suitability predominate in high-altitude regions (such as the Andes), semi-arid zones, and in southern South America, particularly the Southern Cone, suggesting climatic conditions that are less conducive to the occurrence of the modeled vegetation.

Under the low-emission scenario (SSP1-2.6), a relatively broad distribution of areas with moderate to high suitability is observed, with favorable conditions persisting in peripheral sectors of the Amazon, southeastern Colombia, the Guianas, and parts of Brazil's Atlantic coast. This trend is maintained, with slight variations, under the intermediate scenario SSP2-4.5. However, in the more pessimistic scenarios (SSP3-7.0 and SSP5-8.5), a spatial contraction of highly suitable areas is evident, with

an intensification of yellow and orange tones in previously stable regions, indicating a gradual decline in climatic quality for these forests in central Amazonia.

The binary maps were generated by applying the Maximum Sensitivity plus Specificity threshold (MaxSSS), converting continuous suitability values into presence and absence areas. The spatial distribution of presence areas mirrors the patterns observed in the continuous maps but with more clearly defined boundaries.

In the SSP1-2.6 scenario (Figure 3A), most of the Brazilian Amazon, as well as adjacent areas in Colombia, Venezuela, Peru, and Bolivia, are classified as presence zones. Isolated regions of the Atlantic Forest, particularly in southern Bahia, northern Espírito Santo, and eastern Minas Gerais, also retain suitable conditions.

Under SSP2-4.5 (Figure 3B), the spatial pattern remains similar, with a slight reduction in marginal regions and decreased connectivity among presence cores in the Atlantic Forest. In contrast, in the SSP3-7.0 (Figure 3C) and SSP5-8.5 (Figure 3D) scenarios, a more pronounced retraction of presence areas is observed, especially in eastern Amazonia and parts of the northern Atlantic Forest. The fragmentation of suitable areas becomes more marked, reflecting increased climatic stress under high-emission scenarios.

3.2.2 Scenario Comparisons (2021–2040)

A direct comparison among the scenarios reveals a gradual trend of suitable area loss, particularly in central Amazonia, as the intensity of radiative forcing increases across the SSPs. While SSP1-2.6 represents a more conservative pathway, favorable to the maintenance of tropical forests, SSP5-8.5 reflects a scenario of severe climatic degradation, with potential direct impacts on the continuity, extent, and ecological resilience of the TSMBF.

In addition to spatial reduction, changes in connectivity among presence areas are also noteworthy. In SSP1-2.6 and SSP2-4.5, greater spatial cohesion is observed among presence cores, which may facilitate gene flow and species dispersal. In contrast, under SSP3-7.0 and SSP5-8.5, this connectivity is progressively compromised, increasing the risk of population isolation and biodiversity loss in central Amazonia.

3.3 Future Projections of Climatic Suitability (2041–2060)

Projections for the period 2041 to 2060 (Figure 4) indicate progressive changes in the distribution of climatic suitability and the potential presence of TSMBF compared to the previous period (2021–2040). The effects of climate change become more pronounced, especially under the intermediate and pessimistic scenarios, as revealed by the continuous and binary suitability maps in Panel 3.7.

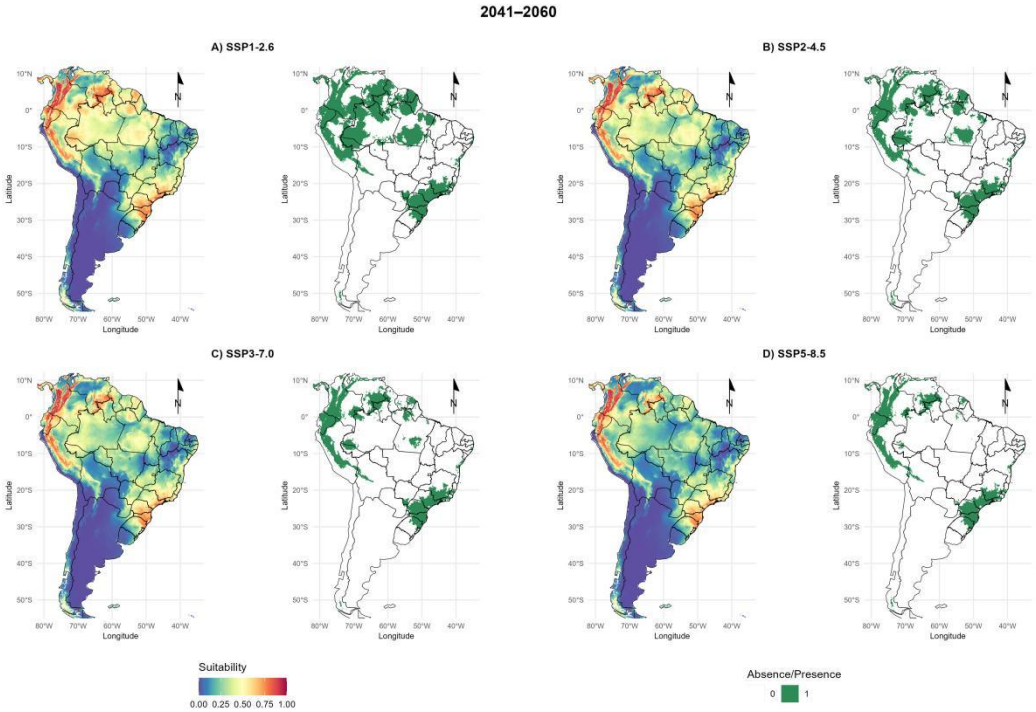

Figure 4. Projections of continuous climatic suitability (left) and binary potential presence (right) of the Tropical and Subtropical Moist Broadleaf Forests (TSMBF) in South America for the period 2041–2060, under four socioeconomic scenarios (SSPs): (A) SSP1-2.6, (B) SSP2-4.5, (C) SSP3-7.0, and (D) SSP5-8.5.

3.3.1 Variations in Continuous Suitability Maps (2041–2060)

The continuous maps exhibit a general pattern similar to the previous period, with the highest suitability values concentrated in western central Amazonia and the northwestern portion of South America. However, an intensification of areas with intermediate values and a relative reduction of high-suitability areas are observed, particularly under the higher-emission scenarios.

In the SSP1-2.6 scenario (Figure 4A), a core of high suitability persists in central Amazonia, although slight retraction is observed in marginal edges and the eastern Atlantic corridor. In the SSP2-4.5 scenario (Figure 4B), this reduction pattern

becomes more pronounced, especially in the western Amazon Basin and along the edges of the Guiana Shield. Yellow tones increase in northern Cerrado, the Chaco region, and southeastern Amazonia.

In the more pessimistic scenarios (SSP3-7.0 and SSP5-8.5), the fragmentation of suitability becomes more evident. Highly suitable areas become more restricted and discontinuous, with an amplification of negative climatic gradients. Southern Amazonia, the western interfluves, and parts of eastern Amazonia show a marked decline in climatic suitability, indicating the progressive degradation of environmental conditions favorable to TSMBF persistence.

Application of the MaxSSS threshold reveals marked changes in the distribution of potential presence areas across the scenarios. In SSP1-2.6 (Figure 4A), presence areas remain extensive throughout Amazonia and are partially connected to fragments of the Atlantic Forest, indicating moderate resilience to projected climate changes. In SSP2-4.5 (Figure 4B), the extent of presence areas remains similar, but fragmentation increases in transition zones between biomes, such as southern Pará, Tocantins, and Maranhão.

The SSP3-7.0 scenario (Figure 4C) shows greater spatial retraction and disconnection between presence areas. Regions that previously sustained marginal conditions become absent, such as northern Mato Grosso and parts of eastern Brazil.

In SSP5-8.5 (Figure 4D), the binary distribution reveals one of the highest levels of fragmentation, with a significant loss of connectivity between Amazonian and Atlantic forest cores, further intensifying the isolation of the modeled plant populations.

3.3.2 Temporal Comparisons and Ecological Implications (2041–2060)

Compared to the period 2021–2040, the maps for 2041–2060 indicate a consistent trend of declining climatic suitability and a reduction in the extent of presence areas under intermediate and high emission scenarios. These changes are particularly concerning under SSP3-7.0 and SSP5-8.5, where suitable areas become not only smaller but also more isolated. Such patterns suggest increasing risks to the ecological resilience of TSMBF, potentially compromising gene flow, migratory routes, and associated ecosystem services.

On the other hand, the SSP1-2.6 scenario still allows for a degree of environmental stability, indicating that effective climate mitigation policies could

curb the projected degradation and preserve a considerable portion of South America's tropical forests in the coming decades.

3.4 Future Projections of Climatic Suitability (2061–2080)

Projections for the period 2061 to 2080 (Figure 5) reveal an intensification of climate impacts on the environmental suitability of Tropical and Subtropical Moist Broadleaf Forests (TSMBF) in South America. The maps show a pattern of progressive retraction and fragmentation of suitable areas for the vegetation, with significant variation across the different emission scenarios.

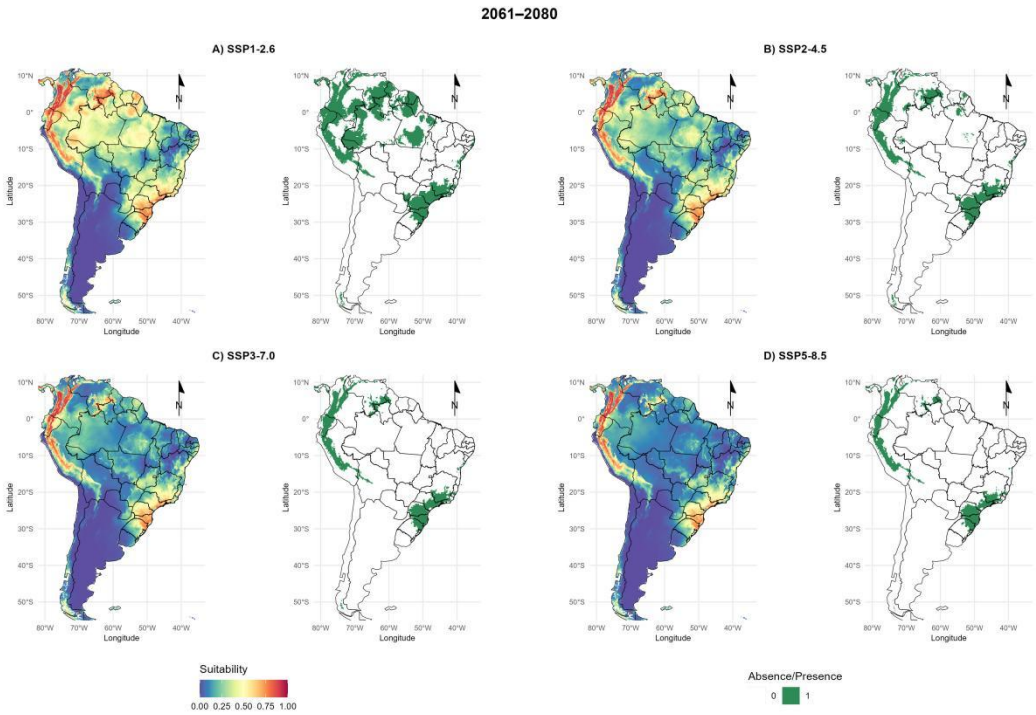

Figure 5. Projections of continuous climatic suitability (left) and binary potential presence (right) of the Tropical and Subtropical Moist Broadleaf Forests (TSMBF) in South America for the period 2061–2080, under four socioeconomic scenarios (SSPs): (A) SSP1-2.6, (B) SSP2-4.5, (C) SSP3-7.0, and (D) SSP5-8.5.

3.4.1 Continuous Climatic Suitability Maps (2061–2080)

In the continuous maps (left panel of each pair), a widespread reduction in climatic suitability values is observed in the marginal areas of both the Amazon and the Atlantic Forest. Even in the most optimistic scenario (SSP1-2.6), although high-suitability cores (red tones) still persist, especially in northern Brazilian Amazonia

and the Guianas, there is a noticeable spread of bluish and greenish tones into areas that were previously more favorable, indicating a decline in environmental quality.

The SSP2-4.5 scenario reveals an intermediate pattern of degradation, with moderately suitable areas (yellow tones) expanding into regions previously classified as highly suitable. The Brazilian Shield and southeastern Amazon regions lose prominence as favorable zones.

In the SSP3-7.0 and SSP5-8.5 scenarios, the effects are more severe. Highly suitable areas become sparse and discontinuous, suggesting a progressive collapse of the environmental conditions that sustain the TSMBF. Low-suitability zones (≤0.25) expand across the edges of the Amazon forest and transitional areas, such as the "Arc of Deforestation" and the Cerrado–Amazonia ecotone, while the Atlantic Forest shows some degree of uniformity, except in the northeastern region.

Conversion to binary maps based on the MaxSSS threshold makes the effects of projected changes more explicit. In the SSP1-2.6 scenario, presence areas remain cohesive in western Amazonia and northern Brazil, although a visible retraction occurs in the eastern and southern parts of the forest. Connectivity with Atlantic Forest fragments remains limited, but some persistence is observed in coastal sectors of the northeast and southeast.

Under SSP2-4.5, there is substantial loss in marginal zones and greater fragmentation of presence cores. The disconnection between Amazonian and Atlantic blocks becomes more evident, with significant reduction of presence in southern Bahia, Espírito Santo, and northern Minas Gerais.

The SSP3-7.0 and SSP5-8.5 scenarios depict a critical situation. Presence areas become extremely reduced, fragmented, and isolated. Under SSP5-8.5, almost the entire eastern and southern fringe of the Amazon is converted to absence, with only small stable cores remaining in the northwestern forest and along humid corridors associated with altitude or persistent river systems. In the Atlantic Forest, potential presence nearly disappears.

3.4.2 Temporal Trend and Implications (2061–2080)

Comparison with previous periods shows that the 2061–2080 interval marks a critical inflection point in the trajectory of climatic suitability for TSMBF, especially under high emission scenarios. Climatic degradation affects not only the extent but also the quality and connectivity of potential habitats. The loss of spatial continuity

may compromise key ecological mechanisms such as dispersal, regeneration, and resilience to disturbances.

The persistence of suitable areas under SSP1-2.6 reinforces the importance of robust and immediate mitigation policies, which could preserve a significant portion of tropical ecosystems. In contrast, SSP3-7.0 and SSP5-8.5 indicate pathways toward ecological collapse, with profound impacts on biodiversity and the regional biogeophysical functioning.

3.5 Future Projections of Climatic Suitability (2081–2100)

Projections for the period 2081 to 2100 (Figure 6) reveal the most extreme scenarios of climatic transformation throughout the 21st century. The previously observed pattern of progressive reduction in suitability and potential presence of TSMBF intensifies significantly, especially under the highest emission scenarios. The map panel shows a clear convergence toward climatic conditions that are increasingly unfavorable for the maintenance of these tropical ecosystems.

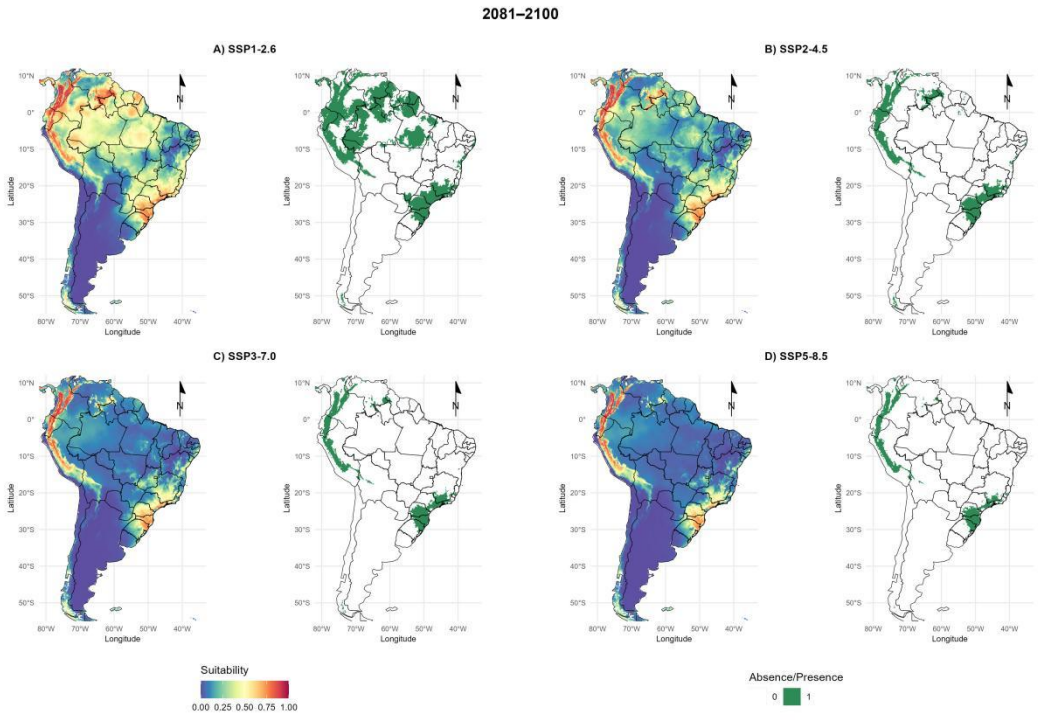

Figure 6. Projections of continuous climatic suitability (left) and binary potential presence (right) of the Tropical and Subtropical Moist Broadleaf Forests (TSMBF) in South America for the period 2081–2100, under four socioeconomic scenarios (SSPs): (A) SSP1-2.6, (B) SSP2-4.5, (C) SSP3-7.0, and (D) SSP5-8.5.

3.5.1 Suitability Maps (2081–2100)

In the continuous maps, a clear contraction of areas with high climatic suitability (≥0.75) is observed, along with an expansion of regions with low to moderate suitability (≤0.50). Even under the SSP1-2.6 scenario, a retraction of the highest-value cores is evident, now limited to central and northern portions of the Amazon Basin. Intermediate ranges dominate the landscape, indicating that although climatic conditions remain favorable in some areas, they no longer support the same extent or connectivity observed in the past.

In SSP2-4.5, climatic suitability continues to decline, with increasing fragmentation and reduction of favorable zones in eastern Amazonia, southern Colombia, and the Brazilian Shield. The expansion of bluish tones in areas previously classified as moderately suitable suggests the progression of a less favorable climate, likely drier and/or thermally unstable.

In the pessimistic scenarios (SSP3-7.0 and SSP5-8.5), suitability becomes drastically compromised. The highest values are largely restricted to small portions of western Amazonia and northwestern South America, while most of the South American territory is dominated by very low values (<0.25). This suggests a widespread climatic collapse of conditions necessary for the persistence of TSMBF.

Conversion from continuous to binary presence–absence maps clearly illustrates the impact of the different emission scenarios:

In SSP1-2.6, extensive areas of potential presence are still observed in Amazonia, although noticeably more fragmented than in previous periods. The Atlantic Forest, in contrast, retains only isolated suitability cores.

In SSP2-4.5, fragmentation intensifies. Presence areas become discontinuous, particularly along the edges of the Amazon biome and in ecological corridors connecting forest domains.

In SSP3-7.0, the potential presence of TSMBF experiences substantial collapse. Only small, isolated blocks remain in western Amazonia and in specific regions such as northern Pará and the Guianas. Presence in the Atlantic Forest becomes residual.

SSP5-8.5 represents the most critical scenario: potential presence areas nearly disappear across most of South America, with the few remaining fragments highly isolated, severely compromising the ecological and functional viability of the modeled ecosystems.

3.5.2 Final Considerations and Implications (2081–2100)

This final time interval projects an alarming scenario for the conservation of South American tropical forests. The progressive erosion of climatic suitability and the consequent retraction of presence areas culminate, under the most pessimistic scenarios, in critical fragmentation that may irreversibly compromise essential ecological processes such as dispersal, recruitment, gene flow, and biodiversity maintenance.

The resilience observed up to the 2040–2060 period nearly vanishes under SSP3-7.0 and SSP5-8.5, suggesting that the accumulated effects of climate change may become irreversible without drastic and immediate mitigation measures. In contrast, the SSP1-2.6 scenario still presents conditions conducive to the maintenance of resilient forest cores, reinforcing the importance of ambitious climate policies and international agreements aimed at reducing greenhouse gas emissions.

4. Discussion

In this study, the modeling of the potential distribution of TSMBF in South America under contemporary and future climate scenarios revealed significant projected contraction and fragmentation of these areas throughout the 21st century, particularly across the vast Amazon Basin and the remaining patches of the Atlantic Forest, under high greenhouse gas emission scenarios.

These projections align with broader trends of warming and moisture alterations projected for various South American terrestrial biomes (Anjos et al., 2021; Reboita et al., 2022; Filho et al., 2024), driven by ongoing and future shifts in temperature and precipitation patterns (Almazroui et al., 2021).

Our analysis for the reference period (1970–2000) indicated that the highest climatic suitability for TSMBF is concentrated predominantly in central and western Amazonia, along northern South America, and in fragmented portions of the Atlantic Forest in Brazil.

The most influential bioclimatic variables in modeling the current distribution were isothermality (BIO3), mean temperature of the wettest quarter (BIO8), precipitation of the coldest quarter (BIO19), mean diurnal temperature range (BIO2), and precipitation of the warmest quarter (BIO18). The relevance of these thermal and hydric variables reflects the ecological requirements for consistent humidity and low temperature variability characteristic of these forests. This aligns with the premise that

large-scale climate conditions are key determinants of the potential distribution of biomes and species (Tonetti et al., 2024; Peterson et al., 2011). Species distribution studies in the region, such as modeling for the harpy eagle, also highlight the importance of climatic variables (Miranda et al., 2019).

Future projections for the 21st century indicate a continuous and progressive decline in climatic suitability for TSMBF, with the 2081–2100 period presenting the most extreme transformation scenarios. Under high-emission pathways (SSP3–7.0 and SSP5–8.5), climatic suitability becomes severely compromised, with higher values restricted to small portions of western Amazonia and the northwestern region of South America. The most pronounced contractions are expected along the eastern and southern edges of the Amazon and in ecotonal zones transitioning to other biomes.

In more pessimistic scenarios, the binary potential presence of TSMBF virtually disappears from most of South America, leaving only highly isolated remnants. This projected replacement of tropical forest by more open formations, such as deciduous forest, savanna, and natural grassland, particularly toward the end of the century, is supported by other dynamic vegetation modeling studies (Lyra et al., 2016; Maksic et al., 2022). For instance, projections indicate drastic reductions (>90%) in tropical forest area in Amazonian states such as Pará, Rondônia, and Acre under the RCP8.5 scenario, closely aligning with our projections of major forest contraction along the eastern and southern Amazon margins (Lyra et al., 2016). Furthermore, recent coupled climate simulations suggest that such savannization, combined with global warming, could extend the duration of severe dry seasons and intensify rainfall reduction from the Amazon to central-southeastern Brazil, exacerbating the isolation of forest remnants (Bottino et al., 2024).

The main mechanisms driving this contraction are the projected changes in temperature and precipitation patterns, particularly increased temperatures and reduced humidity (Anjos et al., 2021). Global and regional climate model projections indicate a persistent and significant rise in mean annual temperature across South America, with the most intense warming occurring in the tropical zone (Anjos et al., 2021; Reboita et al., 2022), along with an increase in the frequency of hot days and nights (Reboita et al., 2022). Regarding precipitation, although the overall pattern across the continent may vary, the tropical zone, including parts of the Amazon, shows a clear trend toward reduced moisture availability (Anjos et al., 2021; Almazroui et al., 2021; Reboita et al., 2022). High-resolution convection-permitting

models also project an increase in the duration and severity of dry spells in the Amazon, particularly under high-emission scenarios (RCP8.5), as well as a shift toward less frequent but more intense rainfall events (Kahana, 2024)

The projected reduction in precipitation over central Amazonia (Almazroui et al., 2021), along with an increase in consecutive dry days (CDD) and a decrease in consecutive wet days (CWD) under future scenarios (Reboita et al., 2022), corroborates our findings of declining climatic suitability in these regions. The weakening of the northeast trade winds and reduced large-scale moisture flux convergence have been identified as potential drivers of declining rainfall in the Amazon (Reboita et al., 2022).

The study by Bottino et al. (2024) goes further, indicating that the combined effects of Amazonian savannization (land-use change) and global warming lead to a significant reduction in rainfall and an extension of the dry season across the Amazon Basin, along with extreme anomalies in maximum temperature (Bottino et al., 2024). The modulation of moisture transport by the South American Low-Level Jet (SALLJ) plays an important role in this dynamic (Bottino et al., 2024).

In addition to contraction, the fragmentation of suitable areas is a striking pattern in future projections, especially under high-emission scenarios. The loss of spatial connectivity among potential presence cores is a significant concern from an ecological perspective. Habitat fragmentation can lead to a collapse in ecosystem functionality (Faria et al., 2023) and negatively affect key processes such as seed dispersal, gene flow, and population persistence (Sales et al., 2021; Gomes et al., 2019). Studies in the Atlantic Forest, a biome already historically fragmented, demonstrate how fragmentation impairs connectivity for species such as primates and jaguars (Pinto et al., 2023; Diniz et al., 2021; Martinez Pardo et al., 2023; Vancine et al., 2024).

The loss of large frugivores due to climate change and habitat fragmentation, for instance, can lead to eco-evolutionary consequences, altering seed dispersal patterns and even the evolution of seed size in palm species such as Euterpe edulis (Sales et al., 2021).

The Atlantic Forest, recognized as a biodiversity hotspot (Santos et al., 2024; Ribeiro et al., 2011), retains climatic suitability in some regions under more optimistic scenarios and during early periods (2021–2040). However, this suitability for endemic species virtually disappears under the most pessimistic scenarios in the distant future

(2081–2100) (Pinto et al., 2023). This biome already faces longstanding conservation challenges, with only about 23% of its original forest cover remaining in 2020 and a highly fragmented landscape in which 97% of forest remnants are smaller than 50 hectares and a large proportion of vegetation is affected by edge effects (Vancine et al., 2024; Ribeiro et al., 2009).

The low level of formal protection only about 10% of the remaining vegetation lies within protected areas or Indigenous territories (Vancine et al., 2024) further increases the biome's vulnerability to projected climate change, since the current network does not cover future priority areas (Tonetti et al., 2024). Endemic Atlantic Forest species, such as primates, are already projected to experience significant net losses in their distributional area under high-emission scenarios, even when potential dispersal is considered (Pinto et al., 2023).

It is essential to recognize that although this study focused on climatic drivers, the interaction with other factors, such as land-use change, is crucial. Deforestation, for instance, is one of the primary drivers of forest loss in South America (Gomes et al., 2019; Mikołajczak et al., 2023; Bottino et al., 2024) and can amplify the impacts of climate change (Anjos et al., 2021; Bottino et al., 2024).

The expansion of agricultural and bioenergy crops can have negative impacts on biodiversity, particularly when replacing natural vegetation (Hirata et al., 2024). Fire regimes, influenced by both climate and land use, are especially important in forest savanna ecotones (Valencia et al., 2024; Uribe et al., 2023).

The forest savanna transition in northern South America, for example, shows that fire frequency and intra-seasonal rainfall are key factors, and savannas can occur under climatic conditions that would otherwise support forests. This highlights the complexity of these transitions and the influence of non-climatic drivers (Valencia et al., 2024).

The CO_2 fertilization effect may theoretically influence forest productivity and distribution (Santos et al., 2024; Chen et al., 2024). Paleoclimatic studies suggest that the historical development of the Atlantic Forest was influenced by atmospheric CO_2 variability (Santos et al., 2024). Models indicate that elevated CO_2 can enhance biomass accumulation (Santos et al., 2024), and CO_2 plays an important role in vegetation growth (Chen et al., 2024).

However, the increasing influence of rising temperatures and declining precipitation under future climate scenarios may offset or even surpass the potential

positive effects of elevated CO_2 (Lyra et al., 2016; Uribe et al., 2023), leading to projected degradation and biomass loss (Uribe et al., 2023). Empirical projections indicate a net reduction in steady-state aboveground biomass under future climate change, despite uncertainties in model capabilities to accurately represent the effects of drought, heat stress, and overestimated CO_2 fertilization responses (Uribe et al., 2023).

Our results, along with comparative literature, reinforce the high vulnerability of Tropical and Subtropical Moist Broadleaf Forests (TSMBF) in South America to projected climate change, particularly under high emission trajectories.

The projected loss of climatic suitability and increased fragmentation pose substantial risks to the vast biodiversity harbored by these biomes and to the ecosystem services they provide (Gomes et al., 2019; Sales et al., 2021; Uribe et al., 2023; Faria et al., 2023).

A recent study on global vegetation resilience including South America projected a significant loss of resilience in equatorial regions in the future, despite an increasing trend in vegetation growth (as indicated by LAI), highlighting a complex and concerning dynamic (Chen et al., 2024).

The urgency of ambitious climate policies, drastic mitigation efforts, and proactive adaptation measures is underscored by the most pessimistic scenarios, in which climate-driven degradation may result in irreversible effects by the end of the century without immediate intervention.

The need for public mitigation and adaptation policies is already evident in drier adjacent biomes, which often receive less research and conservation attention (Filho et al., 2024).

Addressing the socioeconomic and governance barriers that limit on-the-ground conservation efforts is crucial, especially given that economic constraints may hinder local communities from prioritizing nature conservation even when there is a favorable attitude toward it (Mikołajczak et al., 2023).

The effective conservation and future resilience of these ecosystems will depend on integrating landscape-scale planning, expanding and efficiently managing protected areas, and promoting restoration initiatives in degraded regions (Tonetti et al., 2024; Vancine et al., 2024), learning from the lessons of more fragmented biomes such as the Atlantic Forest (Vancine et al., 2024).

5. CONCLUSION

This study modeled the potential distribution of Tropical and Subtropical Moist Broadleaf Forests (TSMBF) in South America under current and future climatic conditions. For the present period (1970–2000), climatic suitability was primarily concentrated in central and western Amazonia, bands across northern South America, and fragmented portions of the Atlantic Forest. The most influential bioclimatic variables were related to thermal stability and water availability during critical periods.

Climate projections for the 21st century reveal a clear trend of spatial contraction and significant fragmentation of climatically suitable areas for TSMBF. This trend intensifies progressively over time, becoming particularly severe under high greenhouse gas emission scenarios (SSP3–7.0 and especially SSP5–8.5). Throughout the century, suitability maps show a gradual decline in climatic quality across previously favorable areas, with increasing fragmentation and loss of connectivity between suitable habitat cores in the Amazon and the Atlantic Forest.

In the most pessimistic scenarios (SSP5–8.5), projections for the end of the century (2081–2100) indicate a widespread climatic collapse of ideal conditions, with suitable areas becoming rare, highly isolated, and the potential presence in the Atlantic Forest virtually disappearing. In contrast, the low-emission scenario (SSP1–2.6) still presents conditions for the persistence of suitability cores and some degree of environmental stability.

However, high-emission pathways point to an imminent ecological collapse, severely compromising the ecological and functional viability of these ecosystems by the end of the century. Our findings demonstrate that projected climate change poses a serious threat to the extent and persistence of TSMBF in South America, highlighting the urgent need for emissions mitigation and the implementation of adaptation strategies to safeguard these vital biomes.

6. REFERENCES

Aiello-Lammens, M.E., Boria, R.A., Radosavljevic, A., Vilela, B. and Anderson, R.P. (2015), spThin: an R package for spatial thinning of species occurrence records for use in ecological niche models. Ecography, 38: 541-545. https://doi.org/10.1111/ecog.01132

Allouche, O., Tsoar, A., & Karni, O. (2006). Assessing the accuracy of species distribution models: Prevalence, kappa and the true skill statistic (TSS). Journal of

Applied Ecology, 43(6), 1223–1232. https://doi.org/10.1111/j.1365-2664.2006.01214.x

Almazroui, M., Ashfaq, M., Islam, M.N. et al. Assessment of CMIP6 Performance and Projected Temperature and Precipitation Changes Over South America. Earth Syst Environ 5, 155–183 (2021). https://doi.org/10.1007/s41748-021-00233-6

Anjos, L. J. S., de Souza, E. B., Amaral, C. T., Igawa, T. K., & de Toledo, P. M. (2021). Future projections for terrestrial biomes indicate widespread warming and moisture reduction in forests up to 2100 in South America. Global Ecology and Conservation, 25, e01441. https://doi.org/10.1016/j.gecco.2020.e01441

Artaxo, P., et al. (2022). Tropical and boreal forest–atmosphere interactions: A review. Tellus B: Chemical and Physical Meteorology, 74(1), 24–163. https://doi.org/10.16993/tellusb.34

Baldwin, R. A. (2009). Use of Maximum Entropy Modeling in Wildlife Research. Entropy, 11(4), 854-866. https://doi.org/10.3390/e11040854

Boria, R. A., Olson, L. E., Goodman, S. M., & Anderson, R. P. (2014). Spatial filtering to reduce sampling bias can improve the performance of ecological niche models. Ecological Modelling, 275, 73–77. https://doi.org/10.1016/j.ecolmodel.2013.12.012

Borma, L. S., Costa, M. H., da Rocha, H. R., Arieira, J., Nascimento, N. C. C., Jaramillo-Giraldo, C., et al. (2022). Beyond carbon: The contributions of South American tropical humid and subhumid forests to ecosystem services. Reviews of Geophysics, 60, e2021RG000766. https://doi. org/10.1029/2021RG000766

Bottino, M. J., Nobre, P., Giarolla, E., Lyra, A. A., Marengo, J. A., & Sampaio, G. (2024). Amazon savannization and climate change are projected to increase dry season length and temperature extremes over Brazil. Scientific Reports, 14, 5131. https://doi.org/10.1038/s41598-024-55176-5

Chen, Z., Fan, P., Hou, X., Wang, Y., Zhang, Y., & Li, Y. (2024). Analysis of global vegetation resilience under different future climate scenarios. Climate Dynamics, 62, 7967–7980. https://doi.org/10.1007/s00382-024-07317-9

Dinerstein, E., Olson, D., Joshi, A., Vynne, C., Burgess, N. D., Wikramanayake, E., Hahn, N., Palminteri, S., Hedao, P., Noss, R., Hansen, M., Locke, H., Ellis, E. C., Jones, B., Barber, C. V., Hayes, R., Kormos, C., Martin, V., Crist, E., Sechrest, W., Price, L., Baillie, J. E. M., Weeden, D., Suckling, K., Davis, C., Sizer, N., Moore, R., Thau, D., Birch, T., Potapov, P., Turubanova, S., Tyukavina, A., de Souza, N., Pintea, L., Brito, J. C., Llewellyn, O. A., Miller, A. G., Patzelt, A., Ghazanfar, S. A., Timberlake, J., Klöser, H., Shennan-Farpón, Y., Kindt, R., Barnekow Lillesø, J. P., van Breugel, P., Graudal, L., Voge, M., Al-Shammari, K. F., & Saleem, M. (2017). An ecoregion-based approach to protecting half the terrestrial realm. BioScience, 67(6), 534–545. https://doi.org/10.1093/biosci/bix014

Diniz, M. F., Coelho, M. T. P., de Sousa, F. G., Hasui, E., & Loyola, R. (2021). The underestimated role of small fragments for carnivore dispersal in the Atlantic Forest. Perspectives in Ecology and Conservation, 19, 81–89.

Elith, J., Phillips, S.J., Hastie, T., Dudík, M., Chee, Y.E. and Yates, C.J. (2011), A statistical explanation of MaxEnt for ecologists. Diversity and Distributions, 17: 43-57. https://doi.org/10.1111/j.1472-4642.2010.00725.x

Eyring, V., Bony, S., Meehl, G. A., Senior, C. A., Stevens, B., Stouffer, R. J., & Taylor, K. E. (2016). Overview of the Coupled Model Intercomparison Project Phase 6 (CMIP6) experimental design and organization. Geoscientific Model Development, 9, 1937–1958. https://doi.org/10.5194/gmd-9-1937-2016

Faria, D., Morante-Filho, J. C., Baumgarten, J., Bovendorp, R. S., Cazetta, E., Gaiotto, F. A., Mariano-Neto, E., Mielke, M. S., Pessoa, M. S., Rocha-Santos, L., Santos, A. S., Soares, L. A. S. S., Talora, D. C., Vieira, E. M., & Benchimol, M. (2023). The breakdown of ecosystem functionality driven by deforestation in a global biodiversity hotspot. Biological Conservation, 283, 110126. https://doi.org/10.1016/j.biocon.2023.110126

Fielding, A. H., & Bell, J. F. (1997). A review of methods for the assessment of prediction errors in conservation presence/absence models. Environmental Conservation, 24(1), 38–49.
Fick, S. E., & Hijmans, R. J. (2017). WorldClim 2: New 1-km spatial resolution climate surfaces for global land areas. International Journal of Climatology, 37(12), 4302–4315. https://doi.org/10.1002/joc.5086

Flantua, S. G. A., Hooghiemstra, H., Grimm, E. C., Behling, H., Bush, M. B., González-Arango, C., Gosling, W. D., Ledru, M.-P., Lozano-García, S., Maldonado, A., Prieto, A. R., Rull, V., & Van Boxel, J. H. (2015). Updated site compilation of the Latin American Pollen Database. Review of Palaeobotany and Palynology, 223, 104–115. http://dx.doi.org/10.1016/j.revpalbo.2015.09.008

Flores, B.M., Montoya, E., Sakschewski, B. et al. Critical transitions in the Amazon forest system. Nature 626, 555–564 (2024). https://doi.org/10.1038/s41586-023-06970-0

GBIF. Global Biodiversity Information Facility. Disponível em: <https://www.gbif.org>. Acesso em: 5 dez. 2024.

Gomes, V. H. F., Vieira, I. C. G., Salomão, R. P., ter Steege, H., Amaral, I. L., de Almeida Matos, F. D., ... Phillips, O. L. (2019). Amazonian tree species threatened by deforestation and climate change. Nature Climate Change, 9, 547–553. https://doi.org/10.1038/s41558-019-0500-2

Grantham, H. S., Duncan, A., Evans, T. D., Jones, K. R., Beyer, H. L., Schuster, R., ... Watson, J. E. M. (2020). Anthropogenic modification of forests means only 40% of remaining forests have high ecosystem integrity. Nature Communications, 11, 5978. https://doi.org/10.1038/s41467-020-19493-3

Hijmans, R. J., Phillips, S. J., Leathwick, J., & Elith, J. (2018). dismo: Species distribution modelling (R package version). https://CRAN.R-project.org/package=dismo

Hirata, A., Ohashi, H., Hasegawa, T., Matsui, T., Nishina, K., Fujimori, S., ... Smith, P. (2024). The choice of land-based climate change mitigation measures influences future global biodiversity loss. Communications Earth & Environment, 5, 259. https://doi.org/10.1038/s43247-024-01433-4

Hubau, W., Lewis, S.L., Phillips, O.L. et al. Asynchronous carbon sink saturation in African and Amazonian tropical forests. Nature 579, 80–87 (2020). https://doi.org/10.1038/s41586-020-2035-0

Jiménez, L., & Soberón, J. (2020). Leaving the area under the receiving operating characteristic curve behind: An evaluation method for species distribution modelling applications based on presence-only data. Methods in Ecology and Evolution, 11(12), 1571–1586. https://doi.org/10.1111/2041-210X.13479

Kahana, R., Halladay, K., Alves, L. M., Chadwick, R., & Hartley, A. J. (2024). Future precipitation projections for Brazil and tropical South America from a convection-permitting climate simulation. Frontiers in Climate, 6, Article 1419704. https://doi.org/10.3389/fclim.2024.1419704

Kramer-Schadt, S., Niedballa, J., Pilgrim, J. D., Schröder, B., Lindenborn, J., Reinfelder, V., Stillfried, M., Heckmann, I., Scharf, A. K., Augeri, D. M., Cheyne, S. M., Hearn, A. J., Ross, J., Macdonald, D. W., Mathai, J., Eaton, J., Marshall, A. J., Semiadi, G., & Wilting, A. (2013). The importance of correcting for sampling bias in MaxEnt species distribution models. Diversity and Distributions, 19(11), 1366–1379. https://doi.org/10.1111/ddi.12096

Koch, A., & Kaplan, J. O. (2022). Tropical forest restoration under future climate change. Nature Climate Change, 12, 279–283. https://doi.org/10.1038/s41558-022-01289-6

Liu, C., White, M., & Newell, G. (2013). Selecting thresholds for the prediction of species occurrence with presence-only data. Journal of Biogeography, 40(4), 778–789. https://doi.org/10.1111/jbi.12058

Lyra, A. de A., Chou, S. C., & Sampaio, G. de O. (2016). Sensitivity of the Amazon biome to high resolution climate change projections. Acta Amazonica, 46(2), 175–188. https://doi.org/10.1590/1809-4392201502225

Marques, M. C. M., Trindade, W., Bohn, A., & Grelle, C. E. V. (2021). The Atlantic Forest: An introduction to the megadiverse forest of South America. In M. C. M. Marques & C. E. V. Grelle (Eds.), The Atlantic Forest: History, biodiversity, threats and opportunities of the mega-diverse forest (pp. 3–23). Springer International Publishing.

Martínez Pardo, J., Saura, S., Insaurralde, A., Di Bitetti, M. S., Paviolo, A., & De Angelo, C. (2023). Much more than forest loss: Four decades of habitat connectivity decline for Atlantic Forest jaguars. Landscape Ecology, 38, 41–57.

Merow, C., Smith, M.J. and Silander, J.A., Jr (2013), A practical guide to MaxEnt for modeling species' distributions: what it does, and why inputs and settings matter. Ecography, 36: 1058-1069. https://doi.org/10.1111/j.1600-0587.2013.07872.x

Mikołajczak, K. M., Barlow, J., Lees, A. C., Ives, C. D., Strack, M., de Almeida, O. T., Souza, A. C., Sinclair, F., & Parry, L. (2023). Evaluating the influence of nature connection and values on conservation attitudes at a tropical deforestation frontier. Conservation Biology, 37, e14067. https://doi.org/10.1111/cobi.14067

Miranda, E. B. P., Menezes, J. F. S., Farias, C. C. L., Munn, C., & Peres, C. A. (2019). Species distribution modeling reveals strongholds and potential reintroduction areas for the world's largest eagle. PLoS ONE, 14(5), e0216323. https://doi.org/10.1371/journal.pone.0216323

Mittermeier, R. A., Mittermeier, C. G., Brooks, T. M., Pilgrim, J. D., Konstant, W. R., da Fonseca, G. A. B., & Kormos, C. (2003). Wilderness and biodiversity conservation. Proceedings of the National Academy of Sciences of the United States of America, 100(18), 10309–10313. https://doi.org/10.1073/pnas.1732458100

Moss, R. H., Edmonds, J. A., Hibbard, K. A., Manning, M. R., Rose, S. K., van Vuuren, D. P., Carter, T. R., Emori, S., Kainuma, M., Kram, T., Meehl, G. A., Mitchell, J. F. B., Nakicenovic, N., Riahi, K., Smith, S. J., Stouffer, R. J., Thomson, A. M., Weyant, J. P., & Wilbanks, T. J. (2010). The next generation of scenarios for climate change research and assessment. Nature, 463, 747–756. https://doi.org/10.1038/nature08823

Myers, N., Mittermeier, R. A., Mittermeier, C. G., da Fonseca, G. A. B., & Kent, J. (2000). Biodiversity hotspots for conservation priorities. Nature, 403(6772), 853–858. https://doi.org/10.1038/35002501

Oliveira Filho, J. (2024). Climate change research in dry environments of South America: Evolution, current state, and future directions. Journal of Soils and Sediments, 24, 3013–3027. https://doi.org/10.1007/s11368-024-03855-1

O'Neill, B. C., Tebaldi, C., van Vuuren, D. P., Eyring, V., Friedlingstein, P., Hurtt, G., Knutti, R., Kriegler, E., Lamarque, J.-F., Lowe, J., Meehl, G. A., Moss, R., Riahi, K., & Sanderson, B. M. (2016). The Scenario Model Intercomparison Project (ScenarioMIP) for CMIP6. Geoscientific Model Development, 9, 3461–3482. https://doi.org/10.5194/gmd-9-3461-2016

O'Neill, B. C., Kriegler, E., Ebi, K. L., Kemp-Benedict, E., Riahi, K., Rothman, D. S., van Ruijven, B. J., van Vuuren, D. P., Birkmann, J., Kok, K., Levy, M., & Solecki, W. (2017). The roads ahead: Narratives for shared socioeconomic pathways describing world futures in the 21st century. Global Environmental Change, 42, 169–180. https://doi.org/10.1016/j.gloenvcha.2015.01.004

Pearson, R. G., Raxworthy, C. J., Nakamura, M., & Peterson, A. T. (2007). Predicting species distributions from small numbers of occurrence records: A test case using cryptic geckos in Madagascar. Journal of Biogeography, 34(1), 102–117. https://doi.org/10.1111/j.1365-2699.2006.01594.x

Peterson, A. T., Soberón, J., & Sánchez-Cordero, V. (1999). Conservatism of ecological niches in evolutionary time. Science, 285(5431), 1265–1267. https://doi.org/10.1126/science.285.5431.1265

Peterson, A. T., Soberón, J., Pearson, R. G., Anderson, R. P., Martínez-Meyer, E., Nakamura, M., & Araújo, M. B. (2011). Ecological niches and geographic distributions. Princeton University Press.

Phillips, S. J., Anderson, R. P., Dudík, M., Schapire, R. E., & Blair, M. E. (2017). Opening the black box: An open-source release of Maxent. Ecography, 40(7), 887–893. https://doi.org/10.1111/ecog.03049

Phillips, S. J., Anderson, R. P., & Schapire, R. E. (2006). Maximum entropy modeling of species geographic distributions. Ecological Modelling, 190(3–4), 231–259. https://doi.org/10.1016/j.ecolmodel.2005.03.026

Pinto, M.P., Beltrão-Mendes, R., Talebi, M. et al. Primates facing climate crisis in a tropical forest hotspot will lose climatic suitable geographical range. Sci Rep 13, 641 (2023). https://doi.org/10.1038/s41598-022-26756-0

Qin, Y., Xiao, X., Dong, J. et al. Improved estimates of forest cover and loss in the Brazilian Amazon in 2000–2017. Nat Sustain 2, 764–772 (2019). https://doi.org/10.1038/s41893-019-0336-9

Reboita, M. S., Kuki, C. A. C., Marrafon, V. H., Cunha, D. A., Llopart, M., & da Rocha, R. P. (2022). South America climate change revealed through climate indices projected by GCMs and Eta-RCM ensembles. Climate Dynamics, 58, 459–485. https://doi.org/10.1007/s00382-021-05918-2

Rezende, C. L., Scarano, F. R., Assad, E. D., Joly, C. A., Metzger, J. P., Strassburg, B. B. N., et al. (2018). From hotspot to hopespot: An opportunity for the Brazilian Atlantic Forest. Perspectives in Ecology and Conservation, 16(4), 208–214. https://doi.org/10.1016/j.pecon.2018.10.002

Ribeiro, M. C., Metzger, J. P., Martensen, A. C., Ponzoni, F. J., & Hirota, M. M. (2009). The Brazilian Atlantic Forest: How much is left, and how is the remaining forest distributed? Implications for conservation. Biological Conservation, 142(6), 1141–1153. https://doi.org/10.1016/j.biocon.2009.02.021

Sales, L. P., Kissling, W. D., Galetti, M., Naimi, B., & Pires, M. M. (2021). Climate change reshapes the eco-evolutionary dynamics of a Neotropical seed dispersal system. Global Ecology and Biogeography, 30(1), 117–127. https://doi.org/10.1111/geb.13271

Santos, T., Bouloubassi, I., Cruz, J., Rodrigues, A., Ledru, M.-P., & others. (2024). Long-term adjustment of the South America Atlantic Forest to atmospheric carbon dioxide concentration (Preprint). HAL. https://hal.science/hal-04764029

Staal, A., Tuinenburg, O.A., Bosmans, J.H.C. et al. Forest-rainfall cascades buffer against drought across the Amazon. Nature Clim Change 8, 539–543 (2018). https://doi.org/10.1038/s41558-018-0177-y

ter Steege, H., Pitman, N. C. A., Killeen, T. J., Laurance, W. F., Peres, C. A., Guevara, J. E., ... & Silman, M. R. (2015). Estimating the global conservation status of more than 15,000 Amazonian tree species. Science Advances, 1(10), e1500936. https://doi.org/10.1126/sciadv.1500936

Tonetti, V., Bocalini, F., Schunck, F., Vancine, M. H., Butti, M., Ribeiro, M. C., & Pizo, M. A. (2024). The Protected Areas network may be insufficient to protect bird diversity in a fragmented tropical hotspot under different climate scenarios. Perspectives in Ecology and Conservation, 22(1), 63–71. https://doi.org/10.1016/j.pecon.2023.12.002

Uribe, M.d.R., Coe, M.T., Castanho, A.D.A. et al. Net loss of biomass predicted for tropical biomes in a changing climate. Nat. Clim. Chang. 13, 274–281 (2023). https://doi.org/10.1038/s41558-023-01600-z

Valavi, R., G. Guillera-Arroita, J. J. Lahoz-Monfort, and J. Elith. (2022). Predictive performance of presence-only species distribution models: a benchmark study with reproducible code. Ecological Monographs 92(1):e01486. 10.1002/ecm.1486

Valencia, S., Salazar, J. F., Hoyos, N., Duque, Á., Agudelo, C. A., Sierra, C. A., ... González, R. (2024). Current forest–savanna transition in northern South America departs from typical climatic thresholds. Ecosystems, 27, 61–76. https://doi.org/10.1007/s10021-023-00872-y

Vancine, M. H., Muylaert, R. L., Niebuhr, B. B., Oshima, J. E. F., Tonetti, V., Bernardo, R., De Angelo, C., Rosa, M. R., Grohmann, C. H., & Ribeiro, M. C. (2024). The Atlantic Forest of South America: Spatiotemporal dynamics of the vegetation and implications for conservation. Biological Conservation, 291, 110499. https://doi.org/10.1016/j.biocon.2024.110499

van Vuuren, D. P., Edmonds, J., Kainuma, M., Riahi, K., Thomson, A., Hibbard, K., Hurtt, G. C., Kram, T., Krey, V., Lamarque, J.-F., Masui, T., Meinshausen, M., & Nakicenovic, N. (2011). The representative concentration pathways: An overview. Climatic Change, 109, 5–31. https://doi.org/10.1007/s10584-011-0148-z

Veloz, S. D. (2009). Spatially autocorrelated sampling falsely inflates measures of accuracy for presence-only niche models. Journal of Biogeography, 36(12), 2290–2299. https://doi.org/10.1111/j.1365-2699.2009.02174.x

Wiens, J. J., & Graham, C. H. (2005). Niche conservatism: Integrating evolution, ecology, and conservation biology. Annual Review of Ecology, Evolution, and Systematics, 36, 519–539. https://doi.org/10.1146/annurev.ecolsys.36.102803.095431

Williams, J. W., Grimm, E. G., Blois, J., Charles, D. F., Davis, E., Goring, S. J., Graham, R., Smith, A. J., Anderson, M., Arroyo-Cabrales, J., Ashworth, A. C., Betancourt, J. L., Bills, B. W., Booth, R. K., Buckland, P., Curry, B., Giesecke, T., Hausmann, S., Jackson, S. T., Latorre, C., Nichols, J., Purdum, T., Roth, R. E., Stryker, M., & Takahara, H. (2018). The Neotoma Paleoecology Database: A multi-proxy, international community-curated data resource. Quaternary Research, 89(1), 156–177. https://doi.org/10.1017/qua.2017.105

4. Final Conclusions and Conservation Implications

This study aimed to investigate the sensitivity and response of Tropical and Subtropical Moist Broadleaf Forests (TSMBF) in South America to major climatic changes, examining both long-term past dynamics, focusing on the Last Glacial Maximum (LGM), and future projections under different climate change scenarios. By integrating a paleoecological perspective with ecological niche modeling under future climate scenarios, we sought to achieve a more comprehensive understanding of the vulnerability and resilience (Scarano & Ceotto, 2015) of these vital ecosystems under contrasting climate regimes. South America's tropical and subtropical forests, including the vast Amazon Rainforest and the fragmented yet biologically rich Atlantic Forest, play crucial roles in both the global and regional biosphere. However, they are increasingly threatened by the combined impacts of human activity and climate change.

Our analysis of potential climatic conditions for TSMBF during the Last Glacial Maximum reveals a scenario markedly different from the present. Through climate suitability modeling based on paleoecological and paleoclimatic data, we established a climatic suitability threshold (0.45997) to generate binary potential distribution maps. This reconstruction of the past allows us to visualize how the climatically favorable area for these forests was configured under cooler temperatures and lower atmospheric CO_2 concentrations (Sato et al., 2021; Pinaya et al., 2019; Behling & Negrelle, 2001; Colinvaux et al., 2000).

The LGM was a period of profound environmental shifts that shaped vegetation distribution, leading to the expansion of grasslands in areas now occupied by forests, and to the persistence of forests either in refugia or with altered structure (Behling et al., 1995; Behling & Negrelle, 2001; Colinvaux et al., 2000; Hermanowski et al., 2012). Although our results for the LGM specifically focus on delineating potential climatic suitability, they align with the broader understanding that humid forests occupied a different extent under glacial climates, providing a valuable reference point for assessing the capacity of these biomes to respond to extreme environmental conditions (Flantua et al., 2015; Maksic et al., 2022).

In contrast, the modeling of potential distribution under contemporary climatic conditions (1970–2000) and projections for the future (2081–2100) presents an alarming scenario. Using the MaxEnt algorithm with WorldClim 2 data for the

baseline period, the contemporary potential distribution of TSMBF, based on an optimal threshold of 0.447, shows a broad continuous belt across the Amazon Basin and fragmented areas compatible with remnants of the Atlantic Forest and southern humid forests. The model demonstrated good predictive performance (AUC = 0.754).

However, future climate projections based on CMIP6 models under Shared Socioeconomic Pathways (SSPs) (Almazroui et al., 2021; Anjos et al., 2021; IPCC, 2023) indicate a persistent temperature increase and a trend toward reduced moisture, particularly in forest biomes (Anjos et al., 2021). Our projections for the 2081–2100 period reveal a progressive erosion of climatic suitability and a consequent contraction of the potential presence areas for TSMBF. Under the most pessimistic scenarios, this contraction culminates in critical fragmentation.

The integration of these findings suggests that although South American TSMBF have shown an ability to adapt to and survive major climatic shifts in the past, as inferred from paleoecological records under glacial conditions (Behling et al., 1995; Behling & Negrelle, 2001; Colinvaux et al., 2000), the speed and magnitude of projected future changes, combined with ongoing anthropogenic pressures, pose an unprecedented challenge. Current habitat fragmentation in the Atlantic Forest already limits essential ecological processes (Ribeiro et al., 2009; Tabarelli et al., 2010), and projected additional climatic fragmentation may lead to an even greater collapse of ecosystem services (Borma et al., 2022). The contraction of climatic suitability and associated fragmentation under future scenarios have the potential to permanently compromise key ecological processes such as seed dispersal, recruitment, gene flow, and the maintenance of high biodiversity levels.

The comparison between the glacial past and a warming future underscores the fundamental difference between long-term natural climate changes, over which ecosystems had millennia to adapt, and the rapid, human-induced changes of the present. The resilience observed in the past may no longer be sufficient to mitigate future impacts (Chen, 2024), especially when climate change interacts synergistically with other stressors such as deforestation, fire, and fragmentation (Malhi et al., 2008; Miranda, 2019; Welch et al., 2013; Sansevero et al., 2020; Grantham et al., 2020). The threat of tipping points in South American forest systems (Nobre & Borma, 2009; Flores et al., 2024) becomes increasingly plausible in light of the widespread erosion of climatic suitability revealed by our modeling.

This study provides critical insights for the conservation and management of South American forests in a rapidly changing world. Areas identified as retaining high climatic suitability, both now and in the future, should be prioritized for protection. Conversely, areas projected to lose climatic suitability or become increasingly fragmented will require adaptation strategies, such as large-scale ecological restoration to enhance landscape connectivity and facilitate species dispersal (Arroyo-Rodríguez et al., 2017; Joly, Metzger & Tabarelli, 2014; Rezende et al., 2018; Sansevero et al., 2020; Vancine et al., 2024). Lessons from the Atlantic Forest, which has a rich history of research on fragmentation, resilience, and restoration, can be adapted and applied to other South American biomes such as the Amazon and the Cerrado (Vancine et al., 2024).

It is important to acknowledge the limitations of this study. Potential distribution modeling is based on correlations between species (or vegetation types) and environmental variables, and does not account for the full complexity of biological interactions and dynamic processes (e.g., dispersal, competition, adaptation) that govern actual distributions (Elith et al., 2010; Dormann et al., 2012). Future projections carry uncertainties associated with climate models and socioeconomic scenarios (Almazroui et al., 2021; Valavi et al., 2022). Species occurrence data may be affected by sampling bias (Feng et al., 2022; Valavi et al., 2022). Likewise, paleoclimatic and paleoecological reconstructions, although essential, have their own uncertainties (Sato et al., 2021; Pinaya et al., 2019; Flantua et al., 2015). Future research should aim to refine models by explicitly incorporating dynamic processes and biotic interactions, using higher-resolution spatial and temporal data, and filling data gaps, particularly in understudied regions or for underrepresented taxonomic groups (Feng et al., 2022; Oliveira Filho, 2024).

In summary, by integrating deep-time perspectives with projections of ongoing climate change, this study reinforces the urgency of effective conservation action. The historical resilience of South American forests to past climatic fluctuations does not guarantee their persistence under the rapid and multifaceted pressures of the 21st century. Projected climatic fragmentation, combined with existing habitat fragmentation, points to a challenging future in which the maintenance of ecological processes and biodiversity will critically depend on proactive and scientifically grounded interventions. The conservation of these forests

is not merely an environmental concern, but a fundamental imperative for regional and global climate stability and for human well-being (Borma et al., 2022).

REFERENCES

Almazroui, M., Ashfaq, M., Islam, M.N. et al. Assessment of CMIP6 Performance and Projected Temperature and Precipitation Changes Over South America. Earth Syst Environ 5, 155–183 (2021). https://doi.org/10.1007/s41748-021-00233-6

Anjos, L. J. S., de Souza, E. B., Amaral, C. T., Igawa, T. K., & de Toledo, P. M. (2021). Future projections for terrestrial biomes indicate widespread warming and moisture reduction in forests up to 2100 in South America. Global Ecology and Conservation, 25, e01441. https://doi.org/10.1016/j.gecco.2020.e01441

Arroyo-Rodríguez, V., Melo, F.P.L., Martínez-Ramos, M., Bongers, F., Chazdon, R.L., Meave, J.A., Norden, N., Santos, B.A., Leal, I.R. and Tabarelli, M. (2017), Multiple successional pathways in human-modified tropical landscapes: new insights from forest succession, forest fragmentation and landscape ecology research. Biol Rev, 92: 326-340. https://doi.org/10.1111/brv.12231

Behling, H. (1995). Investigations into the Late Pleistocene and Holocene history of vegetation and climate in Santa Catarina (S Brazil). Vegetation History and Archaeobotany 4:127-152.

Behling, H., & Negrelle, R. R. B. (2001). Tropical rain forest and climate dynamics of the Atlantic lowland, southern Brazil, during the Late Quaternary. Quaternary Research, 56(3), 383–389. https://doi.org/10.1006/qres.2001.2264

Borma, L. S., Costa, M. H., da Rocha, H. R., Arieira, J., Nascimento, N. C. C., Jaramillo-Giraldo, C., et al. (2022). Beyond carbon: The contributions of South American tropical humid and subhumid forests to ecosystem services. Reviews of Geophysics, 60, e2021RG000766. https://doi. org/10.1029/2021RG000766

Chen, Z., Fan, P., Hou, X., Wang, Y., Zhang, Y., & Li, Y. (2024). Analysis of global vegetation resilience under different future climate scenarios. Climate Dynamics, 62, 7967–7980. https://doi.org/10.1007/s00382-024-07317-9

Colinvaux, P. A., De Oliveira, P. E., & Bush, M. B. (2000). Amazonian and neotropical plant communities on glacial time-scales: The failure of the aridity and refuge hypotheses. Quaternary Science Reviews, 19(1–5), 141–169

Dormann, C. F., Elith, J., Bacher, S., Buchmann, C., Carl, G., Carré, G., García Marquéz, J. R., Gruber, B., Lafourcade, B., Leitão, P. J., Münkemüller, T., McClean, C., Osborne, P. E., Reineking, B., Schröder, B., Skidmore, A. K., Zurell, D., & Lautenbach, S. (2013). Collinearity: A review of methods to deal with it and a simulation study evaluating their performance. Ecography, 36(1), 27–46. https://doi.org/10.1111/j.1600-0587.2012.07348.x

Elith, J., Kearney, M., & Phillips, S. (2010). The art of modelling range-shifting species. Methods in Ecology and Evolution, 1(4), 330–342. https://doi.org/10.1111/j.2041-210X.2010.00036.x

Feng, X., Enquist, B. J., Park, D. S., Boyle, B., Breshears, D. D., Gallagher, R. V., Lien, A., Newman, E. A., Burger, J. R., Maitner, B. S., Merow, C., Li, Y., Huynh, K. M., Ernst, K., Baldwin, E., Foden, W., Hannah, L., Jørgensen, P. M., Kraft, N. J. B., ... López-Hoffman, L. (2022). A review of the heterogeneous landscape of biodiversity databases: Opportunities and challenges for a synthesized biodiversity knowledge base. Global Ecology and Biogeography, 31, 1242–1260. https://doi.org/10.1111/geb.13497

Flantua, S. G. A., Hooghiemstra, H., Grimm, E. C., Behling, H., Bush, M. B., González-Arango, C., Gosling, W. D., Ledru, M.-P., Lozano-García, S., Maldonado, A., Prieto, A. R., Rull, V., & Van Boxel, J. H. (2015). Updated site compilation of the Latin American Pollen Database. Review of Palaeobotany and Palynology, 223, 104–115. http://dx.doi.org/10.1016/j.revpalbo.2015.09.008

Flores, B.M., Montoya, E., Sakschewski, B. et al. Critical transitions in the Amazon forest system. Nature 626, 555–564 (2024). https://doi.org/10.1038/s41586-023-06970-0

Grantham, H. S., Duncan, A., Evans, T. D., Jones, K. R., Beyer, H. L., Schuster, R., ... Watson, J. E. M. (2020). Anthropogenic modification of forests means only 40% of remaining forests have high ecosystem integrity. Nature Communications, 11, 5978. https://doi.org/10.1038/s41467-020-19493-3

Hermanowski, B., Behling, H., Pillar, V. D., Berrio, J. C., Van der Hammen, T., & Bush, M. B. (2012). Environmental changes in southeastern Amazonia during the last 25,000 years revealed from a paleoecological record. Quaternary Research, 77(1), 138–148.

IPCC. (2023). Summary for Policymakers. In H. Lee & J. Romero (Eds.), Climate Change 2023: Synthesis Report. Contribution of Working Groups I, II and III to the Sixth Assessment Report of the Intergovernmental Panel on Climate Change (pp. 1–34). IPCC. https://doi.org/10.59327/IPCC/AR6-9789291691647.001

Joly, C.A., Metzger, J.P. and Tabarelli, M. (2014), Experiences from the Brazilian Atlantic Forest: ecological findings and conservation initiatives. New Phytol, 204: 459-473. https://doi.org/10.1111/nph.12989

Maksic, J., Venancio, M., Shimizu, M. H., Chiessi, C. M., Piacsek, P., Sampaio, G., Cruz, F. W., & Alexandre, F. F. (2022). Brazilian biomes distribution: Past and future. Palaeogeography, Palaeoclimatology, Palaeoecology, 585, 110717. https://doi.org/10.1016/j.palaeo.2021.110717

Malhi, Y., Roberts, J. T., Betts, R. A., Killeen, T. J., Li, W., & Nobre, C. A. (2008). Climate change, deforestation, and the fate of the Amazon. Science, 319(5860), 169–172. https://doi.org/10.1126/science.1146961

Miranda, E. B. P., Menezes, J. F. S., Farias, C. C. L., Munn, C., & Peres, C. A. (2019). Species distribution modeling reveals strongholds and potential reintroduction areas for the world's largest eagle. PLoS ONE, 14(5), e0216323. https://doi.org/10.1371/journal.pone.0216323

Nobre, C. A., & Borma, L. D. S. (2009). "Tipping points" for the Amazon forest. Current Opinion in Environmental Sustainability, 1(1), 28–36. https://doi.org/10.1016/j.cosust.2009.07.003

Oliveira-Filho, A. T., & Ratter, J. A. (2002). Vegetation physiognomies and woody flora of the Cerrado biome. In P. S. Oliveira & R. J. Marquis (Eds.), The Cerrados of Brazil (pp. 91–120). Columbia University Press. https://doi.org/10.7312/oliv12042-007

Rezende, C. L., Scarano, F. R., Assad, E. D., Joly, C. A., Metzger, J. P., Strassburg, B. B. N., et al. (2018). From hotspot to hopespot: An opportunity for the Brazilian Atlantic Forest. Perspectives in Ecology and Conservation, 16(4), 208–214. https://doi.org/10.1016/j.pecon.2018.10.002

Ribeiro, M. C., Metzger, J. P., Martensen, A. C., Ponzoni, F. J., & Hirota, M. M. (2009). The Brazilian Atlantic Forest: How much is left, and how is the remaining forest distributed? Implications for conservation. Biological Conservation, 142(6), 1141–1153. https://doi.org/10.1016/j.biocon.2009.02.021

Sansevero, J. B. B., Garbin, M. L., Sánchez-Tapia, A., Valladares, F., & Scarano, F. R. (2020). Fire drives abandoned pastures to a savanna-like state in the Brazilian Atlantic Forest. Perspectives in Ecology and Conservation, 18(1), 31–36. https://doi.org/10.1016/j.pecon.2019.12.004

Sato, H., Yoshioka, M., Ito, A., Haverd, V., Nishina, K., & Saito, M. (2021). Dry corridors opened by fire and low CO_2 in Amazonian rainforest during the Last Glacial Maximum. Nature Geoscience, 14, 578–585. https://doi.org/10.1038/s41561-021-00774-y

Pinaya, J. L. D., Cruz, F. W., Ceccantini, G. C. T., Corrêa, P. L. P., Pitman, N., Vemado, F., Lopez, M. S., Pereira Filho, A. J., Grohmann, C. H., Chiessi, C. M., Stríkis, N. M., & De Oliveira, P. E. (2019). Brazilian montane rainforest expansion induced by Heinrich Stadial 1 event. Scientific Reports, 9(17912). (2019) 9:17912 https://doi.org/10.1038/s41598-019-53036-1

Tabarelli, M., Aguiar, A. V., Ribeiro, M. C., Metzger, J. P., & Peres, C. A. (2010). Prospects for biodiversity conservation in the Atlantic Forest: Lessons from aging human-modified landscapes. Biological Conservation, 143(10), 2328–2340. https://doi.org/10.1016/j.biocon.2010.02.005

Welch, J. R., Brondízio, E. S., Hetrick, S. S., & Coimbra, C. E. A. (2013). Indigenous burning as conservation practice: Neotropical savanna recovery amid agribusiness deforestation in Central Brazil. PLoS ONE, 8(12), e81226. https://doi.org/10.1371/journal.pone.0081226

Vancine, M. H., Muylaert, R. L., Niebuhr, B. B., Oshima, J. E. F., Tonetti, V., Bernardo, R., De Angelo, C., Rosa, M. R., Grohmann, C. H., & Ribeiro, M. C. (2024). The Atlantic Forest of South America: Spatiotemporal dynamics of the vegetation and implications for conservation. Biological Conservation, 291, 110499. https://doi.org/10.1016/j.biocon.2024.110499

Appendix A

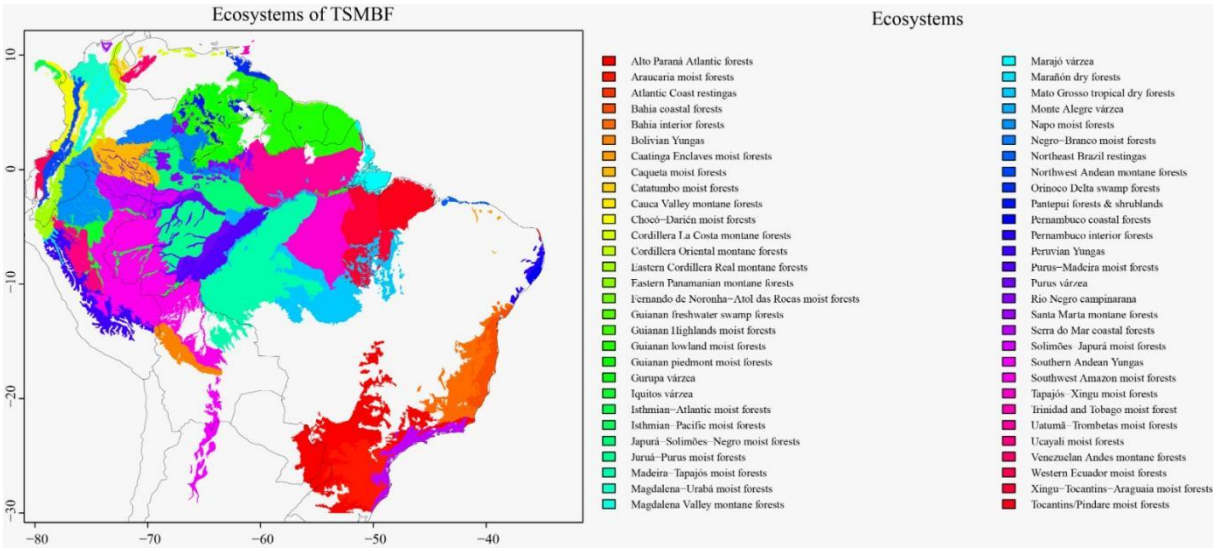
Ecosystems of TSMBF
10
0
−10
−20
−30
−80
−70
−60
−50
−40
Ecosystems
Alto Paraná Atlantic forests
Araucaria moist forests
Atlantic Coast restingas
Bahia coastal forests
Bahia interior forests
Bolivian Yungas
Caatinga Enclaves moist forests
Caqueta moist forests
Catatumbo moist forests
Cauca Valley montane forests
Chocó−Darién moist forests
Cordillera La Costa montane forests
Cordillera Oriental montane forests
Eastern Cordillera Real montane forests
Eastern Panamanian montane forests
Fernando de Noronha−Atol das Rocas moist forests
Guianan freshwater swamp forests
Guianan Highlands moist forests
Guianan lowland moist forests
Guianan piedmont moist forests
Gurupa várzea
Iquitos várzea
Isthmian−Atlantic moist forests
Isthmian−Pacific moist forests
Japurá−Solimões−Negro moist forests
Juruá−Purus moist forests
Madeira−Tapajós moist forests
Magdalena−Urabá moist forests
Magdalena Valley montane forests
Marajó várzea
Marañón dry forests
Mato Grosso tropical dry forests
Monte Alegre várzea
Napo moist forests
Negro−Branco moist forests
Northeast Brazil restingas
Northwest Andean montane forests
Orinoco Delta swamp forests
Pantepui forests & shrublands
Pernambuco coastal forests
Pernambuco interior forests
Peruvian Yungas
Purus−Madeira moist forests
Purus várzea
Rio Negro campinarana
Santa Marta montane forests
Serra do Mar coastal forests
Solimões−Japurá moist forests
Southern Andean Yungas
Southwest Amazon moist forests
Tapajós−Xingu moist forests
Trinidad and Tobago moist forest
Uatumã−Trombetas moist forests
Ucayali moist forests
Venezuelan Andes montane forests
Western Ecuador moist forests
Xingu−Tocantins−Araguaia moist forests
Tocantins/Pindare moist forests

Appendix B

Longitude	Latitude	Family	Genus	Species
-49.936944	-23.776667	Acanthaceae	Justicia	Justicia carnea
-49.121389	-18.530278	Alismataceae	Aquarius	Aquarius longipetalus
-48.738391	-22.077486	Annonaceae	Annona	Annona squamosa
-53.956608	-24.465908	Apiaceae	Coriandrum	Coriandrum sativum
-50.392333	-20.286062	Apiaceae	Eryngium	Eryngium foetidum
-52.454849	-27.075367	Apiaceae	Foeniculum	Foeniculum vulgare
-48.321444	-23.002222	Apocynaceae	Asclepias	Asclepias curassavica
-55.555238	-25.1498	Araceae	Thaumatophyllum	Thaumatophyllum bipinnatifidum
-52.403333	-29.768505	Araceae	Spathicarpa	Spathicarpa hastifolia
-50.216666	-18.18	Araliaceae	Dendropanax	Dendropanax cuneatus
-54.756495	-26.563436	Asparagaceae	Dracaena	Dracaena trifasciata
-50.766667	-19.149444	Asparagaceae	Herreria	Herreria salsaparilha
-56.848892	-26.079405	Begoniaceae	Begonia	Begonia cucullata
-55.788	-26.511621	Bignoniaceae	Dolichandra	Dolichandra cynanchoides
-49.312565	-23.005034	Bixaceae	Bixa	Bixa orellana
-50.804347	-22.83154	Bixaceae	Bixa	Bixa orellana
-48.041667	-18.9125	Burseraceae	Protium	Protium heptaphyllum
-55.519735	-27.391936	Cactaceae	Parodia	Parodia claviceps
-56.351454	-23.618675	Cactaceae	Discocactus	Discocactus hartmannii
-49.631972	-19.612253	Calophyllaceae	Kielmeyera	Kielmeyera rubriflora
-52.678611	-22.805278	Capparaceae	Monilicarpa	Monilicarpa brasiliana
-53.416667	-22.183333	Caryocaraceae	Caryocar	Caryocar brasiliense
-51.41	-20.384444	Caryocaraceae	Caryocar	Caryocar brasiliense
-49.233333	-16.233333	Connaraceae	Rourea	Rourea induta
-53.494258	-28.226379	Convolvulaceae	Ipomoea	Ipomoea grandifolia
-54.852778	-21.223611	Cucurbitaceae	Cucurbita	Cucurbita moschata
-55.25	-24.25	Dennstaedtiaceae	Mucura	Mucura globulifera
-51.388152	-28.994221	Iridaceae	Herbertia	Herbertia lahue
-50.456417	-21.210228	Lecythidaceae	Couroupita	Couroupita guianensis
-49.421667	-17.674444	Lygodiaceae	Lygodium	Lygodium venustum
-56.52	-24.63	Lygodiaceae	Lygodium	Lygodium volubile
-54.557211	-25.5936	Meliaceae	Guarea	Guarea kunthiana
-53.040833	-24.083889	Meliaceae	Trichilia	Trichilia pallida
-48.42	-24.27	Nectriaceae	Cosmospora	Cosmospora flammea
-54.796361	-28.107409	Nyctaginaceae	Mirabilis	Mirabilis jalapa
-53.717495	-29.724081	Onagraceae	Ludwigia	Ludwigia major
-50.635556	-16.987778	Osmundaceae	Osmunda	Osmunda spectabilis
-51.733333	-22.466667	Osmundaceae	Osmunda	Osmunda spectabilis
-53.045	-25.364167	Phytolaccaceae	Trichostigma	Trichostigma octandrum
-54.734839	-29.405894	Polypodiaceae	Pleopeltis	Pleopeltis minima
-53.8425	-23.319722	Pontederiaceae	Pontederia	Pontederia azurea
-49.17	-20.95	Pontederiaceae	Pontederia	Pontederia crassipes
-51.946667	-23.431389	Rhamnaceae	Gouania	Gouania ulmifolia
-50.908301	-29.844729	Rosaceae	Rhaphiolepis	Rhaphiolepis bibas
-49.68	-15.3	Rutaceae	Murraya	Murraya paniculata
-54.916667	-22.197778	Salviniaceae	Salvinia	Salvinia auriculata
-50.759722	-16.048333	Sapotaceae	Chrysophyllum	Chrysophyllum marginatum
-56.001667	-22.689167	Symplocaceae	Symplocos	Symplocos pubescens

-49.951657	-22.186389	Urticaceae	Pilea	Pilea microphylla
-51.693333	-21.453333	Urticaceae	Cecropia	Cecropia pachystachya
-53.98	-27.257778	Violaceae	Pombalia	Pombalia bigibbosa
-45.050521	-22.702806	Amaranthaceae	Gomphrena	Gomphrena globosa
-46.370556	-21.973333	Blechnaceae	Blechnum	Blechnum austrobrasilianum
-41.045209	-22.040422	Convolvulaceae	Ipomoea	Ipomoea imperati
-42.260091	-21.998434	Myrtaceae	Syzygium	Syzygium malaccense
-46.124039	-20.975668	Plantaginaceae	Plantago	Plantago major
-47.544	-22.396472	Polypodiaceae	Pleopeltis	Pleopeltis pleopeltifolia
-44.965278	-21.740833	Ranunculaceae	Clematis	Clematis brasiliana
-47.34	-21.41	Rhamnaceae	Gouania	Gouania lupuloides
-47.41973	-23.492329	Rosaceae	Rhaphiolepis	Rhaphiolepis bibas
-43.875655	-22.374778	Rosaceae	Rhaphiolepis	Rhaphiolepis bibas
-45.942576	-23.182503	Urticaceae	Pilea	Pilea microphylla
-49.274444	-26.359444	Alstroemeriaceae	Bomarea	Bomarea edulis
-52.250833	-24.718056	Anacardiaceae	Schinus	Schinus terebinthifolia
-53.170415	-26.291874	Anacardiaceae	Mangifera	Mangifera indica
-48.765713	-27.556012	Annonaceae	Guatteria	Guatteria australis
-52.418748	-28.256515	Apiaceae	Apium	Apium graveolens
-51.193055	-27.011111	Araceae	Wolffia	Wolffia brasiliensis
-50.357942	-25.827903	Araucariaceae	Araucaria	Araucaria angustifolia
-51.845139	-25.945222	Araucariaceae	Araucaria	Araucaria angustifolia
-49.534167	-28.363611	Begoniaceae	Begonia	Begonia scharffiana
-49.015011	-25.384874	Cactaceae	Hatiora	Hatiora salicornoides
-51.186668	-28.059444	Caryophyllaceae	Stellaria	Stellaria media
-50.026389	-29.175833	Ericaceae	Gaylussacia	Gaylussacia brasiliensis
-51.083556	-23.966389	Ericaceae	Agarista	Agarista pulchella
-50.175556	-27.2925	Gunneraceae	Gunnera	Gunnera manicata
-51.265	-25.205556	Hypericaceae	Hypericum	Hypericum rigidum
-50.006356	-24.786984	Lamiaceae	Ocimum	Ocimum campechianum
-53.021417	-28.553637	Meliaceae	Melia	Melia azedarach
-52.193056	-26.984722	Menispermaceae	Cissampelos	Cissampelos pareira
-51.897217	-28.854253	Oxalidaceae	Oxalis	Oxalis articulata
-52.908177	-25.880731	Passifloraceae	Passiflora	Passiflora alata
-48.835278	-27.6925	Passifloraceae	Passiflora	Passiflora edulis
-51.184867	-26.875493	Passifloraceae	Passiflora	Passiflora eichleriana
-48.571444	-24.298361	Piperaceae	Piper	Piper aduncum
-49.37194	-26.558695	Polypodiaceae	Pleopeltis	Pleopeltis pleopeltifolia
-52.331667	-24.070278	Pontederiaceae	Heteranthera	Heteranthera zosterifolia
-50.425833	-25.821944	Proteaceae	Roupala	Roupala montana
-50.927821	-29.421175	Pteridaceae	Doryopteris	Doryopteris concolor
-49.013731	-25.381589	Rosaceae	Rubus	Rubus niveus
-53.991545	-26.516097	Rubiaceae	Manettia	Manettia paraguariensis
-52.825583	-24.920833	Rutaceae	Citrus	Citrus limon
-51.563889	-25.043889	Salicaceae	Casearia	Casearia sylvestris
-50.236111	-27.361111	Scrophulariaceae	Buddleja	Buddleja grandiflora
-50.499319	-28.474861	Sphagnaceae	Sphagnum	Sphagnum alegrense
-53.826667	-25.136944	Styracaceae	Styrax	Styrax leprosus
-51.343664	-27.914589	Thymelaeaceae	Daphnopsis	Daphnopsis racemosa
-49.816667	-24.133333	Thymelaeaceae	Daphnopsis	Daphnopsis brasiliensis
-53.811192	-27.675954	Verbenaceae	Lippia	Lippia alba

-50.94	-24.12	Violaceae	Pombalia	Pombalia bigibbosa
-51.850833	-25.967222	Xyridaceae	Xyris	Xyris neglecta
-35.403333	-5.243889	Anacardiaceae	Schinus	Schinus terebinthifolia
-35.09407	-6.187971	Nyctaginaceae	Mirabilis	Mirabilis jalapa
-49.625345	-29.21255	Lentibulariaceae	Utricularia	Utricularia tricolor
-50.323333	-30.3875	Scrophulariaceae	Buddleja	Buddleja thyrsoides
-41.475	-22.201389	Eriocaulaceae	Leiothrix	Leiothrix hirsuta
-39.170833	-14.797222	Amaranthaceae	Cyathula	Cyathula prostrata
-38.02	-12.02	Loganiaceae	Spigelia	Spigelia genuflexa
-39.171114	-13.82156	Moraceae	Artocarpus	Artocarpus heterophyllus
-38.509444	-13.004722	Pontederiaceae	Heteranthera	Heteranthera longirachilla
-41.5625	-20.394444	Alstroemeriaceae	Alstroemeria	Alstroemeria cunha
-40.057222	-16.403333	Amaryllidaceae	Griffinia	Griffinia albolineata
-40.0	-19.149294	Apocynaceae	Prestonia	Prestonia coalita
-40.466525	-18.319583	Euphorbiaceae	Euphorbia	Euphorbia pulcherrima
-40.290556	-20.338889	Sapindaceae	Cupania	Cupania emarginata
-40.422222	-17.363056	Selaginellaceae	Selaginella	Selaginella convoluta
-41.081389	-14.827778	Bignoniaceae	Handroanthus	Handroanthus impetiginosum
-40.21382	-14.326811	Bromeliaceae	Bromelia	Bromelia laciniosa
-40.4921	-13.44475	Cactaceae	Arrojadoa	Arrojadoa penicillata
-39.104444	-11.983333	Celastraceae	Monteverdia	Monteverdia acanthophylla
-39.516667	-12.945	Loganiaceae	Spigelia	Spigelia laurina
-40.970278	-21.171667	Amaranthaceae	Dysphania	Dysphania ambrosioides
-41.573889	-19.332778	Apocynaceae	Mandevilla	Mandevilla obovata
-44.168083	-22.107139	Blechnaceae	Blechnum	Blechnum occidentale
-41.474722	-17.826667	Brassicaceae	Lepidium	Lepidium ruderale
-41.755833	-15.498333	Cactaceae	Cereus	Cereus mirabella
-43.020278	-22.016944	Cannabaceae	Trema	Trema micranthum
-42.171666	-16.376944	Celastraceae	Tontelea	Tontelea micrantha
-43.806389	-17.891667	Clusiaceae	Clusia	Clusia nemorosa
-42.528439	-17.699009	Cucurbitaceae	Cyclanthera	Cyclanthera pedata
-42.8664	-20.735458	Cucurbitaceae	Momordica	Momordica charantia
-45.663056	-20.282778	Dioscoreaceae	Dioscorea	Dioscorea multiflora
-42.516944	-19.700278	Dryopteridaceae	Ctenitis	Ctenitis falciculata
-42.190089	-21.414284	Fabaceae	Mimosa	Mimosa caesalpiniifolia
-43.7425	-19.048611	Humiriaceae	Vantanea	Vantanea obovata
-42.7375	-15.615833	Hymenophyllaceae	Trichomanes	Trichomanes pilosum
-43.93575	-19.95117	Iridaceae	Cipura	Cipura paludosa
-41.068547	-16.39938	Malvaceae	Ayenia	Ayenia blanchetiana
-45.0863	-21.099939	Papaveraceae	Argemone	Argemone mexicana
-42.672131	-18.759296	Passifloraceae	Passiflora	Passiflora alata
-45.94812	-19.327957	Pontederiaceae	Pontederia	Pontederia crassipes
-43.8155	-20.967944	Theaceae	Gordonia	Gordonia fruticosa
-40.251814	-15.244316	Verbenaceae	Duranta	Duranta erecta
-44.887615	-19.662544	Vochysiaceae	Vochysia	Vochysia thyrsoidea
-77.75	8.25	Alismataceae	Aquarius	Aquarius tunicatus
-79.408253	9.580143	Amaryllidaceae	Crinum	Crinum amabile
-79.92485	8.684798	Araceae	Philodendron	Philodendron verrucosum
-78.466802	8.94917	Araceae	Monstera	Monstera dubia
-79.352422	9.575279	Combretaceae	Terminalia	Terminalia catappa
-77.766667	8.333333	Connaraceae	Connarus	Connarus williamsii

-78.755664	8.891293	Lygodiaceae	Lygodium	Lygodium venustum
-79.93333	8.68333	Thymelaeaceae	Daphnopsis	Daphnopsis americana
-35.895	-9.710278	Araceae	Anthurium	Anthurium affine
-35.146944	-8.890058	Cyperaceae	Cyperus	Cyperus pedunculatus
-35.746667	-6.97	Lecythidaceae	Eschweilera	Eschweilera ovata
-35.002778	-7.836111	Menispermaceae	Cissampelos	Cissampelos andromorpha
-37.522933	-11.76161	Cyperaceae	Cyperus	Cyperus pedunculatus
-37.009167	-10.618222	Gesneriaceae	Sinningia	Sinningia nordestina
-36.05	-8.01667	Nymphaeaceae	Nymphaea	Nymphaea lasiophylla
-36.504831	-8.88642	Papaveraceae	Argemone	Argemone mexicana
-35.203611	-6.215833	Pontederiaceae	Pontederia	Pontederia diversifolia
-49.217222	-24.7825	Alstroemeriaceae	Bomarea	Bomarea edulis
-49.948889	-26.460278	Bignoniaceae	Pyrostegia	Pyrostegia venusta
-48.04933	-25.17666	Clethraceae	Clethra	Clethra scabra
-50.045278	-29.562778	Elaeocarpaceae	Sloanea	Sloanea guianensis
-48.03845	-23.192583	Loranthaceae	Struthanthus	Struthanthus rhynchophyllus
-48.306792	-24.306667	Marattiaceae	Danaea	Danaea nodosa
-49.507745	-28.489712	Meliaceae	Cabralea	Cabralea canjerana
-48.591667	-25.955833	Polygalaceae	Polygala	Polygala cyparissias
-48.46187	-27.543912	Urticaceae	Urera	Urera nitida
-49.509588	-27.282284	Winteraceae	Drimys	Drimys angustifolia
-45.572648	-22.733436	Alismataceae	Sagittaria	Sagittaria montevidensis
-45.929749	-23.741938	Annonaceae	Guatteria	Guatteria australis
-46.978038	-24.301642	Apiaceae	Eryngium	Eryngium foetidum
-42.047644	-22.010847	Araceae	Anthurium	Anthurium solitarium
-44.727305	-23.35263	Araliaceae	Hydrocotyle	Hydrocotyle bonariensis
-44.538333	-22.336111	Araliaceae	Didymopanax	Didymopanax calvus
-43.541145	-23.050919	Arecaceae	Bactris	Bactris setosa
-46.916667	-22.833333	Asparagaceae	Herreria	Herreria salsaparilha
-43.211636	-22.121893	Bixaceae	Bixa	Bixa orellana
-42.409942	-22.900111	Bixaceae	Bixa	Bixa orellana
-41.871389	-21.850278	Blechnaceae	Austroblechnum	Austroblechnum lehmannii
-42.032629	-22.969233	Capparaceae	Cynophalla	Cynophalla flexuosa
-43.532777	-23.044722	Connaraceae	Connarus	Connarus nodosus
-46.70436	-22.604601	Convolvulaceae	Ipomoea	Ipomoea cairica
-45.616667	-22.751944	Dennstaedtiaceae	Dennstaedtia	Dennstaedtia cornuta
-47.951667	-24.804444	Elaeocarpaceae	Sloanea	Sloanea guianensis
-44.55142	-23.30296	Elaeocarpaceae	Sloanea	Sloanea hirsuta
-47.38	-24.038056	Loganiaceae	Spigelia	Spigelia beyrichiana
-42.843333	-22.0775	Menispermaceae	Cissampelos	Cissampelos andromorpha
-47.65812	-22.92694	Phyllanthaceae	Phyllanthus	Phyllanthus tenellus
-45.342197	-23.915512	Polygalaceae	Polygala	Polygala paniculata
-46.374253	-23.939164	Solanaceae	Brugmansia	Brugmansia insignis
-44.53805	-22.33361	Theaceae	Gordonia	Gordonia fruticosa
-67.23333	-16.95	Alstroemeriaceae	Bomarea	Bomarea ovata
-67.863889	-14.173333	Anacardiaceae	Tapirira	Tapirira guianensis
-67.893057	-16.295016	Asteraceae	Diplostephium	Diplostephium haenkei
-66.001667	-16.119444	Bixaceae	Bixa	Bixa urucurana
-67.071667	-15.228333	Blechnaceae	Blechnum	Blechnum asplenioides
-65.820556	-17.211667	Chloranthaceae	Hedyosmum	Hedyosmum angustifolium
-69.086111	-14.705	Lamiaceae	Salvia	Salvia dombeyi

-68.741164	-13.630292	Meliaceae	Guarea	Guarea gomma
-68.291321	-15.300972	Pentaphylacaceae	Freziera	Freziera angulosa
-63.65	-17.6	Menispermaceae	Odontocarya	Odontocarya diplobotrya
-64.738611	-17.737778	Polygalaceae	Monnina	Monnina herzogii
-39.773056	-3.750278	Alismataceae	Hydrocleys	Hydrocleys martii
-39.281409	-7.277387	Capparaceae	Cynophalla	Cynophalla hastata
-41.1975	-3.3075	Dilleniaceae	Davilla	Davilla cearensis
-40.811389	-4.530278	Myrtaceae	Myrciaria	Myrciaria pilosa
-38.88111	-4.32583	Thymelaeaceae	Daphnopsis	Daphnopsis racemosa
-73.726944	2.723056	Bixaceae	Bixa	Bixa urucurana
-72.465	-0.55361	Bonnetiaceae	Bonnetia	Bonnetia paniculata
-72.875	1.488333	Combretaceae	Terminalia	Terminalia parvifolia
-71.1735	2.178	Connaraceae	Rourea	Rourea puberula
-70.17	0.5	Humiriaceae	Sacoglottis	Sacoglottis ceratocarpa
-74.776314	2.159506	Lecythidaceae	Couroupita	Couroupita guianensis
-71.83333	0.83333	Loganiaceae	Strychnos	Strychnos subcordata
-72.685692	2.497107	Lycopodiaceae	Palhinhaea	Palhinhaea cernua
-71.143931	0.093767	Nephrolepidaceae	Nephrolepis	Nephrolepis hirsutula
-70.8432	1.1911	Olacaceae	Dulacia	Dulacia redmondii
-74.040833	1.494167	Polygalaceae	Polygala	Polygala galioides
-72.934722	0.248333	Rhizophoraceae	Cassipourea	Cassipourea guianensis
-71.60028	-0.93166	Sabiaceae	Ophiocaryon	Ophiocaryon heterophyllum
-70.244444	-0.451389	Schizaeaceae	Actinostachys	Actinostachys pennula
-74.262444	-0.078667	Selaginellaceae	Selaginella	Selaginella exaltata
-69.976109	1.864341	Chrysobalanaceae	Hirtella	Hirtella duckei
-69.533333	-1.083333	Humiriaceae	Sacoglottis	Sacoglottis guianensis
-72.508651	7.898278	Apocynaceae	Nerium	Nerium oleander
-71.78333	8.83333	Lentibulariaceae	Utricularia	Utricularia pusilla
-73.264444	8.508333	Nephrolepidaceae	Nephrolepis	Nephrolepis cordifolia
-72.8986	9.5917	Xyridaceae	Xyris	Xyris jupicai
-76.400235	4.173029	Annonaceae	Guatteria	Guatteria goudotiana
-75.739506	5.747484	Aquifoliaceae	Ilex	Ilex laurina
-75.8226	6.6949	Araliaceae	Aralia	Aralia excelsa
-76.460176	2.498819	Betulaceae	Alnus	Alnus jorullensis
-75.26633	7.44375	Bixaceae	Bixa	Bixa orellana
-75.476472	4.636737	Bromeliaceae	Vriesea	Vriesea tequendamae
-75.293083	5.852667	Dicksoniaceae	Lophosoria	Lophosoria quadripinnata
-76.647017	2.472737	Iridaceae	Trimezia	Trimezia steyermarkii
-76.1054	6.4218	Isoetaceae	Isoetes	Isoetes killipii
-76.148167	3.8095	Juglandaceae	Juglans	Juglans neotropica
-75.459839	4.632586	Plantaginaceae	Veronica	Veronica serpyllifolia
-75.466667	7.166667	Sphagnaceae	Sphagnum	Sphagnum aciphyllum
-67.566171	10.313671	Acanthaceae	Thunbergia	Thunbergia alata
-68.625	10.225	Blechnaceae	Blechnum	Blechnum meridense
-66.522629	10.626259	Combretaceae	Terminalia	Terminalia catappa
-65.76305	10.06805	Lentibulariaceae	Utricularia	Utricularia alpina
-63.878889	10.141111	Amaranthaceae	Iresine	Iresine diffusa
-62.631944	10.680833	Apocynaceae	Asclepias	Asclepias curassavica
-75.706389	1.682778	Bixaceae	Bixa	Bixa orellana
-72.994611	9.985519	Apiaceae	Eryngium	Eryngium humboldtii
-72.09345	5.830654	Asteraceae	Piptocoma	Piptocoma discolor

-73.79433	2.25984	Clusiaceae	Clusia	Clusia columnaris
-74.897611	2.338944	Cyclanthaceae	Cyclanthus	Cyclanthus bipartitus
-73.939935	4.404854	Juglandaceae	Juglans	Juglans neotropica
-73.203333	8.048611	Lycopodiaceae	Palhinhaea	Palhinhaea cernua
-72.3461	7.13472	Marattiaceae	Danaea	Danaea moritziana
-74.15025	3.46903	Sabiaceae	Meliosma	Meliosma tachirensis
-73.426398	5.17485	Solanaceae	Deprea	Deprea bitteriana
-77.688611	-1.323611	Bixaceae	Bixa	Bixa orellana
-78.142842	-2.22776	Cyclanthaceae	Carludovica	Carludovica palmata
-79.440558	-4.711887	Hypericaceae	Hypericum	Hypericum laricifolium
-78.151188	-0.355732	Loranthaceae	Aetanthus	Aetanthus nodosus
-78.337778	-5.139722	Lygodiaceae	Lygodium	Lygodium radiatum
-79.7422	-3.6547	Marattiaceae	Eupodium	Eupodium laeve
-77.333	0.083	Marattiaceae	Danaea	Danaea oblanceolata
-79.3258	-5.74229	Papaveraceae	Bocconia	Bocconia frutescens
-78.610129	-1.242055	Sapindaceae	Dodonaea	Dodonaea viscosa
-78.4383	-3.585	Sphagnaceae	Sphagnum	Sphagnum magellanicum
-76.7303	1.0828	Thelypteridaceae	Christella	Christella hispidula
-79.148322	-2.841337	Violaceae	Viola	Viola arguta
-57.000722	5.929417	Cyperaceae	Cyperus	Cyperus difformis
-55.093682	5.686794	Pontederiaceae	Pontederia	Pontederia crassipes
-66.005	0.806667	Asteraceae	Glossarion	Glossarion bilabiatum
-67.3	4.983334	Bonnetiaceae	Archytaea	Archytaea triflora
-66.05	5.683333	Bonnetiaceae	Bonnetia	Bonnetia celiae
-65.0	6.0	Cyclanthaceae	Thoracocarpus	Thoracocarpus bissectus
-65.3	7.283333	Elaeocarpaceae	Sloanea	Sloanea grandiflora
-66.38	6.56	Erythroxylaceae	Erythroxylum	Erythroxylum mucronatum
-66.350278	4.730556	Hypericaceae	Vismia	Vismia macrophylla
-65.683333	3.65	Smilacaceae	Smilax	Smilax schomburgkiana
-65.25	4.58333	Xyridaceae	Xyris	Xyris atriceps
-61.106389	4.501944	Apocynaceae	Mandevilla	Mandevilla scaberula
-64.683333	2.966667	Aquifoliaceae	Ilex	Ilex laureola
-62.8	1.533333	Begoniaceae	Begonia	Begonia semiovata
-64.37	4.05	Begoniaceae	Begonia	Begonia semiovata
-62.116667	5.05	Bonnetiaceae	Bonnetia	Bonnetia huberiana
-63.833333	2.133333	Calophyllaceae	Caraipa	Caraipa densifolia
-63.558333	6.375	Calophyllaceae	Mahurea	Mahurea exstipulata
-63.532778	3.008056	Caryocaraceae	Caryocar	Caryocar montanum
-63.88	4.95	Cyatheaceae	Cyathea	Cyathea lellingeriana
-63.283056	4.228889	Hymenophyllaceae	Trichomanes	Trichomanes bicorne
-61.354167	6.166111	Lamiaceae	Marsypianthes	Marsypianthes chamaedrys
-60.51016	5.23516	Primulaceae	Myrsine	Myrsine guianensis
-62.518413	5.9739	Rubiaceae	Geophila	Geophila repens
-64.91666	1.33333	Smilacaceae	Smilax	Smilax maypurensis
-61.892222	1.598056	Urticaceae	Coussapoa	Coussapoa viridifolia
-57.5	1.83333	Cyatheaceae	Cyathea	Cyathea andina
-58.699722	1.2775	Hymenophyllaceae	Didymoglossum	Didymoglossum punctatum
-59.4837	5.17947	Lycopodiaceae	Pseudolycopodiella	Pseudolycopodiella meridionalis
-56.16166	3.9025	Sphagnaceae	Sphagnum	Sphagnum perichaetiale
-54.740556	4.268611	Anacardiaceae	Tapirira	Tapirira guianensis
-53.080408	3.024657	Polypodiaceae	Terpsichore	Terpsichore staheliana

-62.933333	7.766667	Boraginaceae	Glandora	Glandora oleifolia
-60.376361	6.377389	Meliaceae	Trichilia	Trichilia rubra
-61.66	8.5	Nephrolepidaceae	Nephrolepis	Nephrolepis biserrata
-61.492861	7.437167	Rutaceae	Zanthoxylum	Zanthoxylum caribaeum
-56.733333	4.716667	Acanthaceae	Ruellia	Ruellia rubra
-55.78333	2.33333	Amaranthaceae	Cyathula	Cyathula prostrata
-58.93333	7.63333	Anacardiaceae	Anacardium	Anacardium giganteum
-57.34	3.37	Anacardiaceae	Spondias	Spondias mombin
-58.0	5.666667	Anacardiaceae	Tapirira	Tapirira guianensis
-59.63	4.15	Anacardiaceae	Cyrtocarpa	Cyrtocarpa velutinifolia
-59.255568	3.330376	Arecaceae	Socratea	Socratea exorrhiza
-59.28	2.07	Aspleniaceae	Asplenium	Asplenium serratum
-58.37	2.33	Aspleniaceae	Asplenium	Asplenium serratum
-57.75	4.5	Capparaceae	Neocalyptrocalyx	Neocalyptrocalyx maroniensis
-58.29972	3.58417	Celastraceae	Peritassa	Peritassa laevigata
-55.566667	4.666667	Celastraceae	Hippocratea	Hippocratea volubilis
-58.83333	6.35	Connaraceae	Rourea	Rourea surinamensis
-58.68531	4.67139	Convolvulaceae	Calycobolus	Calycobolus glaber
-59.95	7.81666	Cyclanthaceae	Asplundia	Asplundia heteranthera
-56.753889	2.363889	Dilleniaceae	Doliocarpus	Doliocarpus spraguei
-55.45	3.33	Dioscoreaceae	Dioscorea	Dioscorea chondrocarpa
-58.0	6.75	Lentibulariaceae	Utricularia	Utricularia foliosa
-59.35	3.25	Loranthaceae	Struthanthus	Struthanthus phillyreoides
-55.16	5.53	Lygodiaceae	Lygodium	Lygodium volubile
-58.63	2.3743	Ochnaceae	Ouratea	Ouratea candollei
-59.73	6.783333	Onagraceae	Ludwigia	Ludwigia affinis
-56.307573	4.989113	Passifloraceae	Passiflora	Passiflora vespertilio
-58.723	6.28453	Passifloraceae	Passiflora	Passiflora costata
-58.9	7.61	Passifloraceae	Passiflora	Passiflora glandulosa
-55.37217	4.4215	Poaceae	Oryza	Oryza sativa
-56.18333	3.93333	Polypodiaceae	Microgramma	Microgramma lycopodioides
-55.2	2.196939	Rhizophoraceae	Cassipourea	Cassipourea guianensis
-57.395243	2.579202	Rubiaceae	Palicourea	Palicourea apoda
-57.15	4.38	Sapindaceae	Paullinia	Paullinia stenopetala
-56.15	2.03	Schizaeaceae	Actinostachys	Actinostachys pennula
-55.45	3.35	Selaginellaceae	Selaginella	Selaginella epirrhizos
-57.981453	5.43716	Simaroubaceae	Quassia	Quassia amara
-59.64333	4.15333	Smilacaceae	Smilax	Smilax schomburgkiana
-58.21147	3.38867	Solanaceae	Solanum	Solanum schomburghii
-59.144444	5.368333	Solanaceae	Solanum	Solanum crinitum
-58.693889	1.2675	Thelypteridaceae	Steiropteris	Steiropteris leprieurii
-57.8167	6.58333	Typhaceae	Typha	Typha domingensis
-58.625	4.58333	Verbenaceae	Petrea	Petrea macrostachya
-59.93333	7.69833	Vitaceae	Cissus	Cissus verticillata
-59.566667	1.983333	Vochysiaceae	Vochysia	Vochysia glaberrima
-53.30211	4.58764	Amaryllidaceae	Hymenocallis	Hymenocallis tubiflora
-53.202222	3.640466	Araceae	Monstera	Monstera gracilis
-51.005278	1.896667	Araceae	Philodendron	Philodendron ornatum
-52.87	2.23	Aspleniaceae	Asplenium	Asplenium hostmannii
-54.61666	2.91666	Celastraceae	Salacia	Salacia impressifolia
-53.5	1.5	Celastraceae	Salacia	Salacia insignis

-51.867367	3.962767	Clusiaceae	Symphonia	Symphonia globulifera
-53.80556	2.51111	Erythroxylaceae	Erythroxylum	Erythroxylum citrifolium
-54.448676	4.937205	Euphorbiaceae	Croton	Croton trinitatis
-54.133753	3.802033	Lygodiaceae	Lygodium	Lygodium volubile
-51.93333	2.08333	Menispermaceae	Abuta	Abuta grandifolia
-51.38	2.8	Proteaceae	Euplassa	Euplassa pinnata
-52.351826	4.838927	Pteridaceae	Adiantum	Adiantum serratodentatum
-54.42444	1.24528	Sapindaceae	Toulicia	Toulicia elliptica
-52.335558	3.170167	Vitaceae	Cissus	Cissus erosa
-66.16666	0.83333	Bonnetiaceae	Bonnetia	Bonnetia neblinae
-66.541667	6.922417	Calophyllaceae	Caraipa	Caraipa parvielliptica
-67.366667	5.616667	Calophyllaceae	Caraipa	Caraipa densifolia
-66.15	3.016667	Calophyllaceae	Caraipa	Caraipa costata
-65.237667	7.362	Commelinaceae	Murdannia	Murdannia nudiflora
-65.343056	4.8575	Connaraceae	Connarus	Connarus punctatus
-65.34	0.471945	Cyatheaceae	Cyathea	Cyathea marginalis
-66.283333	4.666667	Eriocaulaceae	Comanthera	Comanthera reflexa
-67.009	4.002	Loganiaceae	Strychnos	Strychnos rondeletioides
-67.66666	4.75	Loganiaceae	Strychnos	Strychnos guianensis
-66.13333	5.61667	Lythraceae	Cuphea	Cuphea pleiantha
-65.67	1.65	Salviniaceae	Azolla	Azolla caroliniana
-63.75	4.166667	Aquifoliaceae	Ilex	Ilex jenmanii
-61.647222	3.390833	Araceae	Monstera	Monstera adansonii
-64.55	2.933333	Begoniaceae	Begonia	Begonia humilis
-63.4	3.33	Begoniaceae	Begonia	Begonia semiovata
-63.316667	5.283333	Blechnaceae	Salpichlaena	Salpichlaena volubilis
-61.391667	5.963056	Bonnetiaceae	Archytaea	Archytaea triflora
-61.63333	4.38333	Caryocaraceae	Caryocar	Caryocar nuciferum
-63.335833	6.340556	Clethraceae	Clethra	Clethra occidentalis
-61.633611	1.537222	Clusiaceae	Clusia	Clusia nitida
-63.35	0.78	Connaraceae	Rourea	Rourea krukovii
-61.960833	7.370833	Cucurbitaceae	Cucumis	Cucumis anguria
-64.23333	5.03333	Dioscoreaceae	Dioscorea	Dioscorea amazonum
-62.8	4.45	Dioscoreaceae	Dioscorea	Dioscorea amazonum
-64.55	1.616667	Humiriaceae	Endopleura	Endopleura uchi
-62.450581	5.687135	Iridaceae	Sisyrinchium	Sisyrinchium vaginatum
-64.46667	6.2	Loganiaceae	Strychnos	Strychnos mitscherlichii
-60.232222	2.863333	Melastomataceae	Macairea	Macairea theresiae
-62.8	2.60966	Nephrolepidaceae	Nephrolepis	Nephrolepis occidentalis
-61.40743	2.48051	Passifloraceae	Passiflora	Passiflora longiracemosa
-63.35	1.85	Pentaphylacaceae	Ternstroemia	Ternstroemia prancei
-64.21666	7.18333	Schizaeaceae	Schizaea	Schizaea elegans
-62.916667	7.166667	Smilacaceae	Smilax	Smilax purhampuy
-55.08	-1.83	Nymphaeaceae	Victoria	Victoria amazonica
-53.978077	-1.944214	Nymphaeaceae	Victoria	Victoria amazonica
-52.533333	-1.85	Polygonaceae	Symmeria	Symmeria paniculata
-75.47747	-8.957518	Apocynaceae	Asclepias	Asclepias curassavica
-77.33333	-4.75	Connaraceae	Connarus	Connarus fasciculatus
-76.41666	-2.91666	Connaraceae	Connarus	Connarus punctatus
-75.487063	-5.232501	Nymphaeaceae	Victoria	Victoria amazonica
-76.229636	-5.896266	Pontederiaceae	Pontederia	Pontederia crassipes

-75.011944	-7.424444	Pteridaceae	Adiantum	Adiantum poeppigianum
-75.216666	-1.783333	Saccolomataceae	Saccoloma	Saccoloma inaequale
-73.53333	-4.58333	Alismataceae	Sagittaria	Sagittaria sprucei
-74.375627	-9.163761	Alismataceae	Helanthium	Helanthium bolivianum
-73.865556	-5.81	Aspleniaceae	Asplenium	Asplenium juglandifolium
-70.36205	-8.1733	Commelinaceae	Tradescantia	Tradescantia zebrina
-72.926667	-7.555	Connaraceae	Rourea	Rourea camptoneura
-71.81666	-3.33333	Icacinaceae	Leretia	Leretia cordata
-70.176944	-9.13	Loganiaceae	Strychnos	Strychnos malacosperma
-72.68333	-9.2	Loganiaceae	Strychnos	Strychnos gubleri
-70.5	-3.91667	Loganiaceae	Strychnos	Strychnos mitscherlichii
-74.276111	-2.12	Loganiaceae	Strychnos	Strychnos erichsonii
-74.419784	-8.205898	Malvaceae	Theobroma	Theobroma cacao
-74.494444	-4.903611	Menispermaceae	Odontocarya	Odontocarya tripetala
-73.134256	-3.60355	Nymphaeaceae	Victoria	Victoria amazonica
-74.8306	-6.0723	Pontederiaceae	Pontederia	Pontederia crassipes
-71.818333	-7.177222	Saccolomataceae	Saccoloma	Saccoloma inaequale
-74.995314	-3.749918	Saccolomataceae	Saccoloma	Saccoloma inaequale
-71.91666	-4.33333	Schizaeaceae	Schizaea	Schizaea elegans
-69.764722	-6.693889	Amaryllidaceae	Urceolina	Urceolina ulei
-69.2611617	-8.8426936	Capparaceae	Capparidastrum	Capparidastrum solum
-67.566667	-10.066667	Lythraceae	Adenaria	Adenaria floribunda
-68.48658	-10.9428	Rutaceae	Esenbeckia	Esenbeckia almawillia
-70.33972	1.02917	Caryocaraceae	Caryocar	Caryocar glabrum
-67.166667	0.966667	Caryocaraceae	Caryocar	Caryocar gracile
-69.0	-1.833333	Caryocaraceae	Caryocar	Caryocar gracile
-68.666667	-0.3	Cyclanthaceae	Sphaeradenia	Sphaeradenia duidae
-67.088889	-0.13	Dilleniaceae	Doliocarpus	Doliocarpus amazonicus
-68.440524	1.922045	Dioscoreaceae	Dioscorea	Dioscorea amazonum
-67.083333	1.9	Dioscoreaceae	Dioscorea	Dioscorea trichanthera
-67.661629	2.792112	Humiriaceae	Humiria	Humiria balsamifera
-65.666667	-1.833333	Icacinaceae	Casimirella	Casimirella ampla
-66.036667	-0.556944	Lentibulariaceae	Utricularia	Utricularia steyermarkii
-66.895556	-1.372222	Melastomataceae	Miconia	Miconia bullatifolia
-69.732767	1.740639	Menispermaceae	Odontocarya	Odontocarya tamoides
-69.216667	0.966667	Schizaeaceae	Schizaea	Schizaea incurvata
-68.15	-1.4	Schizaeaceae	Schizaea	Schizaea incurvata
-68.92528	2.72194	Selaginellaceae	Selaginella	Selaginella amazonica
-65.089167	-1.028611	Simaroubaceae	Simaba	Simaba polyphylla
-68.136111	0.542222	Urticaceae	Pourouma	Pourouma villosa
-60.786935	-2.5724	Bignoniaceae	Handroanthus	Handroanthus barbatus
-63.5	-0.52	Calophyllaceae	Caraipa	Caraipa densifolia
-62.563477	-3.313436	Clusiaceae	Garcinia	Garcinia madruno
-64.42	-0.42	Connaraceae	Connarus	Connarus ruber
-61.583333	-1.416667	Icacinaceae	Casimirella	Casimirella ampla
-61.95	-2.383333	Moraceae	Ficus	Ficus caballina
-64.748122	-2.486228	Oxalidaceae	Averrhoa	Averrhoa carambola
-61.333333	-3.333333	Pentaphylacaceae	Ternstroemia	Ternstroemia dentata
-63.5	-2.5	Plantaginaceae	Scoparia	Scoparia dulcis
-63.53	-1.6	Simaroubaceae	Simaba	Simaba obovata
-59.926667	-3.080278	Sapotaceae	Pradosia	Pradosia lahoziana

-65.751502	-5.660786	Acanthaceae	Ruellia	Ruellia chartacea
-67.616944	-8.280556	Acanthaceae	Dianthera	Dianthera pectoralis
-66.035833	-4.105833	Annonaceae	Annona	Annona mucosa
-68.023917	-7.475917	Bixaceae	Bixa	Bixa urucurana
-67.6125	-5.888889	Bixaceae	Bixa	Bixa excelsa
-68.252322	-8.932083	Blechnaceae	Salpichlaena	Salpichlaena volubilis
-66.852047	-2.952522	Bromeliaceae	Aechmea	Aechmea poitaei
-65.333056	-4.843056	Burseraceae	Crepidospermum	Crepidospermum rhoifolium
-69.606389	-4.071389	Caryocaraceae	Caryocar	Caryocar glabrum
-66.783333	-6.716667	Caryocaraceae	Anthodiscus	Anthodiscus amazonicus
-66.798611	-4.992778	Convolvulaceae	Calycobolus	Calycobolus glaber
-69.0	-5.0	Dilleniaceae	Doliocarpus	Doliocarpus macrocarpus
-65.55	-3.196667	Humiriaceae	Schistostemon	Schistostemon retusum
-65.833333	-7.333333	Loganiaceae	Strychnos	Strychnos mattogrossensis
-68.0	-5.0	Proteaceae	Panopsis	Panopsis rubescens
-68.524333	-6.096722	Simaroubaceae	Homalolepis	Homalolepis pohliana
-67.2	-3.9075	Sphagnaceae	Sphagnum	Sphagnum magellanicum
-68.069483	-3.459295	Verbenaceae	Stachytarpheta	Stachytarpheta cayennensis
-63.383231	-4.138492	Acanthaceae	Dianthera	Dianthera pectoralis
-64.42	-5.0	Cyclanthaceae	Asplundia	Asplundia xiphophylla
-64.37	-4.05	Pontederiaceae	Pontederia	Pontederia diversifolia
-65.446944	-9.641944	Annonaceae	Onychopetalum	Onychopetalum periquino
-65.36666	-10.81666	Connaraceae	Rourea	Rourea cuspidata
-60.266667	-9.322222	Acanthaceae	Dianthera	Dianthera pectoralis
-64.868056	-11.721111	Annonaceae	Xylopia	Xylopia sericea
-62.8438	-7.893992	Annonaceae	Duguetia	Duguetia flagellaris
-64.327222	-9.231389	Annonaceae	Guatteria	Guatteria guianensis
-61.46924	-11.423882	Araceae	Colocasia	Colocasia esculenta
-63.013854	-9.951252	Asteraceae	Emilia	Emilia fosbergii
-62.016111	-12.435	Asteraceae	Neocuatrecasia	Neocuatrecasia epapposa
-60.172222	-8.158889	Bonnetiaceae	Bonnetia	Bonnetia rubicunda
-61.746944	-13.616389	Calophyllaceae	Calophyllum	Calophyllum brasiliense
-63.173333	-15.922778	Caryocaraceae	Caryocar	Caryocar brasiliense
-62.224073	-6.948409	Caryocaraceae	Caryocar	Caryocar microcarpum
-64.28333	-12.41666	Connaraceae	Rourea	Rourea amazonica
-64.706139	-14.931806	Convolvulaceae	Ipomoea	Ipomoea cryptica
-61.044167	-7.436389	Dilleniaceae	Doliocarpus	Doliocarpus dentatus
-63.641667	-10.858055	Ericaceae	Gaylussacia	Gaylussacia amazonica
-61.407222	-8.581944	Eriocaulaceae	Syngonanthus	Syngonanthus humboldtii
-60.633333	-12.016667	Erythroxylaceae	Erythroxylum	Erythroxylum mucronatum
-63.651986	-13.238669	Euphorbiaceae	Hevea	Hevea brasiliensis
-60.720278	-13.661389	Iridaceae	Cipura	Cipura paludosa
-60.2175	-5.168889	Lauraceae	Ocotea	Ocotea wurdackiana
-62.783333	-14.733333	Loganiaceae	Strychnos	Strychnos nigricans
-62.058964	-9.665672	Lythraceae	Lagerstroemia	Lagerstroemia speciosa
-63.274167	-9.036944	Melastomataceae	Miconia	Miconia tetrasperma
-64.3329	-10.1913	Meliaceae	Guarea	Guarea kunthiana
-63.75	-14.75	Nephrolepidaceae	Nephrolepis	Nephrolepis biserrata
-61.192819	-14.607496	Nymphaeaceae	Nymphaea	Nymphaea oxypetala
-63.058577	-11.735725	Poaceae	Zea	Zea mays
-62.222558	-10.735669	Pteridaceae	Adiantopsis	Adiantopsis radiata

-61.074769	-6.088733	Salicaceae	Casearia	Casearia ulmifolia
-60.933333	-10.6625	Vochysiaceae	Ruizterania	Ruizterania esmeraldae
-55.198333	-9.950278	Acanthaceae	Dianthera	Dianthera pectoralis
-58.079664	-5.203169	Anacardiaceae	Anacardium	Anacardium spruceanum
-55.980743	-4.257059	Apocynaceae	Asclepias	Asclepias curassavica
-59.583333	-4.383333	Aquifoliaceae	Ilex	Ilex divaricata
-58.074444	-8.936389	Araceae	Spathiphyllum	Spathiphyllum juninense
-57.591389	-6.162222	Araceae	Anthurium	Anthurium clavigerum
-55.215278	-3.38	Arecaceae	Mauritia	Mauritia flexuosa
-59.0	-5.166667	Aspleniaceae	Asplenium	Asplenium angustum
-57.053167	-10.2515	Asteraceae	Mikania	Mikania cordifolia
-59.939167	-7.183056	Asteraceae	Echinocoryne	Echinocoryne schwenkiifolia
-59.503056	-10.050833	Burseraceae	Protium	Protium trifoliolatum
-56.686067	-2.187585	Burseraceae	Protium	Protium heptaphyllum
-56.174472	-10.007417	Cannabaceae	Celtis	Celtis iguanaea
-59.0164	-6.8331	Capparaceae	Preslianthus	Preslianthus pittieri
-56.860583	-4.89475	Connaraceae	Connarus	Connarus perrottetii
-59.030278	-11.188056	Convolvulaceae	Distimake	Distimake macrocalyx
-56.780278	-9.330833	Cucurbitaceae	Gurania	Gurania lobata
-55.4475	-11.28	Dilleniaceae	Davilla	Davilla kunthii
-58.7	-4.2	Eriocaulaceae	Syngonanthus	Syngonanthus williamsii
-59.2	-8.999722	Euphorbiaceae	Croton	Croton matourensis
-57.723889	-11.089444	Euphorbiaceae	Sagotia	Sagotia brachysepala
-58.272972	-9.87155	Hypericaceae	Vismia	Vismia guianensis
-57.63333	-4.38333	Loganiaceae	Strychnos	Strychnos guianensis
-58.134351	-7.344654	Loganiaceae	Strychnos	Strychnos peckii
-57.711944	-3.391944	Loganiaceae	Strychnos	Strychnos amazonica
-55.973055	-2.845278	Malpighiaceae	Banisteriopsis	Banisteriopsis muricata
-56.063806	-9.87625	Malvaceae	Ceiba	Ceiba pentandra
-58.178055	-7.279167	Melastomataceae	Miconia	Miconia ciliata
-56.703611	-2.868472	Menispermaceae	Abuta	Abuta grandifolia
-59.508889	-10.060278	Moraceae	Pseudolmedia	Pseudolmedia laevis
-59.6425	-3.725833	Moraceae	Helicostylis	Helicostylis turbinata
-55.758056	-10.987222	Moraceae	Pseudolmedia	Pseudolmedia laevis
-57.25	-4.25	Nectriaceae	Nectria	Nectria lunulata
-59.48	-5.17	Onagraceae	Ludwigia	Ludwigia grandiflora
-58.5	-3.83333	Onagraceae	Ludwigia	Ludwigia decurrens
-56.258611	-4.485278	Polygalaceae	Securidaca	Securidaca bialata
-58.02	-4.97	Proteaceae	Roupala	Roupala obtusata
-57.5	-10.11667	Rutaceae	Metrodorea	Metrodorea flavida
-56.094139	-2.207139	Salicaceae	Casearia	Casearia bicolor
-56.790833	-9.324722	Sapindaceae	Matayba	Matayba purgans
-57.733056	-11.087222	Sapotaceae	Chrysophyllum	Chrysophyllum lucentifolium
-59.833333	-7.166667	Schizaeaceae	Schizaea	Schizaea elegans
-56.93	-5.229722	Simaroubaceae	Picrolemma	Picrolemma sprucei
-57.805556	-9.086667	Solanaceae	Solanum	Solanum anisophyllum
-57.672478	-3.401951	Urticaceae	Cecropia	Cecropia concolor
-59.608333	-8.213611	Urticaceae	Cecropia	Cecropia ficifolia
-59.4	-11.16	Urticaceae	Urera	Urera caracasana
-55.402778	-3.724722	Urticaceae	Cecropia	Cecropia latiloba
-58.495556	-10.332222	Verbenaceae	Lippia	Lippia origanoides

-58.568889	-8.574167	Vochysiaceae	Qualea	Qualea dinizii
-58.189675	-6.327733	Vochysiaceae	Qualea	Qualea paraensis
-54.440561	-10.427955	Cucurbitaceae	Citrullus	Citrullus lanatus
-54.934946	-2.518722	Passifloraceae	Passiflora	Passiflora nitida
-75.135194	9.963889	Anacardiaceae	Spondias	Spondias mombin
-75.08333	8.06667	Caryocaraceae	Caryocar	Caryocar amygdaliferum
-75.878535	8.75098	Commelinaceae	Tradescantia	Tradescantia pallida
-76.665799	7.869771	Urticaceae	Cecropia	Cecropia peltata
-73.7235	8.31265	Alismataceae	Aquarius	Aquarius paniculatus
-74.337917	6.468278	Menispermaceae	Elissarrhena	Elissarrhena longipes
-74.9001	9.042839	Pontederiaceae	Pontederia	Pontederia azurea
-73.877395	7.391716	Sapotaceae	Chrysophyllum	Chrysophyllum cainito
-75.443111	4.593917	Aquifoliaceae	Ilex	Ilex kunthiana
-76.491387	1.958321	Arecaceae	Ceroxylon	Ceroxylon vogelianum
-75.99	3.310528	Celastraceae	Maytenus	Maytenus prunifolia
-75.481638	2.377638	Gesneriaceae	Kohleria	Kohleria amabilis
-75.362573	6.776942	Pinaceae	Pinus	Pinus patula
-72.957286	7.353764	Apocynaceae	Asclepias	Asclepias curassavica
-73.4866	9.201	Celastraceae	Schaefferia	Schaefferia frutescens
-73.608467	5.405447	Eriocaulaceae	Paepalanthus	Paepalanthus alpinus
-74.910632	5.559623	Lecythidaceae	Gustavia	Gustavia romeroi
-72.695506	5.999857	Lentibulariaceae	Pinguicula	Pinguicula elongata
-74.08636	4.5213	Lycopodiaceae	Diphasiastrum	Diphasiastrum thyoides
-74.932528	3.175333	Passifloraceae	Passiflora	Passiflora maliformis
-73.440079	8.462071	Phytolaccaceae	Ledenbergia	Ledenbergia seguierioides
-73.5055	5.313194	Polygalaceae	Polygala	Polygala paniculata
-72.65275	6.092889	Ranunculaceae	Ranunculus	Ranunculus petiolaris
-74.85916	5.898263	Rubiaceae	Isertia	Isertia haenkeana
-74.590889	4.911419	Sabiaceae	Meliosma	Meliosma bogotana
-74.385197	3.925583	Symplocaceae	Symplocos	Symplocos theiformis
-72.958056	7.520139	Symplocaceae	Symplocos	Symplocos uniflora
-74.92475	6.89223	Thymelaeaceae	Schoenobiblus	Schoenobiblus daphnoides
-74.333333	8.0	Thymelaeaceae	Schoenobiblus	Schoenobiblus peruviana
-74.932643	3.175797	Verbenaceae	Duranta	Duranta erecta
-73.637504	6.6835	Violaceae	Leonia	Leonia triandra
-51.43	4.1	Amaranthaceae	Cyathula	Cyathula prostrata
-52.58	-0.67	Anacardiaceae	Astronium	Astronium lecointei
-51.66	-0.99	Apocynaceae	Parahancornia	Parahancornia fasciculata
-50.788278	1.545722	Aspleniaceae	Asplenium	Asplenium serratum
-50.0	-1.0	Dryopteridaceae	Elaphoglossum	Elaphoglossum glabellum
-51.278806	-0.11863	Euphorbiaceae	Euphorbia	Euphorbia thymifolia
-50.000317	0.00045	Myristicaceae	Virola	Virola surinamensis
-50.8777	2.588129	Plantaginaceae	Bacopa	Bacopa aquatica
-50.641111	-1.828611	Primulaceae	Cybianthus	Cybianthus penduliflorus
-48.848889	-1.384444	Lygodiaceae	Lygodium	Lygodium venustum
-49.571667	-2.171389	Malpighiaceae	Byrsonima	Byrsonima coccolobifolia
-77.480222	-8.306222	Celastraceae	Tricerma	Tricerma octogonum
-77.991975	-6.85115	Fabaceae	Senna	Senna pallida
-78.3614	-5.2569	Loganiaceae	Bonyunia	Bonyunia pulchra
-78.85239	-6.099399	Onagraceae	Ludwigia	Ludwigia peruviana
-55.85	-9.45	Acanthaceae	Dianthera	Dianthera calycina

-55.53333	-12.3	Alismataceae	Aquarius	Aquarius subulatus
-57.51666	-7.58333	Amaranthaceae	Alternanthera	Alternanthera martii
-57.04	-9.190555	Annonaceae	Guatteria	Guatteria sellowiana
-55.688056	-10.967222	Araceae	Heteropsis	Heteropsis reticulata
-56.433333	-12.816667	Araliaceae	Didymopanax	Didymopanax distractiflorus
-58.6286	-7.4188	Araliaceae	Dendropanax	Dendropanax macropodus
-58.427722	-6.537386	Arecaceae	Oenocarpus	Oenocarpus minor
-57.183056	-11.011111	Aspleniaceae	Asplenium	Asplenium serratum
-57.985	-12.153806	Asteraceae	Coreopsis	Coreopsis grandiflora
-57.849167	-9.999167	Bignoniaceae	Tanaecium	Tanaecium xanthophyllum
-58.080833	-8.906944	Burseraceae	Protium	Protium paniculatum
-56.356111	-10.333778	Burseraceae	Trattinnickia	Trattinnickia rhoifolia
-56.28	-11.67	Erythroxylaceae	Erythroxylum	Erythroxylum macrophyllum
-56.658611	-8.104167	Fabaceae	Swartzia	Swartzia laurifolia
-58.75	-11.533333	Lycopodiaceae	Palhinhaea	Palhinhaea cernua
-54.46	-11.7	Alismataceae	Aquarius	Aquarius subulatus
-54.12	-10.45	Anacardiaceae	Tapirira	Tapirira guianensis
-51.129444	-8.752306	Apocynaceae	Aspidosperma	Aspidosperma eteanum
-51.156389	-6.564167	Apocynaceae	Mandevilla	Mandevilla scabra
-51.116667	-7.783333	Cactaceae	Epiphyllum	Epiphyllum phyllanthus
-51.5689	-10.6439	Combretaceae	Combretum	Combretum micranthum
-52.7442	-10.8044	Combretaceae	Terminalia	Terminalia tetraphylla
-53.25	-9.85	Connaraceae	Connarus	Connarus suberosus
-54.328611	-12.861389	Convolvulaceae	Cuscuta	Cuscuta racemosa
-51.057778	-9.820833	Dilleniaceae	Doliocarpus	Doliocarpus major
-52.0	-8.0	Eriocaulaceae	Syngonanthus	Syngonanthus humboldtii
-54.895833	-9.759722	Euphorbiaceae	Sapium	Sapium glandulosum
-51.318175	-11.922442	Moraceae	Ficus	Ficus obtusifolia
-53.151944	-12.596111	Myrtaceae	Campomanesia	Campomanesia eugenioides
-54.961944	-8.733611	Poaceae	Guadua	Guadua paniculata
-52.329167	-11.798889	Polygalaceae	Bredemeyera	Bredemeyera floribunda
-51.87	-12.72	Verbenaceae	Stachytarpheta	Stachytarpheta gesnerioides
-52.54	-9.22	Xyridaceae	Xyris	Xyris uleana
-48.898055	-8.730278	Annonaceae	Xylopia	Xylopia aromatica
-49.576472	-9.785472	Annonaceae	Unonopsis	Unonopsis guatterioides
-47.525278	-9.403333	Apocynaceae	Himatanthus	Himatanthus obovatus
-49.62338	-10.791137	Bignoniaceae	Tabebuia	Tabebuia rosea
-48.2	-7.181944	Bromeliaceae	Ananas	Ananas comosus
-49.836111	-7.066667	Chrysobalanaceae	Hirtella	Hirtella triandra
-48.55	-10.666667	Commelinaceae	Floscopa	Floscopa glabrata
-47.41667	-6.33333	Connaraceae	Rourea	Rourea fluminensis
-48.6	-9.72	Lamiaceae	Mesosphaerum	Mesosphaerum suaveolens
-47.503889	-10.704722	Lentibulariaceae	Genlisea	Genlisea aurea
-49.866667	-8.816667	Lythraceae	Physocalymma	Physocalymma scaberrimum
-47.783055	-8.305833	Ochnaceae	Ouratea	Ouratea hexasperma
-48.124444	-5.651111	Onagraceae	Ludwigia	Ludwigia helminthorrhiza
-49.655084	-5.976292	Passifloraceae	Passiflora	Passiflora glandulosa
-49.441111	-7.979444	Poaceae	Axonopus	Axonopus rupestris
-64.91	-11.743889	Annonaceae	Xylopia	Xylopia cuspidata
-63.022809	-7.514708	Asteraceae	Erechtites	Erechtites hieraciifolius
-61.875875	-1.093297	Bignoniaceae	Anemopaegma	Anemopaegma paraense

-62.502397	-4.728728	Bixaceae	Bixa	Bixa orellana
-61.260856	-3.653264	Burseraceae	Protium	Protium hebetatum
-63.013886	-3.988772	Calophyllaceae	Haploclathra	Haploclathra paniculata
-63.93878	-8.835559	Fabaceae	Peltophorum	Peltophorum dubium
-62.082331	-6.39105	Hypericaceae	Vismia	Vismia cayennensis
-60.3809298	-5.1239964	Lentibulariaceae	Utricularia	Utricularia amethystina
-61.300144	-5.831561	Vitaceae	Cissus	Cissus erosa
-56.738582	-2.637701	Anacardiaceae	Anacardium	Anacardium occidentale
-58.169167	-1.989167	Fabaceae	Eperua	Eperua glabra
-58.638897	-3.246967	Lythraceae	Cuphea	Cuphea melvilla
-59.216667	-2.191667	Malvaceae	Scleronema	Scleronema grandiflorum
-56.294444	-1.816944	Piperaceae	Piper	Piper bartlingianum
-59.891944	-3.360833	Polygalaceae	Polygala	Polygala trichosperma
-59.65	-4.366667	Rhizophoraceae	Cassipourea	Cassipourea peruviana
-54.742282	-2.371093	Vitaceae	Cissus	Cissus erosa
-76.441388	-3.754416	Alismataceae	Aquarius	Aquarius horizontalis
-75.666666	-4.75	Alismataceae	Aquarius	Aquarius tunicatus
-75.0	-4.0	Alismataceae	Aquarius	Aquarius grisebachii
-77.45807	-2.07495	Annonaceae	Oxandra	Oxandra xylopioides
-75.170503	-0.971347	Araceae	Caladium	Caladium bicolor
-77.898124	-1.070953	Bignoniaceae	Crescentia	Crescentia cujete
-77.363463	0.02612	Bixaceae	Bixa	Bixa orellana
-75.19644	1.78269	Bixaceae	Bixa	Bixa urucurana
-76.533333	-1.5	Caryocaraceae	Caryocar	Caryocar villosum
-75.984722	1.331944	Connaraceae	Rourea	Rourea camptoneura
-76.325991	0.46774	Lecythidaceae	Grias	Grias neuberthii
-75.199528	0.803194	Menispermaceae	Abuta	Abuta grandifolia
-75.633333	-1.8	Saccolomataceae	Saccoloma	Saccoloma inaequale
-75.433333	-2.85	Saccolomataceae	Saccoloma	Saccoloma inaequale
-77.333333	-4.25	Saccolomataceae	Saccoloma	Saccoloma inaequale
-76.47	-2.8	Saccolomataceae	Saccoloma	Saccoloma inaequale
-77.913889	-3.020833	Thymelaeaceae	Schoenobiblus	Schoenobiblus daphnoides
-76.394693	-0.468029	Urticaceae	Cecropia	Cecropia utcubambana
-73.1	-3.483333	Alismataceae	Limnocharis	Limnocharis flava
-74.083333	-4.433333	Marattiaceae	Danaea	Danaea nigrescens
-74.598444	-0.028472	Menispermaceae	Curarea	Curarea tecunarum
-74.172133	-2.294842	Nymphaeaceae	Victoria	Victoria amazonica
-71.7842	2.3432	Bixaceae	Bixa	Bixa orellana
-70.579822	3.166822	Eriocaulaceae	Paepalanthus	Paepalanthus chiquitensis
-72.066063	3.206793	Polypodiaceae	Pleopeltis	Pleopeltis orientalis
-72.72833	2.44917	Thymelaeaceae	Schoenobiblus	Schoenobiblus peruviana
-68.337861	3.047778	Aquifoliaceae	Ilex	Ilex divaricata
-66.083889	-0.129444	Araceae	Anthurium	Anthurium trinervium
-69.075556	3.658333	Bromeliaceae	Aechmea	Aechmea penduliflora
-67.111389	2.004167	Combretaceae	Terminalia	Terminalia pulcherrima
-66.46	1.16	Connaraceae	Connarus	Connarus coriaceus
-67.43805	2.92111	Dilleniaceae	Doliocarpus	Doliocarpus ortegae
-65.45	3.18333	Eriocaulaceae	Comanthera	Comanthera reflexa
-67.8	4.416667	Linderniaceae	Vandellia	Vandellia diffusa
-69.995914	4.025608	Melastomataceae	Miconia	Miconia affinis
-69.3725	2.743333	Myristicaceae	Iryanthera	Iryanthera paradoxa

-67.083889	-0.127778	Poaceae	Lasiacis	Lasiacis procerrima
-65.73	1.82	Saccolomataceae	Saccoloma	Saccoloma inaequale
-66.38333	2.95	Xyridaceae	Xyris	Xyris lomatophylla
-63.911111	-0.3525	Celastraceae	Hippocratea	Hippocratea volubilis
-61.921667	-0.136389	Lauraceae	Pleurothyrium	Pleurothyrium parviflorum
-62.983333	-0.133333	Myristicaceae	Virola	Virola venosa
-64.933333	-0.528572	Pentaphylacaceae	Ternstroemia	Ternstroemia candolleana
-64.566667	2.316667	Phyllanthaceae	Hieronyma	Hieronyma alchorneoides
-41.73431	-2.912959	Anacardiaceae	Anacardium	Anacardium occidentale
-40.490928	-2.829217	Apocynaceae	Funastrum	Funastrum clausum
-42.808527	-2.729633	Arecaceae	Mauritia	Mauritia flexuosa
-43.919722	-2.8175	Lamiaceae	Amasonia	Amasonia campestris
-78.872832	-0.724435	Alstroemeriaceae	Bomarea	Bomarea multiflora
-76.694199	3.335382	Alstroemeriaceae	Bomarea	Bomarea linifolia
-76.741056	2.238306	Amaryllidaceae	Phaedranassa	Phaedranassa lehmannii
-78.238328	0.459228	Apiaceae	Foeniculum	Foeniculum vulgare
-76.49655	7.7688	Apocynaceae	Asclepias	Asclepias curassavica
-78.184005	1.358828	Apocynaceae	Mandevilla	Mandevilla sagittarii
-76.432243	4.262753	Araliaceae	Sciodaphyllum	Sciodaphyllum digynum
-76.31115	6.76324	Aspleniaceae	Asplenium	Asplenium radicans
-78.689479	-2.095932	Asteraceae	Baccharis	Baccharis latifolia
-79.142639	0.145267	Begoniaceae	Begonia	Begonia glabra
-79.597599	-3.252815	Begoniaceae	Begonia	Begonia acerifolia
-76.086521	5.207673	Begoniaceae	Begonia	Begonia lehmannii
-77.28863	1.05269	Betulaceae	Alnus	Alnus jorullensis
-76.674517	3.744513	Cactaceae	Pilosocereus	Pilosocereus lanuginosus
-77.8863	0.428225	Elaeocarpaceae	Vallea	Vallea stipularis
-76.698333	1.979167	Elaeocarpaceae	Vallea	Vallea stipularis
-76.115143	8.010627	Fabaceae	Pentaclethra	Pentaclethra macroloba
-76.219847	4.762031	Fabaceae	Calliandra	Calliandra haematocephala
-76.183989	5.851664	Gesneriaceae	Glossoloma	Glossoloma schultzei
-78.233333	1.28333	Humiriaceae	Sacoglottis	Sacoglottis ovicarpa
-79.15396	0.498805	Melastomataceae	Pleroma	Pleroma urvilleanum
-76.171028	6.90733	Pinaceae	Pinus	Pinus caribaea
-79.265673	-0.40852	Polygalaceae	Polygala	Polygala paniculata
-79.181206	-1.766697	Rutaceae	Murraya	Murraya paniculata
-79.364041	-2.785589	Scrophulariaceae	Alonsoa	Alonsoa meridionalis
-78.319327	-0.458167	Solanaceae	Brugmansia	Brugmansia sanguinea
-77.6	1.966667	Sphagnaceae	Sphagnum	Sphagnum tenerum
-77.2212	1.06327	Xyridaceae	Xyris	Xyris subulata
-68.3	10.78333	Rhizophoraceae	Rhizophora	Rhizophora mangle
-60.20028	8.30028	Calophyllaceae	Clusiella	Clusiella impressinervis
-61.916667	8.583333	Connaraceae	Cnestidium	Cnestidium guianense
-61.06666	9.18333	Onagraceae	Ludwigia	Ludwigia affinis
-62.984722	10.3125	Rhizophoraceae	Rhizophora	Rhizophora harrisonii
-61.916667	9.583333	Smilacaceae	Smilax	Smilax siphilitica
-59.2833	7.85	Commelinaceae	Callisia	Callisia serrulata
-65.53	4.42	Bonnetiaceae	Bonnetia	Bonnetia crassa
-65.72	3.38	Bonnetiaceae	Bonnetia	Bonnetia tristyla
-66.2	5.76666	Bonnetiaceae	Bonnetia	Bonnetia celiae
-65.2	6.316667	Connaraceae	Rourea	Rourea sprucei

-65.2	5.35	Eriocaulaceae	Eriocaulon	Eriocaulon jauense
-65.96667	0.83333	Ophioglossaceae	Cheiroglossa	Cheiroglossa palmata
-67.000983	5.000717	Xyridaceae	Xyris	Xyris pratensis
-61.5	4.5	Bonnetiaceae	Archytaea	Archytaea triflora
-63.92	4.77	Bonnetiaceae	Bonnetia	Bonnetia cordifolia
-64.67333	4.08333	Bonnetiaceae	Bonnetia	Bonnetia sessilis
-63.6667	5.81667	Bonnetiaceae	Bonnetia	Bonnetia lanceifolia
-61.45	6.016667	Bromeliaceae	Pitcairnia	Pitcairnia maidifolia
-62.3	5.01	Caryocaraceae	Anthodiscus	Anthodiscus mazarunensis
-62.56667	5.93333	Clethraceae	Clethra	Clethra guyanensis
-62.75	3.83	Cyatheaceae	Cyathea	Cyathea platylepis
-63.354167	2.366667	Cyperaceae	Lagenocarpus	Lagenocarpus eriopodus
-60.788195	5.180354	Lentibulariaceae	Utricularia	Utricularia quelchii
-61.773611	1.716111	Myrtaceae	Eugenia	Eugenia anastomosans
-64.22	3.05	Proteaceae	Panopsis	Panopsis parimensis
-56.5	3.65	Cucurbitaceae	Cayaponia	Cayaponia racemosa
-59.1225	5.21067	Violaceae	Noisettia	Noisettia orchidiflora
-78.850279	-6.104774	Apocynaceae	Mandevilla	Mandevilla subsagittata
-78.035647	-7.827653	Betulaceae	Alnus	Alnus acuminata
-76.83333	-8.13333	Burseraceae	Dacryodes	Dacryodes peruviana
-76.802091	-9.223986	Caryophyllaceae	Polycarpon	Polycarpon tetraphyllum
-77.885	-5.7025	Hydrangeaceae	Hydrangea	Hydrangea weberbaueri
-75.351667	-10.530278	Hymenophyllaceae	Hymenophyllum	Hymenophyllum ruizianum
-76.537347	-10.445158	Lamiaceae	Lamium	Lamium amplexicaule
-75.681633	-9.072975	Piperaceae	Peperomia	Peperomia serpens
-77.646305	-6.863765	Ranunculaceae	Krapfia	Krapfia clypeata
-76.183333	-6.533333	Schizaeaceae	Actinostachys	Actinostachys pennula
-75.750748	-11.425392	Scrophulariaceae	Buddleja	Buddleja coriacea
-78.9	-7.38	Thymelaeaceae	Daphnopsis	Daphnopsis weberbaueri
-73.190173	-13.914739	Begoniaceae	Begonia	Begonia veitchii
-72.54243	-13.168461	Begoniaceae	Begonia	Begonia bracteosa
-71.679795	-13.67518	Boraginaceae	Borago	Borago officinalis
-74.98168	-12.507374	Cactaceae	Cleistocactus	Cleistocactus morawetzianus
-74.160453	-13.578642	Convolvulaceae	Ipomoea	Ipomoea pubescens
-71.401445	-12.787358	Dryopteridaceae	Mickelia	Mickelia lindigii
-74.820556	-11.516944	Gesneriaceae	Glossoloma	Glossoloma serpens
-74.249685	-10.618076	Passifloraceae	Passiflora	Passiflora miniata
-73.959059	-12.570492	Phytolaccaceae	Phytolacca	Phytolacca rivinoides
-73.341	-11.78	Proteaceae	Roupala	Roupala montana
-70.461977	-13.649963	Proteaceae	Roupala	Roupala monosperma
-72.3	-12.3	Scrophulariaceae	Buddleja	Buddleja americana
-69.547296	-14.267874	Amaryllidaceae	Hippeastrum	Hippeastrum bukasovii
-66.185	-8.865	Clusiaceae	Tovomita	Tovomita laurina
-65.0	-8.416667	Eriocaulaceae	Syngonanthus	Syngonanthus nitens
-65.451388	-9.634167	Lecythidaceae	Gustavia	Gustavia hexapetala
-63.919003	-8.313858	Arecaceae	Attalea	Attalea speciosa
-64.421389	-9.145278	Arecaceae	Geonoma	Geonoma maxima
-64.078333	-7.408889	Commelinaceae	Dichorisandra	Dichorisandra villosula
-60.710053	-3.41927	Euphorbiaceae	Euphorbia	Euphorbia milii
-60.016667	-4.333333	Lygodiaceae	Lygodium	Lygodium venustum
-63.079444	-7.6375	Malpighiaceae	Byrsonima	Byrsonima ligustrifolia

-61.988889	-5.311667	Myristicaceae	Virola	Virola mollissima
-61.313889	-4.306944	Poaceae	Olyra	Olyra latifolia
-61.02	-5.371428	Schizaeaceae	Actinostachys	Actinostachys pennula
-62.980556	-6.666111	Simaroubaceae	Simaba	Simaba polyphylla
-59.678947	-3.438103	Araceae	Anthurium	Anthurium gracile
-71.81247	-0.86688	Alismataceae	Aquarius	Aquarius horizontalis
-70.388917	1.494278	Aquifoliaceae	Ilex	Ilex jenmanii
-74.007222	0.710167	Aspleniaceae	Asplenium	Asplenium serratum
-71.506083	-2.227333	Aspleniaceae	Asplenium	Asplenium hallii
-73.046333	-0.973611	Caryocaraceae	Caryocar	Caryocar glabrum
-72.785056	1.152139	Caryocaraceae	Caryocar	Caryocar microcarpum
-70.183333	-0.583333	Cyclanthaceae	Ludovia	Ludovia integrifolia
-73.526111	1.7275	Hymenophyllaceae	Trichomanes	Trichomanes pinnatum
-71.15486	0.9861	Hymenophyllaceae	Trichomanes	Trichomanes accedens
-72.13333	0.03333	Rhizophoraceae	Sterigmapetalum	Sterigmapetalum guianense
-71.0	0.00417	Thymelaeaceae	Tepuianthus	Tepuianthus colombianus
-65.08583	-4.14444	Alismataceae	Sagittaria	Sagittaria sprucei
-65.28	-7.47	Amaryllidaceae	Crinum	Crinum amazonicum
-65.37	-2.666667	Apiaceae	Eryngium	Eryngium foetidum
-66.080337	-3.760208	Aspleniaceae	Asplenium	Asplenium hallii
-67.483333	-5.583333	Blechnaceae	Salpichlaena	Salpichlaena volubilis
-66.894495	-2.822978	Bromeliaceae	Aechmea	Aechmea poitaei
-66.9944	-1.8861	Caryocaraceae	Caryocar	Caryocar glabrum
-69.741389	-2.484722	Connaraceae	Connarus	Connarus fasciculatus
-68.466944	-9.344444	Dilleniaceae	Davilla	Davilla nitida
-67.7	-4.042222	Eriocaulaceae	Syngonanthus	Syngonanthus longipes
-67.478889	-8.566667	Hypericaceae	Vismia	Vismia japurensis
-67.527945	-9.583627	Lamiaceae	Leonotis	Leonotis nepetifolia
-68.949444	-3.484444	Malpighiaceae	Banisteriopsis	Banisteriopsis martiniana
-67.936768	-3.097643	Piperaceae	Piper	Piper peltatum
-68.883333	-6.6	Saccolomataceae	Saccoloma	Saccoloma inaequale
-65.873476	-1.912	Urticaceae	Cecropia	Cecropia ficifolia
-68.434417	-1.971611	Verbenaceae	Lippia	Lippia alba
-62.977778	-5.28	Annonaceae	Annona	Annona foetida
-63.269744	-3.769122	Clusiaceae	Tovomita	Tovomita choisyana
-64.4	-3.55	Plantaginaceae	Scoparia	Scoparia dulcis
-64.330278	-6.3025	Rutaceae	Zanthoxylum	Zanthoxylum compactum
-69.492194	1.058722	Apocynaceae	Odontadenia	Odontadenia glauca
-67.5475	-0.826389	Calophyllaceae	Caraipa	Caraipa savannarum
-66.023333	-0.795278	Clusiaceae	Clusia	Clusia cerroana
-65.1	-0.754361	Cyclanthaceae	Asplundia	Asplundia vaupesiana
-66.73	3.83	Dilleniaceae	Doliocarpus	Doliocarpus leiophyllus
-68.154057	1.387945	Loganiaceae	Strychnos	Strychnos rondeletioides
-67.73333	4.36666	Onagraceae	Ludwigia	Ludwigia hyssopifolia
-68.175111	0.044417	Passifloraceae	Passiflora	Passiflora foetida
-67.96667	3.45	Smilacaceae	Smilax	Smilax maypurensis
-60.84233	1.42294	Annonaceae	Annona	Annona foetida
-61.635278	0.789444	Bignoniaceae	Amphilophium	Amphilophium racemosum
-62.636667	0.842222	Bonnetiaceae	Bonnetia	Bonnetia sessilis
-64.059722	-0.0825	Capparaceae	Crateva	Crateva tapia
-63.26	-0.8754	Caryocaraceae	Caryocar	Caryocar microcarpum

-60.688889	-0.053333	Humiriaceae	Humiria	Humiria balsamifera
-62.5604	-0.24481	Pentaphylacaceae	Ternstroemia	Ternstroemia campinicola
-70.65478	-2.52631	Aquifoliaceae	Ilex	Ilex laureola
-74.136246	-2.022176	Begoniaceae	Begonia	Begonia stenotepala
-72.399583	-1.627694	Celastraceae	Hippocratea	Hippocratea volubilis
-70.766667	-1.466667	Loganiaceae	Strychnos	Strychnos gubleri
-74.33333	-1.0	Loganiaceae	Strychnos	Strychnos gubleri
-71.08333	-3.33333	Nephrolepidaceae	Nephrolepis	Nephrolepis rivularis
-72.966667	-3.5	Sabiaceae	Ophiocaryon	Ophiocaryon klugii
-72.0	-3.333333	Saccolomataceae	Saccoloma	Saccoloma inaequale
-69.966667	-4.158889	Araceae	Philodendron	Philodendron nullinervium
-69.423	-1.383	Caryocaraceae	Caryocar	Caryocar glabrum
-64.882481	-22.306091	Amaranthaceae	Gomphrena	Gomphrena meyeniana
-63.931944	-21.423056	Anacardiaceae	Cardenasiodendron	Cardenasiodendron brachypterum
-64.583333	-18.85	Apiaceae	Eryngium	Eryngium nudicaule
-63.985828	-24.202252	Apocynaceae	Vallesia	Vallesia glabra
-63.792563	-22.345055	Apocynaceae	Philibertia	Philibertia gilliesii
-64.910332	-26.457897	Asteraceae	Cnicothamnus	Cnicothamnus lorentzii
-63.8575	-20.511944	Begoniaceae	Begonia	Begonia wollnyi
-64.974065	-25.499337	Bixaceae	Bixa	Bixa orellana
-64.937019	-23.648606	Boraginaceae	Cynoglossum	Cynoglossum amabile
-63.875372	-18.173969	Cannabaceae	Cannabis	Cannabis sativa
-63.88305	-19.51944	Cannabaceae	Celtis	Celtis iguanaea
-64.90361	-21.11083	Commelinaceae	Commelina	Commelina elliptica
-64.969379	-25.486055	Euphorbiaceae	Ricinus	Ricinus communis
-64.963678	-23.529575	Fabaceae	Coursetia	Coursetia hassleri
-63.678968	-22.033044	Fabaceae	Poissonia	Poissonia hypoleuca
-63.722373	-18.191425	Gesneriaceae	Seemannia	Seemannia sylvatica
-64.588365	-18.916223	Lamiaceae	Salvia	Salvia retinervia
-64.9167	-22.25	Oxalidaceae	Oxalis	Oxalis tuberosa
-63.994982	-24.166609	Papaveraceae	Argemone	Argemone subfusiformis
-64.43333	-21.41667	Scrophulariaceae	Buddleja	Buddleja tucumanensis
-64.886514	-26.487401	Solanaceae	Solanum	Solanum symmetricum
-64.046012	-20.479868	Solanaceae	Solanum	Solanum sisymbriifolium
-63.904444	-22.9175	Solanaceae	Physalis	Physalis viscosa
-63.88666	-19.58333	Violaceae	Rinorea	Rinorea ovalifolia
-75.372283	-11.046744	Acanthaceae	Hypoestes	Hypoestes phyllostachya
-71.397002	-12.898221	Acanthaceae	Pachystachys	Pachystachys lutea
-70.95	-10.2	Alismataceae	Aquarius	Aquarius grisebachii
-71.398726	-11.878947	Araceae	Monstera	Monstera obliqua
-73.724569	-12.589226	Arecaceae	Iriartea	Iriartea deltoidea
-72.34889	-6.458055	Begoniaceae	Begonia	Begonia buddleiifolia
-73.98333	-8.25	Bixaceae	Bixa	Bixa urucurana
-72.916667	-3.75	Caryocaraceae	Anthodiscus	Anthodiscus amazonicus
-72.320556	-9.043611	Connaraceae	Connarus	Connarus ruber
-71.121944	-6.820556	Cyclanthaceae	Asplundia	Asplundia schizotepala
-70.406389	-13.478611	Dicksoniaceae	Lophosoria	Lophosoria quadripinnata
-71.376944	-7.988333	Gesneriaceae	Nautilocalyx	Nautilocalyx fasciculatus
-73.666611	-7.39975	Gesneriaceae	Nautilocalyx	Nautilocalyx fasciculatus
-74.3	-11.79	Juglandaceae	Juglans	Juglans neotropica
-73.760278	-5.858333	Marattiaceae	Danaea	Danaea leprieurii

-74.588508	-7.115972	Menispermaceae	Abuta	Abuta sandwithiana
-73.223465	-10.618179	Moraceae	Poulsenia	Poulsenia armata
-72.18333	-12.41666	Nephrolepidaceae	Nephrolepis	Nephrolepis pectinata
-70.208708	-4.31636	Nymphaeaceae	Victoria	Victoria amazonica
-73.758173	-4.958932	Nymphaeaceae	Victoria	Victoria amazonica
-71.402432	-4.44404	Rhizophoraceae	Cassipourea	Cassipourea peruviana
-70.25	-7.65	Rhizophoraceae	Paradrypetes	Paradrypetes subintegrifolia
-70.2665	-12.4531	Sabiaceae	Meliosma	Meliosma herbertii
-72.82	-5.13	Sabiaceae	Ophiocaryon	Ophiocaryon duckei
-72.88	-11.8083	Schizaeaceae	Schizaea	Schizaea elegans
-73.201853	-9.618519	Thymelaeaceae	Schoenobiblus	Schoenobiblus peruviana
-72.71779	-7.562522	Urticaceae	Cecropia	Cecropia concolor
-70.12388	-9.52222	Vitaceae	Cissus	Cissus microcarpa
-71.309258	-9.333333	Vitaceae	Cissus	Cissus pseudoverticillata
-66.816472	-10.048167	Araceae	Philodendron	Philodendron deflexum
-67.55838	-11.10266	Arecaceae	Attalea	Attalea phalerata
-68.46875	-6.339944	Burseraceae	Protium	Protium klugii
-68.297222	-8.094444	Capparaceae	Preslianthus	Preslianthus pittieri
-65.45	-9.749528	Chrysobalanaceae	Couepia	Couepia bracteosa
-67.52625	-14.44791	Clusiaceae	Clusia	Clusia spruceana
-69.533611	-10.295	Connaraceae	Rourea	Rourea puberula
-65.49083	-16.53666	Cyclanthaceae	Thoracocarpus	Thoracocarpus bissectus
-69.383333	-13.483333	Dilleniaceae	Davilla	Davilla nitida
-66.116667	-11.866667	Dilleniaceae	Curatella	Curatella americana
-68.346088	-13.474691	Ephedraceae	Ephedra	Ephedra rupestris
-66.1	-14.5	Isoetaceae	Isoetes	Isoetes panamensis
-66.59	-15.3	Loranthaceae	Struthanthus	Struthanthus acuminatus
-68.951111	-9.131111	Meliaceae	Cedrela	Cedrela fissilis
-65.717926	-10.976696	Myristicaceae	Osteophloeum	Osteophloeum platyspermum
-67.0625	-12.06917	Nyctaginaceae	Neea	Neea bangii
-65.04521	-12.820989	Nymphaeaceae	Victoria	Victoria boliviana
-65.23333	-15.51666	Onagraceae	Ludwigia	Ludwigia grandiflora
-69.114286	-12.225833	Passifloraceae	Passiflora	Passiflora auriculata
-68.455083	-10.601889	Passifloraceae	Passiflora	Passiflora miniata
-69.380314	-11.221611	Piperaceae	Piper	Piper aduncum
-68.902778	-3.551944	Polypodiaceae	Microgramma	Microgramma baldwinii
-69.45	-6.516666	Pteridaceae	Adiantum	Adiantum obliquum
-69.32	-5.216667	Rhamnaceae	Gouania	Gouania pyrifolia
-68.175556	-12.354167	Salicaceae	Casearia	Casearia gossypiosperma
-68.1291	-9.72296	Sapindaceae	Allophylus	Allophylus divaricatus
-69.526667	-8.219722	Sapotaceae	Micropholis	Micropholis williamii
-67.08333	-13.08333	Xyridaceae	Xyris	Xyris laxifolia
-64.983333	-14.65	Capparaceae	Crateva	Crateva tapia
-64.32916	-17.25888	Hypericaceae	Vismia	Vismia gracilis
-63.375	-16.83	Primulaceae	Ardisia	Ardisia guianensis
-64.427222	-16.100833	Rhamnaceae	Sarcomphalus	Sarcomphalus mistol
-55.093889	-6.087778	Bignoniaceae	Handroanthus	Handroanthus capitatus
-55.39427	-8.422189	Blechnaceae	Blechnum	Blechnum asplenioides
-55.333333	-7.416667	Commelinaceae	Dichorisandra	Dichorisandra hexandra
-55.981389	-6.414722	Cyperaceae	Eleocharis	Eleocharis interstincta
-55.079722	-5.081389	Fabaceae	Dalbergia	Dalbergia spruceana

-56.060556	-5.359722	Malpighiaceae	Byrsonima	Byrsonima stipulacea
-56.2244	-4.4364	Melastomataceae	Aciotis	Aciotis viscida
-57.08	-7.0	Rhizophoraceae	Cassipourea	Cassipourea guianensis
-57.393333	-6.060556	Rutaceae	Conchocarpus	Conchocarpus acuminatus
-55.07	-4.0	Verbenaceae	Petrea	Petrea volubilis
-52.585459	-7.204003	Alstroemeriaceae	Bomarea	Bomarea edulis
-53.8	-5.633333	Araliaceae	Hydrocotyle	Hydrocotyle umbellata
-53.822222	-7.933611	Cannabaceae	Celtis	Celtis iguanaea
-54.000528	-9.000639	Chloranthaceae	Hedyosmum	Hedyosmum brasiliense
-53.838333	-6.651111	Combretaceae	Terminalia	Terminalia oxycarpa
-52.56056	-5.85028	Dilleniaceae	Davilla	Davilla nitida
-52.916667	-2.166667	Humiriaceae	Vantanea	Vantanea parviflora
-53.908725	-3.042808	Lecythidaceae	Bertholletia	Bertholletia excelsa
-52.882486	-3.440785	Myrtaceae	Eugenia	Eugenia stipitata
-53.920833	-9.959961	Phyllanthaceae	Phyllanthus	Phyllanthus orbiculatus
-54.949444	-2.845556	Piperaceae	Piper	Piper erectipilum
-54.0	-4.0	Rutaceae	Conchocarpus	Conchocarpus guyanensis
-51.688889	-3.120833	Salicaceae	Banara	Banara guianensis
-61.566111	0.686389	Araceae	Philodendron	Philodendron hylaeae
-60.310004	2.563254	Betulaceae	Ostrya	Ostrya virginiana
-61.849444	-0.945555	Bignoniaceae	Fridericia	Fridericia spicata
-61.0025	1.736667	Lecythidaceae	Eschweilera	Eschweilera parvifolia
-60.061389	-1.986111	Piperaceae	Piper	Piper peltatum
-60.418056	0.946111	Piperaceae	Peperomia	Peperomia serpens
-61.001389	-1.818333	Piperaceae	Piper	Piper arboreum
-60.766666	-0.166666	Pteridaceae	Adiantum	Adiantum tuomistoanum
-60.059444	-1.053889	Xyridaceae	Abolboda	Abolboda grandis
-56.462694	-1.856806	Acanthaceae	Justicia	Justicia oldemanii
-57.63	1.370762	Araliaceae	Didymopanax	Didymopanax decaphyllus
-59.57	1.37076	Araliaceae	Didymopanax	Didymopanax morototoni
-56.0	0.0	Asteraceae	Centaurea	Centaurea schousboei
-55.507389	-1.916333	Bignoniaceae	Tanaecium	Tanaecium duckei
-58.27	-0.668889	Calophyllaceae	Caraipa	Caraipa foveolata
-58.86	-3.24	Cannabaceae	Trema	Trema micranthum
-59.151389	-0.441389	Cannabaceae	Trema	Trema micranthum
-55.5175	-0.966944	Clusiaceae	Clusia	Clusia leprantha
-58.315833	0.660917	Cyperaceae	Calyptrocarya	Calyptrocarya bicolor
-56.45	1.7	Dilleniaceae	Davilla	Davilla kunthii
-57.315416	-0.200052	Erythroxylaceae	Erythroxylum	Erythroxylum macrophyllum
-59.93964	-3.006361	Fabaceae	Eperua	Eperua manausensis
-57.509728	-2.397562	Nymphaeaceae	Victoria	Victoria amazonica
-55.583333	1.0	Pentaphylacaceae	Ternstroemia	Ternstroemia dentata
-58.0	-1.6	Plantaginaceae	Scoparia	Scoparia dulcis
-59.01116	-2.11094	Rhizophoraceae	Cassipourea	Cassipourea guianensis
-57.22	-1.15	Simaroubaceae	Homalolepis	Homalolepis cedron
-56.88056	0.75833	Urticaceae	Coussapoa	Coussapoa latifolia
-54.433333	0.916667	Alstroemeriaceae	Alstroemeria	Alstroemeria amazonica
-53.106667	0.276389	Aspleniaceae	Asplenium	Asplenium stuebelianum
-50.911547	1.505083	Aspleniaceae	Asplenium	Asplenium serratum
-54.4333	-0.916667	Aspleniaceae	Asplenium	Asplenium serratum
-54.189722	-2.026111	Bignoniaceae	Adenocalymma	Adenocalymma magnificum

-52.166667	0.883333	Cyatheaceae	Cyathea	Cyathea surinamensis
-50.974863	2.490275	Lentibulariaceae	Utricularia	Utricularia myriocista
-51.966667	1.783333	Loganiaceae	Strychnos	Strychnos mitscherlichii
-52.359444	-1.173889	Marattiaceae	Danaea	Danaea ulei
-53.368889	1.226389	Nyctaginaceae	Neea	Neea madeirana
-54.87	0.0	Papaveraceae	Hypecoum	Hypecoum imberbe
-51.78333	-0.1	Polygonaceae	Coccoloba	Coccoloba paraensis
-77.339023	-6.700278	Amaranthaceae	Celosia	Celosia argentea
-76.020272	-9.320181	Araceae	Anthurium	Anthurium oxycarpum
-76.208056	-8.196667	Bixaceae	Bixa	Bixa arborea
-75.241111	-8.358611	Bixaceae	Bixa	Bixa platycarpa
-75.3	-10.15	Bixaceae	Bixa	Bixa platycarpa
-76.004722	-7.0625	Bonnetiaceae	Bonnetia	Bonnetia paniculata
-76.133097	-5.91591	Euphorbiaceae	Ricinus	Ricinus communis
-78.35	-4.38333	Lygodiaceae	Lygodium	Lygodium venustum
-77.46375	-5.698	Thymelaeaceae	Schoenobiblus	Schoenobiblus daphnoides
-77.5	-4.8	Typhaceae	Typha	Typha latifolia
-74.176384	-10.874445	Begoniaceae	Begonia	Begonia glabra
-74.598333	-9.472778	Pentaphylacaceae	Ternstroemia	Ternstroemia circumscissilis
-71.666667	7.8	Bonnetiaceae	Bonnetia	Bonnetia paniculata
-71.119837	8.681592	Polygonaceae	Persicaria	Persicaria capitata
-70.25	9.75	Styracaceae	Styrax	Styrax glaber
-69.983334	8.866667	Dioscoreaceae	Dioscorea	Dioscorea polygonoides
-69.266667	9.716667	Marattiaceae	Danaea	Danaea nigrescens
-79.809701	0.884707	Cucurbitaceae	Momordica	Momordica charantia
-79.228249	0.111144	Euphorbiaceae	Jatropha	Jatropha integerrima
-79.897219	-2.197467	Meliaceae	Azadirachta	Azadirachta indica
-78.761908	1.682965	Myrtaceae	Psidium	Psidium guajava
-79.703308	-0.892064	Verbenaceae	Petrea	Petrea volubilis
-50.015632	-5.45404	Araceae	Philodendron	Philodendron maximum
-52.559167	-8.257222	Araliaceae	Didymopanax	Didymopanax burchellii
-51.516667	-9.916667	Commelinaceae	Dichorisandra	Dichorisandra hexandra
-51.05	-1.216667	Connaraceae	Connarus	Connarus erianthus
-50.392222	-6.4025	Dioscoreaceae	Dioscorea	Dioscorea convolvulacea
-50.107222	-9.139444	Elaeocarpaceae	Sloanea	Sloanea eichleri
-51.7	-5.299444	Lamiaceae	Hyptis	Hyptis crenata
-50.171667	-7.534167	Lentibulariaceae	Utricularia	Utricularia physoceras
-52.363333	-9.4125	Lentibulariaceae	Utricularia	Utricularia praelonga
-50.601436	-8.338033	Lythraceae	Diplusodon	Diplusodon virgatus
-51.564167	-8.403056	Myristicaceae	Virola	Virola peruviana
-50.5	-10.08333	Ochnaceae	Ouratea	Ouratea hilaireana
-51.71667	-4.16667	Phytolaccaceae	Phytolacca	Phytolacca rivinoides
-50.683333	-4.166667	Rhamnaceae	Ampelozizyphus	Ampelozizyphus amazonicus
-51.647222	-2.005278	Simaroubaceae	Homalolepis	Homalolepis cedron
-52.5167	-4.8167	Verbenaceae	Lantana	Lantana camara
-50.761111	-2.407222	Violaceae	Amphirrhox	Amphirrhox longifolia
-51.420556	-6.530833	Xyridaceae	Xyris	Xyris brachysepala
-49.100556	-5.443333	Annonaceae	Guatteria	Guatteria punctata
-48.772222	-7.766667	Araceae	Philodendron	Philodendron wullschlaegelii
-49.713611	-2.275278	Arecaceae	Oenocarpus	Oenocarpus bataua
-49.296667	-6.979722	Asteraceae	Ageratum	Ageratum conyzoides

-48.563333	-6.1725	Eriocaulaceae	Paepalanthus	Paepalanthus chiquitensis
-49.67	-4.05	Lauraceae	Ocotea	Ocotea bracteosa
-49.496944	-8.342222	Malvaceae	Waltheria	Waltheria indica
-46.096944	-1.6825	Acanthaceae	Dianthera	Dianthera angustifolia
-45.83333	-3.66666	Araceae	Philodendron	Philodendron distantilobum
-47.0167	-5.03333	Arecaceae	Syagrus	Syagrus vermicularis
-48.268467	-1.210383	Asteraceae	Acmella	Acmella oleracea
-46.792444	-1.032222	Blechnaceae	Telmatoblechnum	Telmatoblechnum serrulatum
-49.025	-3.075	Chrysobalanaceae	Parinariopsis	Parinariopsis licaniiflora
-47.94	-4.14	Malvaceae	Herissantia	Herissantia tiubae
-48.799166	-2.176111	Melastomataceae	Miconia	Miconia egensis
-46.43	-2.716667	Myristicaceae	Virola	Virola michelii
-47.696667	-3.265	Poaceae	Paspalum	Paspalum pilosum
-46.7625	-3.681667	Pteridaceae	Adiantum	Adiantum lucidum
-45.235	-2.205833	Salviniaceae	Salvinia	Salvinia auriculata
-48.166667	-5.077222	Solanaceae	Solanum	Solanum crinitum
-47.296944	-1.821944	Vitaceae	Cissus	Cissus verticillata